POLITECNICO DI MILANO

Facoltà di Ingegneria dell'Informazione

Corso di Laurea Specialistica in Ingegneria Elettronica

Tesi di Laurea

SPRAY COATING TECHNIQUE FOR ORGANIC SOLAR CELLS FABRICATION

Relatore:
Prof. MARCO SAMPIETRO

Laureando:
DAVIDE MOIA
MATR. 721527

ANNO ACCADEMICO 2009-2010

"Skies will may change
in your world,
but not your soul"

Morningyes

Alla mia famiglia

Acknowledgments

First of all I would like to thank Jan Genoe, who gave me the opportunity to have this internship in IMEC.
Thanks to the whole organic group which I spend this months with.
Especially to:
Kris, friendly desk-mate with musical heart; David, I swear...we will work out the Voc.. Andrea e Alessandro, compagni druse (..nooooo); Adrian, thanks for the brazilian energy; Bjoern, Barry, Robert, Luuk, Sasha and all the others who let me feel welcome in the group.
To Claudio, great supervisor but not only that... Grazie! for your support during these months, for spurring me on to trust myself. I will miss our talks about...everything.

Un ringraziamento sincero va al Prof. Marco Sampietro, per la Sua presenza umana e scientifica e per avermi sempre ascoltato e dedicato tempo, dal momento in cui ho espresso il desiderio di andare all'estero e durante questi mesi nonostante la distanza.

Grazie ai miei Amici:
Alessandro, mio fratello (e mai smetterò di dirlo con fierezza), per essere fonte di ispirazione e compagno di vita.
Oggio, con le sue trovate over 18 (che noi tutti faremmo volentieri a meno...o forse no), per ricordarmi in ogni occasione che l'amicizia è fedeltà.
Marco, con la sua anti-prudenza, per avermi regalato tanta felicità in questi anni e per la tua contagiosa voglia di libertà.
Aurora, quella piemontese no?.., con cui ho imparato che in tanti momenti, avere qualcuno vicino fa la differenza.
Bicio, con i suoi 'orco diaz e le lezioni serali, per la sincerità dei tuoi consigli.
Athos, compagno di stanza, di griffin, di blink..,
Kikka, con i suoi vani tentativi per una via sacchini più pulita,
per l'atmosfera di famiglia che hai trasmesso alla casa.
Ad Ale my if teacher..work in progress, Diana, Robi, Lucilla, Anna, Salvatore e

Jessica per i momenti passati insieme in questi anni che mai dimenticherò.

Ai compagni con cui ho vissuto la musica: l'intraprendente e fascinoso Richard, l'appassionato e buon superbilly, il geniale ex-druse Ale. Perchè Morningyes lo abbiamo costruito insieme ed ora è dentro di noi.
I Cookiesyes, per le splendide avventure.
A Marco, il mio ghidas.

Infine, un grazie, che più di tutti vorrebbe ripagare ciò che ho ricevuto, va ai miei genitori. Mio Papà, maestro di vita di sport e di lavoro, ma anche grande amico. Mia Mamma, perchè quando c'è di mezzo il sangue le parole non servono.

Abstract

The energetic issues, that lately arose from the continuous increasing demand, underlie the recent significant diffusion of photovoltaics. Such renewable source is found to be in tune with the, by now, common pursuit of sustainable solutions. Important effort has been put in the development of the field, especially for what concerns the silicon-based technology, which nowadays represents the benchmark for the industry.

Other streams, which refer to alternative materials, are found to participate in this growth. A particularly innovative contribution has been given by the organic technology. Considering the mature development of coating and printing techniques in various fields of the industry, it becomes evident how the potential of solution processable devices, which involve organic semiconductors, can be decisive for an effective production of electronic systems. In particular, considering large area applications like photovoltaics, an important impact of this alternative is expected .

Among solution processing techniques, the coating of surfaces via spray deposition has been drawing the attention of the scientific community as well as of the industry. Its compatibility with roll-to-roll processes, the easy patterning, together with the high speed are only some of the advantages which portray the undeniable suitability of this method for large area production. So that a obvious question arises:
"Is it possible to spray a solar cell?", and mainly "Is it worth it?"

While the first question already found a positive answer from the recent research results, the second question needs definitely a much higher level of understanding on several figures of evaluation. The aim of my work was to contribute in such understanding, focusing on the fabrication and the characterization of small ($\sim$1 cm^2) area devices.

The starting point of my investigation consisted in the analysis of solution properties, in terms of coating. The main issues concerning the lack of control

on the deposited liquid, which spray coating simplicity turns into, had to be analysed. A deep study on the solution composition, as well as on the process parameters influences was pursued.

In a second stage of my work, organic layers deposited via spray coating were inserted in solar cells structures. The physical properties of the films were investigated in order to optimize devices' performances. Particular attention was paid to the active layer morphology, which basically determines all the main optical and electrical features of the full structure.

Ultimately, a evaluation of the results achieved is drawn, referring to the performance of spin coating process, benchmark of solution processing.

Sommario

La questione energetica che preoccupa le nuove generazioni e la continua sensibilizzazione verso il raggiungimento di soluzioni ad alta sostenibilità offrirà nei prossimi anni l'occasione per una diffusione in larga scala del fotovoltaico. L'industria sta perciò impiegando risorse nell'abbattimento del costo per Watt dei moduli, in modo da poter offrire un'alternativa valida e competitiva per la produzione energetica per piccole e grandi utenze. Gran parte degli investimenti sono stati destinati allo sviluppo della tecnologia a base di silicio, attuale *benchmark* per l'industria fotovoltaica.

Alcune alternative che coinvolgono materiali di diversa specie suscitano in questo contesto un interesse che sembra essere sempre più crescente. Tra queste, la tecnologia organica ha subito negli ultimi due decenni una rapida evoluzione. L'entusiasmo che ne ha spinto lo sviluppo, specialmente nel settore fotovoltaico, è riconducibile alla sua innegabile compatibilità con i processi *large-area*. Focalizzandoci in particolare sulla realizzazione di dispositivi *solution-processed*, è facile intuire come la maturità raggiunta nelle tecniche di coating e printing, raffinate in numerosi ambiti industriali, e l'assenza di specifiche stringenti di processo (vacuum-free, room temperature) rappresentino i punti di forza dell'*organic photovoltaic* (OPV). I valori di efficienza raggiunti (record 7.9% certificati) sono ancora molto bassi se confrontati con gli standard dei moduli basati su materiali inorganici (over 20%). Considerando inoltre le ancora scarse prestazioni di lifetime, si giustifica come la tecnologia organica non abbia ancora i numeri per dare un sostanzioso inizio alla produzione industriale, tanto meno per permettere ai primi timidi tentativi di fabbricazione di prodotti commerciali di avere un impatto sul mercato.
Per quanto l'efficienza sia la prima cifra di merito da considerare nella valutazione di una tecnologia di fotoconversione, non si tratta però della principale direzione a cui la ricerca OPV deve puntare per raggiungere una sufficiente competitività; Bensì, fondamentale è la messa a punto di processi di deposizione roll-to-roll compatibili, che garantiscano d'altra parte il mantenimento delle prestazioni che

le tecniche di deposizione quali spin-coating definiscono come stato dell'arte.

L'introduzione di tecniche spray per la deposizione di materiali organici da soluzione è stata negli ultimi cinque anni una delle proposte che più hanno attirato l'attenzione della comunità scientifica, nonchè dell'industria. L'alta compatibilità con processi roll-to-roll, la possibilità di eseguire facilmente un patterning del substrato, l'importante riduzione nello scarto di materiale, l'assenza di significativi limiti nella velocità di deposizione, rappresentano ulteriori vantaggi dello spray coating nel già interessante ambiente del *solution processing*.

Nel mio lavoro di tesi ho affrontato l'analisi di questa tecnica, investigando la realizzazione di film sottili per la fabbricazione di celle solari organiche. Il metodo spray consiste nella deposizione di soluzioni su substrato, previa nebulizzazione. Tale operazione è svolta dallo spray coater, costituito da un ugello dotato di testina vibrante ad ultrasuoni. La semplicità del processo è chiaramente il principale punto di forza in vista di una sua estensione nel campo industriale.
Tuttavia, risulta fondamentale il fatto che la tecnica spray non preveda alcuna forza esterna agente sulla soluzione depositata che assicuri una sua corretta distribuzione. Tecniche classiche di solution processing, quali spin coating e blade coating prevedono, dopo la deposizione, opportune sollecitazioni esterne per ottenere un film liquido sottile ed uniforme. In questo modo è infatti possibile assicurare che, a seguito del processo di evaporazione, il layer organico presenti accettabile regolarità nello spessore.
L'uniformità non è quasi mai un problema nelle applicazioni spray per coating industriale. Le cose cambiano considerando le specifiche legate alla produzione di dispositivi elettronici, dove le accuratezze coinvolte sono nell'ordine delle decine di nanometri.

Particolare attenzione alla scelta dei solventi può essere decisiva in questo senso. In letteratura è ormai assodato il fatto che la natura del solvente sia un indizio primario per la valutazione della finale morfologia dei layers depositati. Essi infatti, influenzano profondamente l'organizzazione a livello molecolare delle speci organiche durante il processo di evaporazione. Nel caso del processo spray, i parametri fisici di tali componenti risultano particolarmente determinanti anche nell'effettiva possibilità di rendere la tecnica capace di riprodurre film sottili con accettabile accuratezza e uniformità. Tensione superficiale, gradienti di tensione superficiale diventano le *driving forces* che hanno diretta ripercussione sulla qualità macroscopica della deposizione e sull'effettiva scalabilità del precesso.

Una profonda comprensione del fenomeno di evaporazione delle soluzioni è stata perciò necessaria per l'interpretazione dei risultati, in modo da individuare

le questioni critiche che influenzano la qualità di una deposizione spray. Particolare attenzione è stata dedicata a ciò che rappresenta una delle principali fonti di disuniformità per tutte le deposizioni del tipo *solution casting*, conosciuto in letteratura come *coffee ring effect*. Tale fenomeno è infatti alla base del fatto che a seguito della totale evaporazione del solvente (acqua) di una goccia di caffè posta su una superficie piana, è possibile ossevare come la macchia risultante mostri un significativo accumulo di soluto ai bordi. Analoghi problemi di controllo della distribuzione del materiale organico sono stati riscontrati nel corso del mio studio.

Focalizzandomi sugli aspetti di coating, nella prima fase del mio lavoro ho formulato una procedura riproducibile per la deposizione di alcuni film organici. Dato l'insuccesso di tutti i tentativi di deposizione da singolo solvente, ho proceduto nel considerare una tecnica a due solventi. Un'opportuna progettazione di tale miscela è in grado di portare, in primo luogo ad un miglioramento delle proprietà di wetting della soluzione. Inoltre, creando un opportuno gradiente di tensione superficiale, è stato possibile risolvere il problema della prematura contrazione del layer liquido durante l'evaporazione. Quest'ultimo fenomeno rappresentava infatti la principale causa di degradazione di uniformità nella superficie finale dei film organici.

Valutati gli effetti dei parametri di processo in gioco, mi sono concentrato sull'ottimizzazione di layers organici coinvolti nelle tipiche strutture di celle solari. E' stato perciò condotto un dettagliato studio sulla deposizione dei blend PEDOT:PSS e P3HT:PCBM.

Una seconda fase di analisi è stata dedicata alla caratterizzazione di celle solari fabbricate via spray coating. L'ottimizzazione delle proprietà elettriche dei materiali coinvolti è stata conseguita con l'introduzione di opportune tecniche di processo e di annealing. Concentrandomi in particolare sul layer attivo, il dimensionamento dello spessore ottimale e di un trattamento termico ha portato ad apprezzabili miglioramenti nelle prestazioni.

Sorprendentemente, un confronto finale con lo stato dell'arte mi ha permesso di dimostrare come le performance di celle solari processate via spray coating, che rappresentano quindi in riassunto questo lavoro di tesi, siano in grado di raggiungere i livelli stabiliti dal processo di riferimento.

Principali contributi innovativi

La tecnica di spray coating si dimostra essere tanto ad alto potenziale, quanto delicata dal punto di vista della riproducibilità. L'estrema semplicità del processo

di deposizione si riflette nella variabilità del risultato finale.
Il mio studio degli aspetti di fluidodinamica e termodinamica di evaporazione della soluzione depositata ha contribuito nell'identificazione degli aspetti centrali per lo sviluppo di una tecnica affidabile ed efficace.

In primo luogo, l'adozione del metodo Single Pass si è rivelato cruciale per superare le intrinseche limitazioni derivanti dalla deposizione spray interpretata in modo classico. Lo studio di tale tecnica viene infatti intrapreso da numerosi gruppi di ricerca mantenendo un'evaporazione del liquido nebulizzato rapida e indipendente tra le singole gocce. Tale evoluzione ha devastanti ripercussioni sulla qualità del layer impossibilitando il controllo dello spessore e compromettendo le prestazioni del dispositivo. Il Single Pass prevede la formazione di unico layer liquido a seguito della deposizione. Ciò determina difficoltà nel controllo dell'evoluzione fluido e termodinamica, ma apre la strada alla realizzazione di layers con proprietà di *smoothness* accettabili.

Le investigazioni di composizioni multisolvente si sono rivelate una strada risolutiva al deficit di uniformità macroscopica mostrato dallo spray-coating. Il controllo dei flussi di Marangoni regolati dalle variazioni di tensione superficiale ha costituito un'intuizione risolutiva delle limitazioni intrinsiche della tecnica. L'assenza di forze esterne che garantiscano lo *spreading* della soluzione e l'uniformità del layer risultante è stata compensata dall'induzione di una forza interna che implementi tale funzione. L'efficacia di tale forza ha una portata chiaramente limitata se confrontata con la forza centrifuga coinvolta nel processo di spin coating. Tuttavia l'effetto complessivo si è scoperto essere sufficiente per il raggiungimento di accettabili qualità dei layers.

Concentrando l'attenzione sull'applicazione finale, la formulazione di una ricetta per la realizzazione di celle solari aventi tutti i componenti organici depositati via spray coating ha permesso di eguagliare le performance attribuibili ai processi identificati come stato dell'arte della tecnologia.

Struttura della tesi

Nel **Capitolo 1**, un'introduzione sul ruolo del fotovoltaico nel panorama energetico mondiale è seguita da un approfondimento sulla struttura e sul funzionamento delle celle solari organiche. Infine, una panoramica sui processi con cui tali dispositivi possono essere fabbricati porterà ad una prima presentazione della tecnica di spray coating.

Il **Capitolo 2** ha il compito di inquadrare il setup sperimentale con cui questo

lavoro è stato realizzato. Partendo dall'architettura scelta per i dispositivi oggetto di studio, verrà poi illustrato nei dettagli il funzionamento dello spray coater. Una panoramica sugli strumenti coinvolti negli esperimenti e nelle caratterizzazioni dei campioni concluderà la sezione.

Il **Capitolo 3** è dedicato alla discussione delle principali proprietà dei fluidi che è bene tener in considerazione quando si parla di deposizioni da soluzione. Particolare attenzione verrà data ai parametri fisici coinvolti nella fisica di evaporazione.

Nel **Capitolo 4** è mostrata la prima fase dell'analisi sperimentale. Tutte le investigazioni sul problema del coating con deposizione spray vengono approfondite prendendo in considerazione il *processing* di layers costituiti da PEDOT:PSS e P3HT:PCBM. Le più importanti constatazioni sulle caratteristiche della tecnica sono descritte in questa sezione.

Con il **Capitolo 5** si introduce la caratterizzazione di dispositivi in cui nella fase di processo è stato adottato lo spray coating. Una dettagliata ottimizzazione dell'anodo e in particolare del layer attivo porterà alla formulazione di una ricetta per la fabbricazione di una cella ottenuta via tecnica spray.

Infine, nel **Capitolo 6**, un diretto confronto dei risultati ottenuti in questo lavoro verrà fatto riferendosi al processo di spin coating. Partendo dalla valutazione delle performance in termini di coating, concluderò con i dati sperimentali che mettono in evidenza la portata dei risultati ottenuti in termini di efficienza, confrontati con lo stato dell'arte.

Contents

List of Figures

Chapter 1

Introduction

1.1 Photovoltaics as renewable energy source

The crisis of oil market and the need of a sustainable production of energy are influencing more and more relevantly the economic and ecological policy of developed countries, forcing national governments to invest in renewable energy sources. The countries of European Union (EU) constitute the main world power in the field of development and use of renewable energy. European leaders signed up in March 2007 to a binding EU-wide target to source 20% of their energy needs from renewable sources by 2020 [1].

Photovoltaic (PV) conversion of largely available solar light into directly usable electricity is one of the brightest prospects for the future generation of clean energy, being the sun the primary source of energy for the whole planet. Sunlight is an attractive energy source not only for the production on the large scale as in the case of widely extended photovoltaic power plants. In fact, solar panels can also be placed upon the rooftop of a building to satisfy the domestic energy consumption of a family. Nowadays, the photovoltaic market is dominated by crystalline silicon solar cells, as found on rooftops, with a share of 95%. Amorphous silicon solar cells are worth 4% of the market, and the remaining 1% is filled by newly introduced thin film technologies.

Silicon solar cells are well established in energy generation. It is not uncommon for monocrystalline silicon to obtain power conversion efficiencies of around 24%. Commercially available solar cells are typically fabricated on the multicrystalline silicon technology that is less expensive but at the same time less efficient. Typical power conversion efficiencies are around 14-19%. However, the most significant disadvantage of silicon remains the cost of energy production, in terms of

both financial and environmental costs. Silicon photovoltaic systems need several years of activity in order to recover the energy involved in their fabrication. In addition, there is a large number of hazardous chemicals needed to produce crystalline silicon, as well as a significant amount of water. A further disadvantage of silicon and other such crystalline devices is that they are inflexible and generally very fragile, limiting the possible applications.

Over the past decade, thin-film PV technologies, so called second generation technologies such as a-Si (amorphous silicon), CIGS (copper indium gallium diselenide), and CdTe (cadmium telluride) have rapidly caught up in terms of performance and production technology and are now undergoing a rapid expansion in production. The next few years will determine whether this indicates the beginning of the end of the dominance of the PV market by crystalline Si. The time frame for a PV technology to go from laboratory concept to market is approximately 20 to 30 years. With a-Si, CIGS, and CdTe now becoming established in the market, the question arises as to what photovoltaic technology platform(s) will follow.

Research into such platforms is currently proceeding in two directions: ultrahigh efficiencies and ultralow production costs. For lowest cost PV production, solution-processable solar cell technologies based on both organic and inorganic light absorbers, including polymer-blend, small-molecule, dye-sensitized, and inorganic nanoparticulate devices, are all receiving extensive attention. molecular and inorganic [2].

1.2 Organic solar cells

Organic materials represent an inexpensive and easily processable alternative to silicon. Indeed, semiconducting polymers and molecules combine the optoelectronic properties of conventional semiconductors with the excellent mechanical and processing properties of plastic materials.

1.2.1 Organic semiconductors basic properties

In order to understand the physical properties of organic materials, the basic theory of chemical bonds in carbon based molecules and polymers has to be discussed. Since this work is mainly focused on device processing, only some basic concepts are shown. Further detailed descriptions can be found in [3].

Organic semiconductors are molecules characterized by an extended π-conjugation, where the orbitals of sp^2 or sp hybridized carbon atoms interact to create a delocalized electron clouds over the whole molecular plane, while π orbitals give rise to strong covalent bonds which define the molecular backbone.
π orbitals, therefore, form the frontier orbitals for this class of materials, thus being responsible for their optoelectronic properties. Conjugated molecules can be roughly divided in two categories: polymers and small molecules. Polymers are molecular systems formed by the regular repetition of a fundamental unity called monomer. The molecules where the number of repetitive units is of the order of 8-10 or smaller are indicated as oligomers and, together with molecules that do not show any fundamental unity repetition, belong to the small molecules class.

Condensation of such systems lead to the creation of molecular solids, where each molecular unit is bound to the other through weak van der Waals bonds. The formation energy of such bonds is equal to 10 kcal/mol, much smaller than the 76kcal/mol formation energy of the silicon covalent bond for example, and for this reason the interaction between adjacent molecules results limited. This has important applicative consequences:

- organic semiconductors show high mechanical flexibility, thus allowing the fabrication of flexible electronic devices;
- they are solution-processable materials and allow low-cost and low-temperature deposition techniques compatible with plastic and large area substrates.

The limited molecular interactions imply also that the optoelectronic properties of the solid are not so different from those of the single molecule. This means, for example, that starting from molecules characterized by an efficient radiative recombination of the excited states, it is possible to obtain an electro-luminescent device with a high quantic yield. This, together with the possibility to cover the whole visible spectral range (organic semiconductors show typically energy gaps in the range of 1 to 4 eV), fostered an intense research activity in this field that has led to the recent commercialization of the first examples of organic displays [4].

The absorption of light within organic materials is similar to inorganic counterparts. When a photon is absorbed, an electron is promoted from the Highest Occupied Molecular Orbital (HOMO) to the Lowest Unoccupied Molecular Orbital (LUMO), leaving a hole in the lower energy level. Any photons with energy less than the HOMO-LUMO energy gap cannot be absorbed.

The absorption window of organic materials is rather limited compared to that of classical inorganic crystalline semiconductors. In crystals, absorption is allowed over a broad range due to the presence of broad bands. Conversely, organic materials have no bands, or small bands at best. This limits the absorption mostly to the first electronic transition and some extra vibrational modes. In polymers, the absorption range can be somewhat extended due to energetic disorder originating from differences in conjugation lengths and local inter-chain interactions but, however, the absorption range is not as broad as in inorganic semiconductors. Most of the red and infrared light cannot typically be absorbed.

Due to the Coulombic attraction between the photo-generated electron and hole, the result of absorption is a bound state known as exciton. The nature of excitons in organic materials is different from that of inorganic counterparts. This occurs for the reason that organic materials are characterized by a low dielectric constant (typically 2-4) compared to inorganic semiconductors (typically 14-15), so that the generated electrons and holes can "sense" each other stronger and over a longer distance. Considering excitons in inorganic semiconductors, it means to refer to lightly bound Wannier type excitons. These excitons have a Coulombic radius much larger than the lattice constant and a weak binding energy in the order of 10 meV. Since the thermal energy (kT) at room temperature is 26 meV, these bound species dissociate spontaneously in free electron-hole pairs.

In organic materials, on the other hand, excitons are Frenkel type excitons and are located across a small number of conjugated units with an approximate radius below 0.5 nanometers. Frenkel excitons have a strong binding energy, ranging from 0.2 eV to even 1 eV, so that they can not spontaneously dissociate at room temperature. Moreover, the electric field provided by an organic solar cell is not sufficient to break-up these photogenerated excitons either.

In conjugated polymers, also charged excited species can result out of photon absorption. Upon adding a charge to a polymer chain, the molecule will suffer a local distortion in the conjugated structure. The combination of a charge and a distortion is known as polaron, which can be positive or negative depending on the sign of the charge. Polaron formation is characterized by energetic relaxation, with the polaron energy level lying inside the HOMO-LUMO gap. It should be noted that for the creation of polarons upon photon absorption, the electron and hole must be separated sufficiently in space, so that there is no Coulomb attraction binding them together. This can be achieved only by removing the photogenerated electron or hole from the molecule within femtoseconds or by trapping one of the charges at an impurity or defect. The addition of a further charge, hole or electron, will reform the original conjugation configuration,

producing a positive bi-polaron or a negative bi-polaron respectively. In addition to this, neutral bi-polarons (electron and hole distortions) can be formed, although these are thought to be quickly reduced into excitons due to Coulombic attraction.

1.2.2 Structure and working principle

An organic solar cell is basically made of a stack of layers with the following functions:

- The **anode** is an high work function material, which is responsible of hole extraction.
- The **active layer** hosts all the most important mechanisms of device's working. It consists typically in the coupling of a donor (low electronic affinity) and an acceptor (high electronic affinity) materials. This is by far, the most effective configuration for organic photovoltaic devices.
- The **cathode** is a low work function specie and accomplishes to the photo-generated electrons harvesting.

Indeed, the difference in work function of the electrodes represents the main driving force for charges extraction. In short circuit conditions in fact, an average electric field proportional to such difference is established in the active layer. Moreover, the Fermi levels of the anode and the cathode have to approximately match respectively the HOMO level of the donor and the LUMO level of the acceptor material, so that during the harvesting no energy is further lost.

In order to clarify the most significant factors which influence the performance of an organic solar cell, here we explain the basic principles which underlie the physical behaviour of a lighted device (Figure 1.1).

- Photons entering the solar cell from a transparent electrode and which are absorbed in the active layer generate electron-hole pairs either in the donor or in the acceptor material. Due to the physical properties of organic materials the coulomb interaction between such carriers is high enough to keep them tied and make them form an exciton with a binding energy much higher than the thermal energy (1).
- The following diffusion of the excitons permits to part of these pairs to reach the donor-acceptor interface. The diffusion length (L_d) for an exciton is typically 5 to 10 nanometers (2).

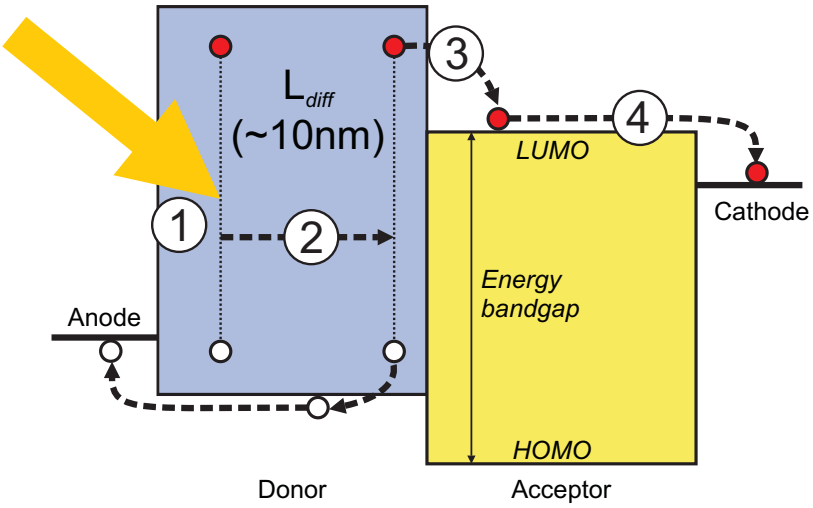

Figure 1.1: Basic working of an organic solar cell: (1) creation of the exciton from photon absorption; (2) diffusion of the exciton towards the donor acceptor interface; (3) charge transfer between the two species driven by the difference in electronic affinity; (4) transport of the carriers towards the respective electrodes.

- The exciton splits through a charge transfer mechanism, driven by the LUMO levels shift, so that free hole in the donor material and free electron in the acceptor material are available (3).
- Subsequently, a successful transport of the two carriers along the two different phases and their proper harvest to the anode and the cathode completes the conversion (4).

In fact, the combination of these processes results in the availability of one effective electrical charge to the potential equal to the voltage of the cell.

By measuring the current-voltage (I-V) characteristic of an organic solar cell, a profile as the one shown in Figure 1.2 can be observed.

The main electrical parameters which permit to evaluate the performance of a solar cell from the I-V curve are now shown:

- The short-circuit current (I_{sc}) is the current flowing in the illuminated device at 0 V bias. This value is significantly dependent on the portion of the solar spectrum which is covered by the absorption window of the active layer.
- The open-circuit voltage (V_{oc}) is the voltage that the device generates in open circuit conditions (no current flowing in the device). It is found to be limited by the difference between the LUMO level in the acceptor and the HOMO level in the donor material.

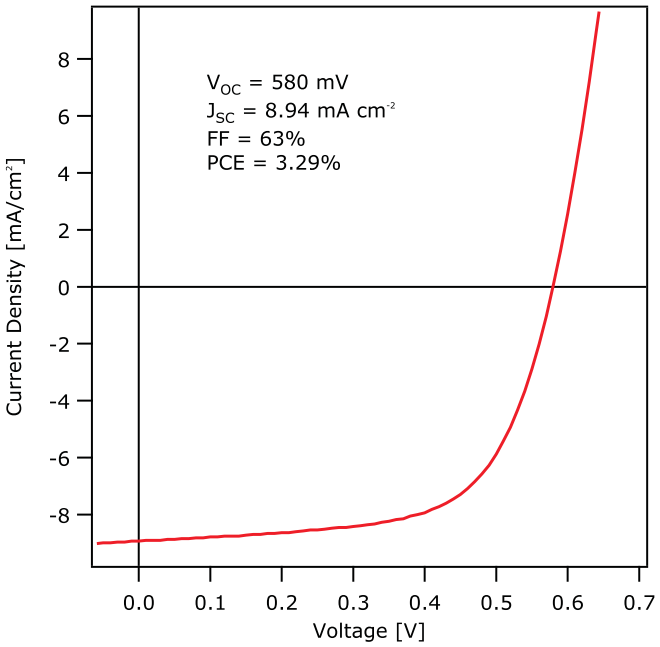

Figure 1.2: Typical profile for I-V curve of an organic solar cell.

- The fill factor (FF) gives information about how similar the I-V curve in the forth quadrant is with a rectangular shape whose area is equal to the product I_{sc} times V_{oc}. It is a very important figure of merit in regard to the transport performance in the active layer as well as in the electrodes.

Indeed the Power Conversion Efficiency (PCE, η) can be written as:

$$\eta = \frac{I_{sc} V_{oc} FF}{P_{in}} \tag{1.2.1}$$

where the numerator represents the maximum power extractable from the device, while P_{in} is the optical incident power. For typical testing, P_{in} refers to 1 sun power at standard conditions, namely solar spectrum intensity with zenith angle 48.19 °C

1.2.3 Architectures

Indeed, the working of an organic solar cell involves a sequence of several physical processes whose correct fulfilment leads to an effective extraction of electrical power. It is evident how all such processes are intimately connected with the optical and electrical properties of the active layer. For this reason, the adoption of suitable architectures which couple the donor and the acceptor materials in various geometry have been investigated.

A first effective architecture is very similar to the scheme shown in Figure 1.1. A bilayer structure consists in fact, in the deposition of pure donor and acceptor materials one on top of each other. This solution is very common for small molecules based devices.

For solution processed solar cells most of the effort in the recent years has been pointed towards the development of bulk heterojunction (BHJ) architecture. In such structure, donor and acceptor materials are processed from the same solution and in the same deposition step. Indeed, this gives rise to a heterogeneous environment within the active layer, where the alternate presence of the two species leads to a geometrical topology detailed to the sub-micrometer scale. This architecture is preferred to the simpler bilayer structure because it permits to overcome the limitations due to the short diffusion length of the exciton. In fact, the effective volume in the active layer where photo-generation of electron-hole couples is followed by a correct charge separation is narrowed to the set of molecules which are $\sim L_d$ far from the donor-acceptor interface. The BHJ philosophy is therefore to extend such interface to the whole volume of the layer, by creating a dual and complementary network with the two materials. The improvement due to the enhanced exciton dissociation efficiency is partially damped by a less efficient transport of the carriers in the donor and acceptor matrix. In fact, the environment which the electrical charges have to travel through is less homogeneous in a BHJ than in a bi-layer, where the transport takes place in a bulk single material.

1.2.4 Pocessing in organic electronics

Deposition of organic materials typically involve, as already mentioned, low cost techniques. This represents the main advantage of adopting such technology instead of traditional inorganic platforms. Whereas for small molecule-based devices, the adoption of vacuum evaporation is typically preferred, polymer-based organic electronics involves in most of the cases depositions from solution. In this work I will focus on the description of solution processing techniques, since spray coating belongs to such family.

In regard to coating techniques, the following are found to be the most suitable for electronics applications:

- Spin coating is a well-understood process for the deposition of thin-film coatings with high precision. It basically consists in an high speed spinning of a substrate on which the solution is previously dispensed. By taking ad-

vantage of centrifugal force, thin and very uniform layers can be processed (see Appendix D for details). The method requires little formulation work and is quite forgiving over a considerable range of viscosities. Wetting can be guaranteed by surface pretreatment of the substrate. The film thickness is controlled by a combination of spinning speed, acceleration, solution viscosity, and temperature; typical spin-coated films are between 50 and 5,000 nm. Typical spin-coating machines handle substrates up to 20 cm in diameter. The disadvantages of spin coating are the large material losses(more than 90%) and the incompatibility with roll-to-roll processing. Whereas the former problem can be minimized by collecting and purifying the residuals from the spin bowl, the incompatibility with roll-to-roll processing preclude its employment for large area production.

- Doctor blading was demonstrated to overcome many of the disadvantages of spin coating. It involves a blade that is drawn over a substrate and homogenously spreads the ink. Doctor blading is fully compatible with roll-to-roll processing. Ink formulation for doctor blading is quite comparable to that for spin coating. Four parameters determine the film formation: the concentration (responsible for the viscosity of the ink), the temperature of the solution, the speed of the blade, and the distance between the blade and the substrate (i.e., the volume of ink being deposited).

Also for printing techniques, here I name the most common ones for organic semiconductor layers deposition. Interestingly, very different principles underlie their workings:

- In gravure printing, the printing pattern is engraved into the printing plate (or film cylinder). During inking, the engraved cells of the plate are filled, and during imprinting, the substrate removes and takes up the ink from the cells. Gravure printing can give outstandingly high resolution and registration for relatively low-viscosity inks.

- In screen printing, a stencil is patterned by closing selected areas of a screen. Upon imprint, ink is forced through open meshes by means of a blade. Screen printing typically requires 10 to 100 times higher viscosity inks than those used for spin coating or doctor blading.

- Inkjet printing has evolved as the most popular printing method for the production of multicolor polymer light-emitting diode (PLED) displays and, by now, is probably the most widely used printing method in organic electronics. Nevertheless, inkjet printing of solar cells has different requirements

than inkjet printing of PLEDs. Indeed, only a few research groups worldwide work on the application of mass printing for the fabrication of large-area PV [2].

1.3 State of the art

A proper understanding of the role which my investigations played in the recent development of solution processable organic solar cells needs a portrait of the current situation in this field.

The state of the art concerning devices' performance will be presented, followed by an overview on the main processes which spray coating has to be compared with. Ultimately, recent results achieved by other groups in spray deposition of organic layers will be shown.

1.3.1 Performance of organic solar cells

The most common materials nowadays employed in the active layer of organic solution processed solar cells are poly(3-hexylthiophene) (P3HT) and the C_{60} derivative PCBM ([6,6]-phenyl-C61-butyric acid methyl ester). The optimization of this combination led to the achievement of efficiency in excess of 4% [27].

Theoretical analyses of the optimum device performance achievable as a function of particular materials properties have guided strategies to make further improvements in device performance beyond P3HT:PCBM. Such analyses have identified two key strategies to achieve further advances. First, aiming to improvements in the voltage output of the solar cell by using polymers with larger ionization potentials. In fact, this voltage is limited by the free energy of the photo-induced charge-separated state and, therefore, by the energy difference between the polymer HOMO level and PCBM LUMO level. Secondly, important enhancements in photo-current occur by lowering the polymer's optical bandgap to enhance the absorption of longer wavelength light. These two requirements clearly give rise to a trade off in the determination of the optimal HOMO LUMO levels. Indeed, the past few years have seen an intense program of polymer design, synthesis, and evaluation based on balancing both such strategies.

A first notable success has been the low-bandgap benzothiadiazolefused thiophene copolymer PCPDTBT. When blended with the C_{70} analogue of PCBM, this polymer yielded efficient photocurrent generation out to 850 nm and a white-

light power conversion efficiency of up to 5.5% [5].

More recent researches ended up with the breakthrough of a 7.9% certified efficiency for a single active layer solution processed solar cell, shown by *Solarmer* in December 2009 [6]. The increasing interest in the field, let us expect further improvements in performance in the next few years.

1.3.2 Deposition processes

Most of the important results in organic solar cells research have been achieved by mean of spin coating process. Indeed, such method still represents the benchmark for what concern film quality and device performance. Its incompatibility with roll-to-roll (Figure 1.3) production is therefore the reason which underlies the intense search for a deposition process enabling the extension of spin coating results to large area fabrication.

Figure 1.3: Basic idea of a roll-to-roll process: Unrolling the substrate, processing, rolling again. The high throughput and low cost of such systems are perfectly tuned with PV industry requirements.

Based on this, spray coating technique finds a very coherent role in organic solar cells fabrication. Before presenting such method, an overview on all the other alternatives is needed.

Concerning printing techniques, inkjet printing shows the possibility to print up-scaled organic layers. The development of inks that dry sufficiently slowly, in combination with a printing scheme that fires droplets sufficiently narrowly spaced, make sure that single pixels coalesce over a reasonably large area before drying. Following these design rules, 2.9% efficient P3HT:PCBM solar cells were inkjet printed from a solvent mix of a high-boiling and a low-boiling solvent,

demonstrating the potential of the technique [7]. Nevertheless, the low throughput achievable still represents the main obstacle between this technique and mass production.
Screen printing of OPV has been reported a few times, but the requirement for high viscosities limits the available materials. Only conjugated polymers with high molecular weights and high solubilities are suitable for high quality screen printed solar cells.

The first gravure printing trials of P3HT:PCBM blends reported excellent film quality [8]. The homogeneity and the surface roughness of gravure-printed P3HT:PCBM films were comparable to those of spin-coated layers. This example, in combination with the high-throughput production compatibility, make gravure printing the most promising printing method for mass production of OPV.

Among coating technique, Blade coating, as well as other methods with similar principle, is nowadays the only one which acceptably accomplishes to the requirements for an effective and complete roll-to-roll organic solar cells fabrication (Figure 1.4).

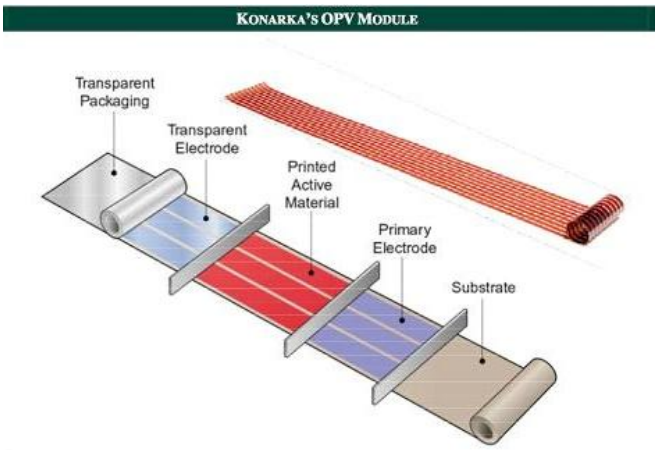

Figure 1.4: Scheme of a blade coating process for complete organic solar cells production [9].

The temperature profile and the drying kinetics of the wet film during blading are quite different from those encountered during spin coating and can lead to different solid-state morphologies. However, detailed investigations have shown that blading can result in fully optimized solar cells with performances identical to those of cells prepared by spin coating [10], reaching very interesting values of efficiency (3.8% for P3HT:PCBM based solar cell) [15]. Indeed, the first commercial items electrically supplied by organic solar cells (Figure 1.5) have been shown recently and confirmed blade coating as robust roll-to-roll deposition process [9].

Figure 1.5: Solar bag with internal laptop battery charger supplied by organic solar cell (Konarka Technologies [9]).

1.3.3 Spray coating

In this context, spray coating technique for organic solar cells fabrication has been recently introduced. The method basically consists in the atomization of the solution into 1 to 10 micrometers small droplets as well as in its ejection from a nozzle over the substrate. The evaporation of the solvent leads consequently to the formation of a covering layer.

Such technique has been investigated for several decades in a lot of industrial fields and, nowadays, the production of most of general purpose coated items involves spray depositions. Typical requirements for such applications consist in uniformity of the coating layer within the micrometer scale, affordable for the nature of the process.

The employment of spray coating for the deposition of layers involved in electronic devices seemed, in the first attempts, to have some intrinsic limitations though. Indeed, the attainment of films with thickness in the order of the tens of nanometers gives rise to much stricter constraints, if compared with typical industrial coatings.

The substantially different approach that spray coating implements in the deposition of a liquid layer underlies the challenge of its employment. In fact, printing technique take advantage of an highly controlled dosage and positioning of elementary amounts of solution, in order to attain a pattern which easily evolves towards a uniform liquid film of solution.
Coating techniques, on the other hand, involve a coarse dosage, but the intervention of an external force provides a regularization in terms of amount and distribution of the solution.

Spray coating joins the simplicity of the two deposition processes families. Indeed, the dosage of the solution occurs accurately, but the positioning of the droplets completely relies on statistics. This entails that much higher deposition speed can be adopted; the drawback is that a "shot-like noise" affects the distribution of the liquid at the time of landing. Moreover, the solution, once deposited, does not undergo any external force which acts in order to flatten it, nor to control its volume. Thus, a free evaporation evolution of the liquid occurs. This permits, for example, to easily pattern the deposition by placing a opportune mask on the substrate. Indeed, most of coating techniques do have a limited potential to deposit patterned layers and have to include post-pattern steps on coated films. Moreover, the substrate must not be necessarily flat. Relatively simple adjustments of nozzle settings can, in principle, introduce such degree of freedom. However, this lack of control on the deposited solution leads to very significant disadvantages. While the random distribution is found to be quite forgiving, the fluid dynamics involved in a free evaporation evolution can strongly degrade the quality of the deposition.
Such issues will represent key points latter on in this work.

I want to conclude this introduction by citing some of the most important researches that, so far, resulted in successful employments of spray coating in organic solar cells fabrication.

- Vak et al. showed the achievement of 2.8% efficiency in the implementation of P3HT:PCBM based organic solar cells, by spraying the active layer with a handheld air-brush [31]. Indeed, despite of the over 50 nanometers for the root mean square values for the roughness of the layer, spray coated organic films demonstrated to correctly work within full device.

- By using similar setup, Girotto et al. reported equal efficiency performance. In this work, the Single Pass technique, that I will present into details in Chapter 3, was introduced. Such method permitted to achieve remarkable quality in terms of smoothness of the organic layer. Root mean square values (rms) for the roughness in the order of 10 nanometers on a 5 by 5 μm^2 area were assessed (comparable with spin coated films). [20].

- Green et al. investigated the spray deposition of P3HT:PCBM by mean of different solvent and showed an optimization of solar cell's performance via thermal treatment. Efficiency value of 2.35% were shown, referred to active layers deposited from a chlorobenzene solution and annealed at 110°C for 10 minutes. In this work, the very rough surface of the film led to significantly low fill factors (lower than 50%) [22].

- In [24] Hoth et al. showed the employment of a two solvents technique, optimized for inkjet printing deposition, for the spray deposition of the active layer. Such strategy led to slight improvement in the smoothness of the film. Due to independent evaporation of single droplets, the topography of the surface still showed limited uniformity (24 nanometers rms over a 50 by 50 μm^2 area). Nevertheless, 2.7% efficiency was reported for devices with both the anode and the active layer deposited via spray coating.

1.4 Outline

In **Chapter 2**, the experimental setup adopted will be shown. The presentation of devices architecture as well as the procedure involved in their fabrication will be followed by an introduction of the spray coater employed in this work.

Chapter 3 will be focused on those liquid properties which are fundamental "characters" in solution processing. An overview on spray deposition techniques will then be made.

Chapter 4 presents the first experimental part of my work, considering the coating of substrates via spray deposition. The study of PEDOT:PSS and P3HT:PCBM processing will be considered, with particular attention on the optimization of the uniformity of the layers.

In **Chapter 5** the characterization of solar cells devices involving spray coated organic layers will be shown. The analysis of the active layer will be, in particular, focused on its morphology and will lead to a specific recipe for an optimized processing.

Ultimately, in **Chapter 6**, I will present an evaluation of the results achieved, referring to the spin coated reference for solution processed organic solar cell. The performance of devices with both the organic layers deposited via spray coating will conclude this work.

Chapter 2

Experimental setup

2.1 Solution processed organic solar cells

Organic electronics differs from other technologies because of the absence of a fixed bulk material which represents the substrate and the core of the final device. The design of an organic solar cell always starts in fact from the choice of all the materials involved in its structure. Especially the choice of the donor and acceptor species, which form the active layer, is a crucial point for what concern the final performance of the device. Indeed, important differences can be observed by changing either of the two components.

This suggests how the research in the chemical synthesis of new organic molecules is the main concerning in order to achieve remarkable efficiency values. This is definitely an important factor in order to increase the impact of organic technology in the photovoltaic market. On the other hand, the development of processes which permit to exploit the potentiality of such materials does matter even more in this context. In fact, it contributes to the optimization of device performance, but it mainly represents the concrete advantage that distinguishes organic electronics in comparison with all the other competitor technologies. In this sense, improvement in the implementation of roll-to-roll low cost processes such as spray coating could really represent the turning point.

Thus, our attention was not focused on the research of cutting-edge materials, but rather on the investigation of the effectiveness of spray coating, compared with other state of the art deposition processes, in the implementation of well-established solar cell structures.

The research on solution processed solar cells focused in the last years on the

development of architectures, which show some basic common features. Among them, the structure we chose for this work represents a very significant reference, therefore it suited perfectly with the requirements previously discussed.

Such architecture, that from now on will be identified as "standard structure", involves the following elements:

- The **anode** is implemented by coupling a Transparent Conductive Oxide (usually Indium Tin Oxide), and an organic layer of PEDOT:PSS.
- The **active layer** is a bulk heterojunction, where the donor material is the polymer P3HT and the acceptor material is the small molecule PCBM.
- Ultimately, the **cathode** finds more variability; in my work I considered a thin film of Ytterbium which provides an opportune work function to face to the active layer, and on top a thicker layer of aluminium which accomplishes to the current extraction.

The spray deposition of PEDOT:PSS and P3HT:PCBM layers was investigated. A brief discussion of the main features of such materials is needed.

2.1.1 Anode: PEDOT:PSS material

PEDOT is the outcome of the polymerization of bicylic 3,4-ethylenedioxythiophenes (EDOT). This material is one of the most common intrinsically conducting polymers in modern organic electronics applications. Thanks to its very stable oxidized state, and to its low HOMO LUMO bandgap, PEDOT shows good electrical conductivity. Therefore, it represents an interesting option when a low resistance electrode is needed. In order to stabilize the oxidized state of each monomer of the polymeric chain, a counterion has to be introduced. Such condition can be accomplished by coupling PEDOT with polystyrene sulfonic acid (PSS), as shown in Figure 2.1. PEDOT:PSS is usually found in dispersions where gel particles of the blend with size around 50 nanometers are dissolved in a water based solvent. Due to the insolubility of PEDOT in water and to the hydrophilic behaviour of PSS, the former is normally surrounded by the latter in the hydrated environment. After the deposition, such arrangement still affects the solid morphology. Considering the size of the particles swollen in solvent molecules, PEDOT:PSS gives rise to dispersions. Nevertheless, since in this work such detail was not relevant, I will often use the simpler and general term "solution".

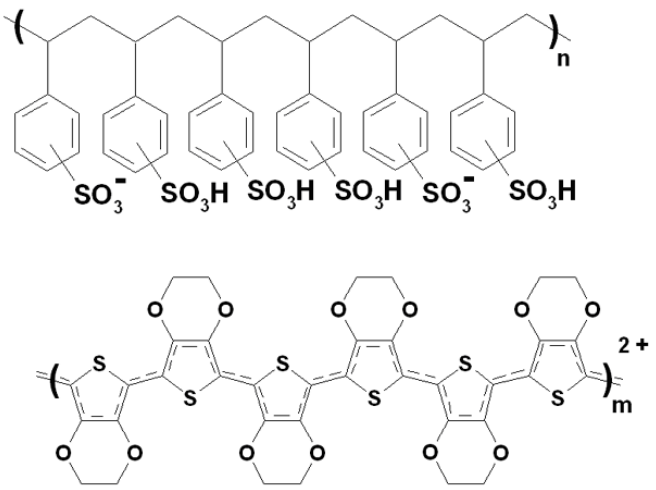

Figure 2.1: Chemical structure of PEDOT:PSS.

The electrical properties of PEDOT:PSS blend are found to be in tune with the figures of merit which define a good "p-type" electrode in organic semiconductor devices. Indeed, the blend of the two polymers shows a work function of around 5 eV, higher compared with the 4.2 eV of pure PEDOT, leading to improved performance in hole accepting-injecting contacts. The conduction in the material gets slightly worse due to the morphology of the blend. In fact, crystalline structure of pure PEDOT is not anymore achievable because of the heterogeneous composition of PEDOT:PSS. Moreover, the presence of PSS "shell" entails energy barrier limitations for charge carrier transport. Despite of these aspects, the conductivity of PEDOT:PSS layers is in most of cases sufficient, and it rarely represents a significant drawback when the material is chosen in device fabrication [11].

2.1.2 Active layer: PCBM and P3HT materials

(6,6)-phenyl C_{61}-butyric acid methyl ester (PCBM) is the most common acceptor material. Such small molecule is a C_{60} derivative where a side group is added in order to allow a broader range of solvents to properly dissolve it. C_{60}, also called bucky ball, is part of the fullerene family, discovered in 1985 by Curl, Kroto and Smalley (Nobel prize in Chemistry, 1996). It has a band-gap of 1.8 eV but, since the HOMO-LUMO transition is forbidden due to the symmetry of the molecule, its contribution to the absorption is negligible. The most attractive property of C_{60} is the fast electron transfer process which occurs from the excited state of a semiconducting polymer to such small molecule (order of femtoseconds time span).

PCBM shows very similar performance in term of charge acceptance and electron transport in photo-electrical devices. Very good electron mobilities in the order of 10^{-3} cm^2 V^{-1} s^{-1} are achievable within a bulk-heterojunction structure. Despite of its low absorption contribution, no other acceptor materials has been found to parallel PCBM in electron acceptance and transport properties. Its coupling with suitable donor materials results in very effective blends, so that its choice represents the state of the art in the most common BHJ structures.

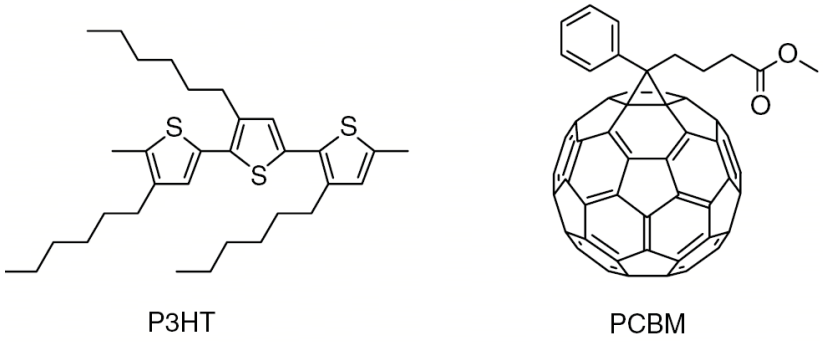

Figure 2.2: Chemical structure for Poly(3-hexylthiophene) (P3HT) and (6,6)-phenyl C_{61}-butyric acid methyl ester (PCBM). Such materials represent respectively the donor and the acceptor species adopted for the active layer fabrication in all the devices investigated in this work.

The choice of the donor material involves a much wider set of possible molecules. In particular, a lot of polymers are found to fulfil the requirements for an effective absorption as well as an acceptable hole mobility. The energy levels of the donor material have to match some constraints in order to give rise to effective photo-conversion. First of all, a significant shift (at least the exciton binding energy) in the LUMO levels of the donor and acceptor materials is needed, so that a proper driving force which causes the charge transfer can be established. Moreover, considering the relatively low width of the absorption windows of organic materials (about 400 nanometers), in the "design" of the optimal bandgap a trade-off have to be considered. Indeed, by lowering the E_{gap} of the polymer, a better matching of the maximum in absorption and the maximum of sun's photon flux is achievable, but, on the other hand, a significant reduction in the V_{oc} arises, so that the overall efficiency drops. A value of 1.5 eV defines the ideal polymer that has to be coupled with PCBM in order to optimize device performance.

Poly(3-hexylthiophene) (P3HT) was found to be the best candidate for our purposes. Other polymers which led to better performance have been recently investigated. Nevertheless, the wide study undertaken from the scientific community in the last years on the P3HT:PCBM blend was a very good starting point in

order to focus our attention on the deposition study. It was possible therefore to consider a reliable device reference for the final comparison with other processes.

P3HT is a polythiophene derivative which received considerable attention in polymer semiconductor research. Polythiophene is barely processable and it was only with the development of soluble forms like P3HT with alkyl side chains added that possibilities grew. Furthermore, in 1992 a way was found to attach the sidechains in fixed pattern, called regioregular alkyl-substituted polythiophene. Such structure was found to be very interesting for its enhanced absorption and hole transport properties. Indeed, nowadays best performance P3HT based solar cells usually involves highly regioregular polymers.

P3HT shows a energy gap between 1.8 and 2 eV according to the production process. Its lower limit in absorption (typically 660 nm) is close to the peak in the photon flux of AM 1.5 spectrum (around 700 nm), so that acceptable performance in term of photo-generation are expectable. Together with the quite good hole mobility (up to 10^{-5} cm^2 V^{-1} s^{-1} within bulk heterojunction structure, after annealing), this factor enabled the achievement of some very important results during last years' investigations.

The coupling of P3HT to PCBM provides a 1 eV shift in the LUMO levels, which represents a sufficient driving force for interfacial charge separation. The free energy of the charge-separated state, approximated by the difference in energy between the PCBM LUMO and P3HT HOMO levels, generates a reasonable output voltage of over 600 mV.

As already mentioned, bulk-heterojunction architectures involve a intimate mixture of donor and acceptor material which gives rise to complementary networks. A lot of fundamental features of the full device are found to depend on the geometry which defines the separation of the two materials, but also on the intermolecular interaction and disposition of the elementary compounds within the same phase. In fact, these aspects affect the optical absorption as well as the exciton separation and the carriers transport, namely all the processes which contribute to the power conversion. The morphology of the active layer refers therefore to a broad range of geometrical, chemical and physical properties. By tuning them, a substantial optimization of the final device performance is achievable. In Chapter 5, a deeper description of such properties will be shown, supported by experimental data.

2.2 Solar cells fabrication procedure

The formulation of the solution is the most fundamental factor how to control the outcome of organic film deposition as well as the first step of the procedure towards solar cells fabrication. After the preparation, solutions containing PEDOT:PSS and P3HT:PCBM underwent a continuous stirring (by mean of magnetic stirrers), in order to prevent the aggregation of the solute. Moreover, right before the deposition, a filtering was performed, so that eventual particles could be removed.

Figure 2.3: PEDOT:PSS (blue) and P3HT:PCBM (red) solutions.

Kintec 1.25 by 1.25 cm^2 area glass substrates with two 3 mm wide ITO contact stripes were adopted (Figure 2.4a). The procedure for the fabrication of standard structure solar cells involved the following steps:

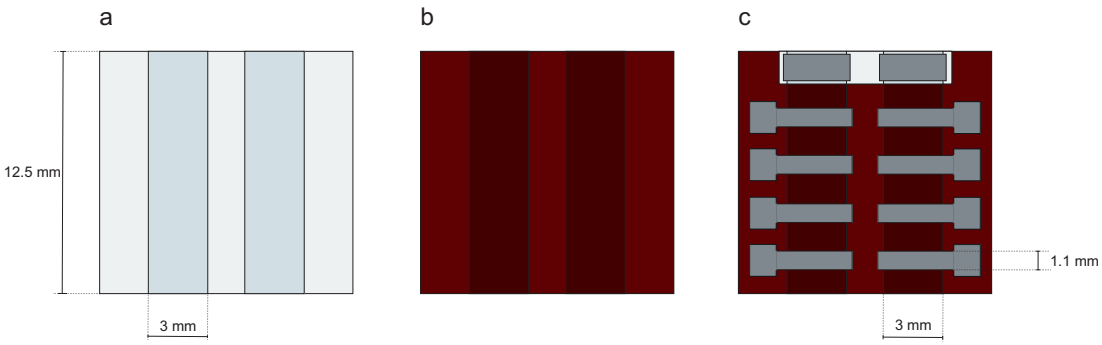

Figure 2.4: Procedure for the fabrication of organic solar cells with standard structure: (a) starting from cleaned glass substrates with ITO stripes, (b) the organic films are deposited via solution processing. (c) The evaporation of the metal cathode through a mask leads to the definition of eight independent devices with 0.33 cm^2 area.

- Glass substrates with ITO (Figure 2.4a) underwent several cleaning steps

as well as an UV ozone treatment. The details of such procedure are shown in appendix A.

- Organic films of PEDOT:PSS and P3HT:PCBM were deposited by solution processing (Figure 2.4b). This represented the main stage of the procedure for what concerns the performance of the final device as well as all the investigations pursued on spray coating process. To be noticed, the "standard procedure", which represented the reference in this work in terms of performance, involves the processing of both PEDOT:PSS and P3HT:PCBM layers by mean of spin coating process. As already discussed, this technique represents the state of the art for solution processing in organic electronics and leads to the best performance in organic solar cells research. The details of the standard procedure are shown in Appendix B. After this step, on a border region of the sample, a removal of the organic layers was performed in order to permit the access to the ITO electrodes.

- The two layers of Ytterbium and Aluminium were deposited by mean of an Angstrom evaporator system. The use of a mask during the evaporation led to the formation of a patterned deposition (Figure 2.4c). The materials ended up on the ITO stripes on one edge of the sample, implementing the anode connection. On top of the active layer, the mask defined eight separated regions. By doing so, eight independent devices could be obtained from each substrate (Figure 2.5).

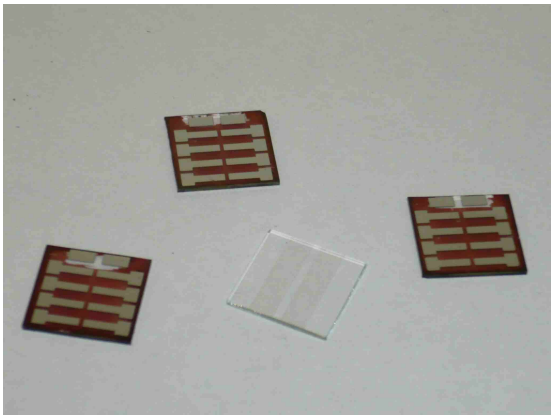

Figure 2.5: Glass substrate with ITO stripes and organic solar cells processed with standard structure ITO / PEDOT:PSS / P3HT:PCBM / Yb / Al.

The final step of the experimental work was the assessment of device's performance. Current voltage (I-V) characterization was performed in a glove box under a controlled nitrogen environment using a Keithley 2602A Source-Measure Unit and an Abet solar simulator with AM1.5 illumination (Figure 2.6). A reliable estimation of the efficiency in standard conditions could be drawn.

Figure 2.6: Solar simulator for organic solar cells testing. The illumination of the lamp refers to 1 sun AM 1.5 spectrum.

2.3 Organic layers assessment tools

A first deep study on solution processed layers was pursued before the implementation of solar cell devices. Such investigations involved depositions on 1.25 by 1.25 cm^2 area glass substrates. Glass is not the material which the organic layers we studied had to eventually be deposited on. Anyway, since no evident differences in the wetting behaviour arose, a preliminary optimization could be considered meaningful. Thanks to such substrates' flatness and transparency, the following measurements could be performed on the organic films:

- 1 cm^2 scan of layers surface in order to assess their macroscopic uniformity. Such measurement is implemented by a Dektak D150 (Veeco Instruments) tool and basically consists in the dragging of a tip along substrate length. By performing this linear scan 300 hundreds times on parallel and 33 micrometers close to each others lines, measurement data could be plotted on a two dimensional graph. The limit in resolution for the height goes down to the nanometer scale. On the planar dimensions, the size of the tip (approximately 12 micrometer radius spherical edge) permitted an accurate evaluation of the macroscopic regularity of the surface. Such assessment was found to be very useful especially in the first stage of my work, when the performance in coating of spray technique was investigated.

- Atomic Force Microscopy with acoustic tapping mode performed with Picoscan PicoSPM LE permitted to deeper evaluate surface features. In fact,

by limiting the scan to a 5 by 5 μm^2 area, important information could be drawn on the microscopic roughness as well as on the topography of the layers. The evaporation evolution of the solution and eventual annealing steps had evident effects on the morphology of the layer, turning in important change assessable by AFM measurement.

- Ultraviolet-visible (UVvis) absorbance spectra of the layers could be measured by mean of a Shimadzu UV-1601PC UV-Visible spectrophotometer. The absorbance of a medium at fixed wavelength is defined as:

$$Abs = -\log\left(\frac{I}{I_0}\right) \tag{2.3.1}$$

where I_0 is the probe light intensity (incident light) and I is the light intensity exiting from the sample (transmitted light). Since the intensity profile within the layer undergoes an exponential extinction, namely

$$I = I_0 \exp(-\Sigma L) \tag{2.3.2}$$

the absorbance is a useful mean how to draw information on the absorption coefficient (Σ) as well as on layer thickness (L). In fact, linear dependences relate it to both these parameters. UVvis measurement gave feedbacks on the optical properties of the layers in terms of magnitude and shape of the absorption window.

2.4 Spray coater: structure and settings

The experimental setup I had available for spray coating technique study consisted in an automated ExactaCoat system from Sono-Tek Corporation equipped with an AccuMist ultrasonic atomizing nozzle. Such tool was inserted in a glovebox and therefore in nitrogen atmosphere. Indeed, by limiting the exposure to oxygen and water vapour, improvements in reliability could be reached while dealing with air unstable materials. The instrument consisted in a nozzle, whose position could be controlled externally. A dedicated program was provided, so that the nozzle could be taught to travel in the three dimensions. In the planar dimensions, positioning over a 50 by 50 cm^2 plate was possible (Figure 2.7).

The solutions were inserted in Hamilton syringes, and could reach the nozzle through small pipes. The dispensing was implemented by mean of an electromechanical system which, according to the deposition rate set, acted on syringe's

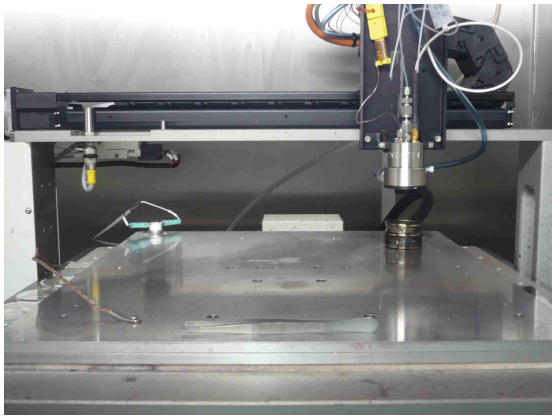

Figure 2.7: Spray coater complete structure. Nozzle's position could be controlled and defined all over the underlying hot plate.

piston.

Figure 2.8: Solution loaded in a syringe, ready to be sent to the nozzle through a small pipe by mean of an electromechanical dispenser.

2.4.1 The nozzle

The atomization and the ejection of the solution was accomplished by the nozzle. Such component was supplied with the solution as well as with a nitrogen flux.

When activated, a piezoelectric system made the head of the tool vibrating at ultrasounds frequency. Such vibration provided the atomization of the solution. According to the range of viscosity of the liquids adopted, a average droplet's radius of 10 micrometers was expected.

The head did not provide any control on the direction and the velocity of each elementary dose of liquid. A conic flux of nitrogen was therefore adopted, in order to force all the droplets to fall on the underlying surface within a circular section. The area of such section could be controlled by varying the height of the nozzle referred to the plate, the nitrogen pressure and the reciprocal position

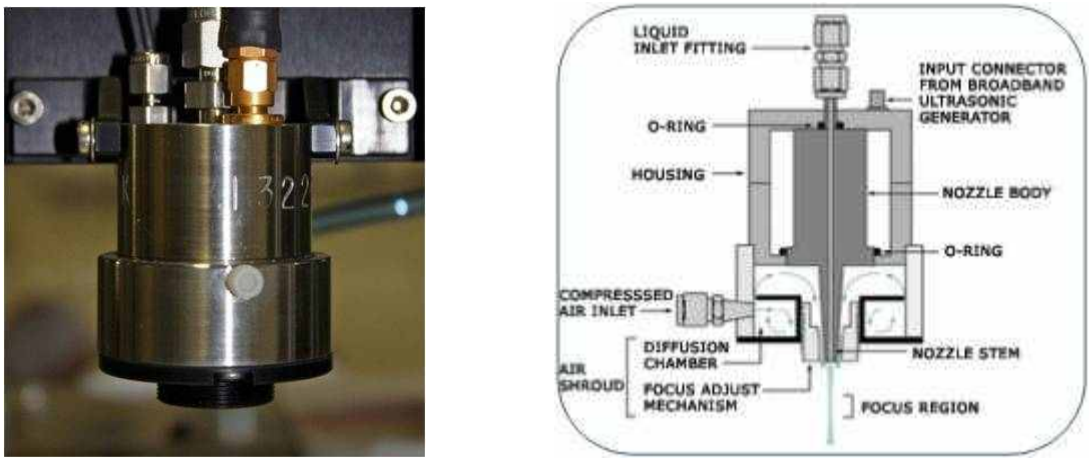

Figure 2.9: Nozzle picture and scheme of the cross section.

of the head with its confining cylinder. A 1.5 cm long diameter was achieved by properly setting the latter, while a constant height of the nozzle of about 10 centimeters was adopted for all the depositions made (Figure 2.10). The pressure of nitrogen flux was kept as low as possible in order not to perturb the solution after the deposition. A 40 mbar overpressure could guarantee a correct focus of the solution, without any significant affection on the dynamics of the deposited liquid.

The control interface permitted an independent activation of the dispenser, the atomizing head and the nitrogen flux. For the deposition techniques we adopted, the activation of such components was made at the same time with eventual small delays, in order to obtain a correct atomization of the solution from the beginning of the dispensing.

2.4.2 Deposition parameters

Considering the settings previously presented, the main parameters to steer for the deposition control were:

- The deposition rate, measured in millilitres per minute (ml/min), which permitted to define the extent of the ejected solution. In a first approximation order, for a generic deposition method, the amount of solution which ended up on the substrate had a linear dependence from such parameter.
- The definition of proper sequences of operations permitted to implement different kinds of deposition techniques. Considering a generic travel of the spray coater over a substrate, the speed was found to be another parameter which enabled the control on the amount of deposited solution.

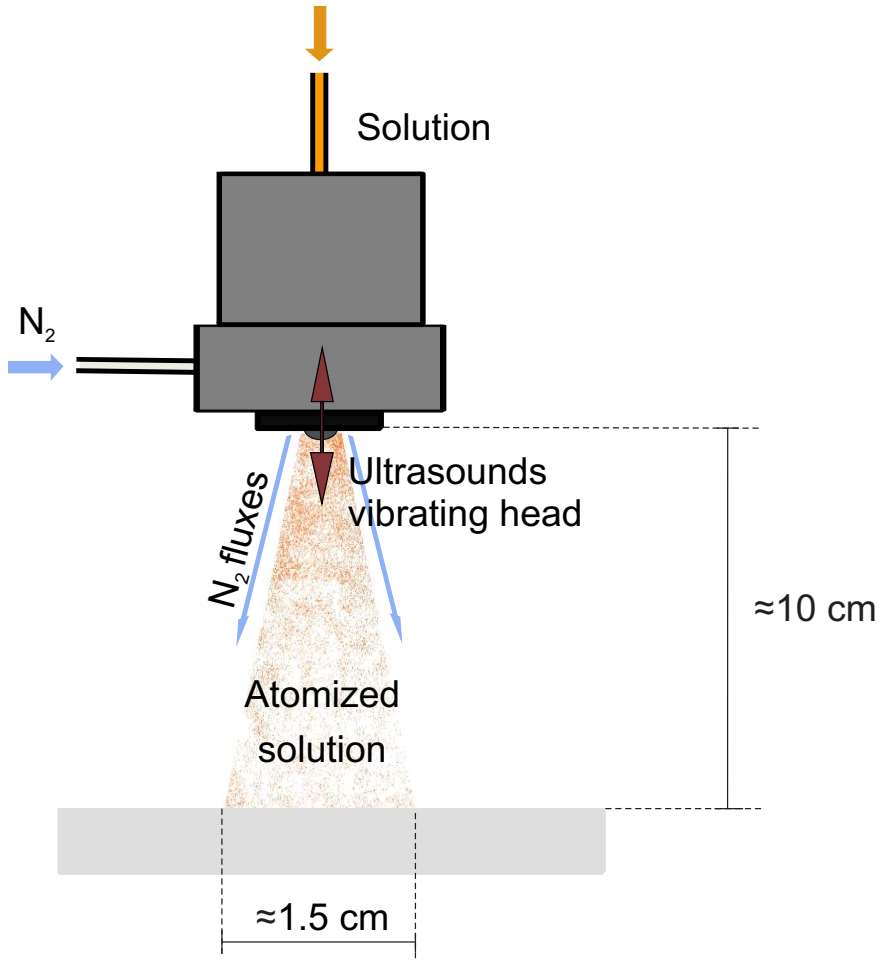

Figure 2.10: Scheme of the settings adopted for the spray coater.

- The temperature of the hot plate was found to be one of the most crucial points in the whole study. Indeed, important changes in the properties of deposited solutions and especially a sensitive control on their evaporation occurred by investigating such parameter.

Chapter 3

Solution properties

The attainment of solid thin films always involves a manipulation of the starting material. In fact, only once its elementary compounds are separated, they can be rearranged in a way that satisfies certain requirements. This means, in most of the cases, that an intermediate stage, where the specie assumes the gaseous phase, have to be considered. Indeed, such state of matter is, by definition, a state of independence among the elementary parts.

This is not the only way how to reach this condition. In fact, the insertion of the material in a host environment can produce very similar effects from the interaction point of view. In particular, the choice of a liquid as host matter, a solvent, can reproduces some features of the gaseous phase for the dissolved material (mobility and diffusion). Furthermore, the attainment and the employment of such heterogeneous mixture is much easier than considering the pure gaseous specie. Indeed, the confinement and the protection of the solute is accomplished by the solvent, so that atmospheric pressure can be adopted.

Organic materials are especially suitable for such manipulation. Their structure involves elementary molecules which interact among each others with mild electrostatic forces (Van der Waals), without any chemical bond involved. Namely, the separation of such molecules and their dissolution can be easily achieved by mean of a proper liquid.

This is the reason why, beside the traditional evaporation of molecules, solution processing is found to be an even more attractive technique how to deposit an organic material. The idea is therefore to aim to uniform layer deposition, by taking advantage of liquid properties. By forcing the solution to form a thin liquid film and to undergo a uniform evaporation all over its surface, the formation of a uniform thin layer of solute is enabled. This statement simply resume the

two main constraints which guarantee the effectiveness of a deposition process. Especially for spray coating, the fulfilment of such requirements is not obvious. Therefore, a deeper understanding of some liquid properties and of liquid evaporation is fundamental.

3.1 Surface tension

Despite of the weak interaction among the elementary compounds of a liquid, the potential energy of a molecule is found to be much lower in the bulk, where it is completely surrounded by like molecules, than on the surface, where a lack of interaction occurs. Therefore, the presence of molecules on the surface represents an excess of energy for the whole liquid, referring to the case of an infinite bulk system. This is the reason why a liquid does not naturally disintegrate, but rather tents to minimize the ratio between its surface and its volume. Such tendency is strongly related to the extent of the excess energy per unit area. For this reason it is called surface energy, it is an intrinsic property of the liquid and depends also on the specie which the liquid faces on its surface. Surface energy is defined as very generally concept, so that it can be used considering whichever interface between two species. For liquids, the name surface energy is commonly replaced by surface tension. The latter better enhances how the elasticity which affects the surface of a liquid is ascribable to this phenomenon.

3.1.1 Temperature influence

Surface tension has a common dependence from temperature among all liquids. An increase in temperature leads to a drop in surface tension. Empirical models show decreasing trends which reach 0 at the critical temperature. As instance, Guggenheim Katayama proposed the following dependence [12]:

$$\gamma(T) = \gamma_0 \left(1 - \frac{T}{T_c}\right)^n \tag{3.1.1}$$

where γ_0 is a constant specific for each liquid and T_c its critical temperature. For organic liquid, n assumes the value of 11/9.

3.1.2 Contact angle in Young equation

Liquids "have no shape". Actually, they always have one but, unlike to solids, such shape sensitively changes according to the field strength that acts on them. Considering an isolated liquid, surface tension is found to be the only field strength, so that a spherical shape is solution of the minimization of potential energy. The solution does not change even if a gaseous specie surrounds the liquid.

Let's consider now how such system will evolve if a planar solid material is introduced. The liquid will interact with the solid surface as long as its energy undergoes a decrease. If this happens the definition of a contact line occurs. The contact line is the collection of points which belong to all the three phases.

Concerning the interface with the gaseous specie, a spherical cap shape still represents the lower energy arrangement. Considering V the volume of the liquid, A_{lg} and A_{sl} the areas of respectively the liquid-gas and the solid-liquid interface, R the radius of the spherical cap, and r the radius of the solid-liquid interface circumference:

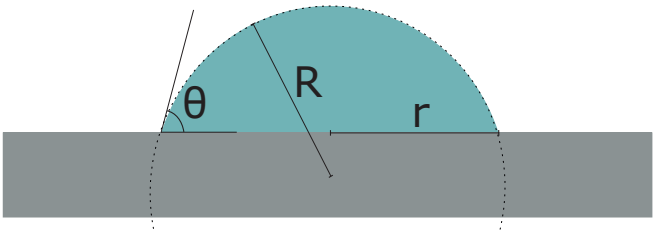

Figure 3.1: Interaction of a liquid with a solid surface. A spherical cap shape always minimizes (if no external forces act on the liquid) the potential energy of the system. By varying the solid, liquid and gaseous species, different contact angles theta are observed.

$$V = \frac{1}{3}\pi R^3(1-\cos\theta)^2(2+\cos\theta) \tag{3.1.2}$$

$$A_{lg} = 2\pi R^2(1-\cos\theta) \tag{3.1.3}$$

$$A_{sl} = \pi r^2 \tag{3.1.4}$$

Where θ is the contact angle of the liquid with the solid phase. This parameter is a fundamental index of the wetting properties of a liquid on a substrate.

If γ_{lg}, γ_{sg} and γ_{sl} represent the surface energies referred to the three interfaces, the free energy F for the system is

$$F = \gamma_{lg} A_{lg} + (\gamma_{sl} - \gamma_{lg}) A_{sl} \tag{3.1.5}$$

Since the system as presented, for a fixed volume V, shows only one degree of freedom, the equilibrium of the system can be calculated from the minimization of F considering only one of the free parameters θ, r, R. By expressing r and R in terms of θ and V, the calculation of $\frac{dF}{d\theta} = 0$ leads to the finding of minimums in the F function, thus to the thermodynamic equilibrium states for the system

$$\gamma_{lg} \cos\theta + \gamma_{sl} - \gamma_{lg} = 0 \tag{3.1.6}$$

3.1.6 is known as Young's equation and defines the contact angle expression, function of the surface energies of the interfaces. Such expression can be interpreted in terms of forces balance which define the position of the contact line [33].

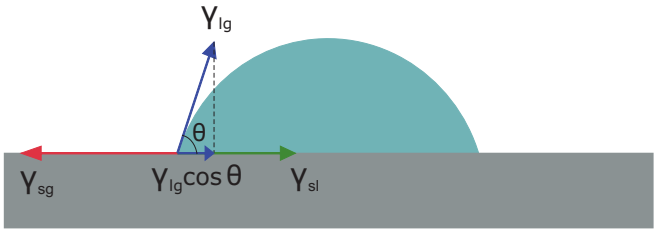

Figure 3.2: The contact angle theta represents the state of equilibrium drawn from the balance of three forces which act on the contact line. Such forces refer to the excess energies due to the presence of interfaces among the three species.

3.1.3 Capillary length

Considering now the effect of gravity on the liquid, it is expectable the situation to change. In particular, it has to be defined when gravity plays a dominant role in the force balance. The introduction of a dimensionless parameter accomplishes to this task. The Bond number is defined as

$$Bo = \frac{\rho L^2 a}{\gamma} \tag{3.1.7}$$

where L is the characteristic length, ρ the density and a the generic acceleration applied to the liquid. For $Bo \ll 1$, it is possible to neglect the effect of the

external acceleration. The liquid will assume a spherical-cap shape and all the consideration previously discussed keep being valid. For $Bo \gg 1$, the acceleration gives the main contribution to the determination of liquid distribution, so that, in case of gravity, a more flat arrangement is expected. Nevertheless, in proximity of the contact line, the force balance which controls the contact angle is not strongly affected from the presence of gravity. This means that young equation still estimates the way how the three phases join.

Arising from the definition of Bond number, the capillary length (λ_c) of a liquid is defined as the length scale which makes the Bond number going to 1:

$$\lambda_c = \sqrt{\frac{\rho\, g}{\gamma}} \tag{3.1.8}$$

The capillary length normally refers to gravity acceleration (g), and permits to infer whether it is important to consider external acceleration effect on liquid distribution. For my purposes, it was important to assess that the study on spray deposition could be meaningful also in view of a scaling of the problem. Indeed, all the solvents adopted in this work showed a capillary length shorter than the size of the substrate. By scaling the process significant change in the dynamics of evaporation and matter transfer can be expected. At least, for what concerns surface tension effects on liquid distribution, useful information could be already drawn from the analysis of ~ 1 cm small substrate.

3.1.4 Advancing and receding contact angles

From the theory shown previously, for fixed liquid, gaseous and solid species, one and only one contact angle is predicted. Real cases show how such statement has limitations. Indeed, by considering factors as roughness and heterogeneity of the solid surface, it is demonstrated that hysteresis behaviours underlie the arrangement of droplets on a surface.

In fact, a liquid drop can remain stuck on a tilted plane, despite gravity, if the contact angle is different at the front and at the rear of the drop (contact angle hysteresis). The rear angle being smaller than the front one, a capillary force exists, which opposes the gravity force.

3.1.5 Gradient in surface tension: Marangoni effect

Surface tension is an index of the force which strains the molecules of a liquid along its surface. For a homogeneous specie in thermodynamic equilibrium, such force contributes to the definition of the steady state distribution of the liquid. If the extent of the interaction among molecules changes, a resultant pulling force is observed in the region where the interaction is higher. This produces a macroscopic transfer of mass from regions with low surface tension to regions with high surface tension. As previously discussed, surface tension is function of temperature. Therefore, a non isothermal liquid will lead to gradient in surface tension, hence to Marangoni effect [34] [25]. The extent of such phenomenon is quantified by mean of the Marangoni number defined as follow:

$$Mg = -\frac{d\gamma}{dT}\frac{\Delta T\, L}{\eta\, \alpha} \tag{3.1.9}$$

where $\frac{d\gamma}{dT}\Delta T$ is an estimation of the difference in surface tension due to temperature variations, η is the dynamic viscosity of the liquid, L is the characteristic length of the system, and α its thermal diffusivity. The Marangoni number considers therefore a comparison between the mass transfer due to surface tension gradient (Marangoni effect) and the heat transfer capability of the medium represented by the diffusivity. According to which one is the dominant component, the equilibrium can be reached by mean of different effects.

Marangoni effects can occur also because of gradients in composition. In fact, considering the presence of surfactants in a liquid, variations in the concentration of such species along the surface of the liquid can lead to surface tension gradients and to important driving forces for the matter flux balance. The contribution of Marangoni effect underlies the formation of bubbles as well as the stability of foam [13].

Furthermore, surface tension differences can derive from heterogeneity within a multiple solvent mixture. Such phenomenon is very common because, even for perfectly miscible liquids, differences in volatility among the species and non uniform evaporation along the liquid surface lead to significant change in the volume fractions of the components.

3.2 Evaporation

3.2.1 Sessile drop

The understanding of the evaporation of liquids is a fundamental point, in order to properly interpret the outcome of material deposition from solution. Such phenomenon basically consists in the passage of molecules of a specie from a liquid state to a gaseous state. Evaporation occurs as long as an equilibrium between the two states of matters is not reached, even at temperature lower than the boiling point of the liquid. In the open space, this means that every liquid, at any temperature condition, eventually completely evaporates.

In order to consider the most useful information for our purposes, let's describe qualitatively only few physical aspects of evaporation. For doing this, some general conclusions can be drawn by referring to the case of a sessile drop. It is observed that two pure modes occur in the evaporation of a liquid drop on a surface: one at constant contact area and one at constant contact angle.

Based on Young equation, the ideal process would involve a fully constant contact angle evaporation, namely a gradual contraction of the drop without any change in θ value.

The second mode considers the presence of an energetic barrier which does not allow the contact line to move, so that the evaporation takes place as a lowering of the height of the drop but with a constant solid liquid interface area. Such phenomenon is known as contact line pinning.

Most of real cases involve the combination of the two processes. In the simplest situation, an evolution as depicted in Figure 3.3 is observed. The initial contact angle θ_0 necessarily belongs to the range of possible values within a particular hysteresis window, specific for the coupling of the three phases considered. The first stage of the evaporation involves a drop in volume at constant area. This means that the contact angle decreases and at a certain point reaches the value of the receding contact angle θ_r. At that point, a gradual contraction of the drop at constant contact angle occurs, till the liquid completely changes phase.

Similar basic phenomenology is observed also in the evaporation of larger liquid depositions. In Chapter 4, the consequences of such behaviour will be discussed concerning organic layers deposition.

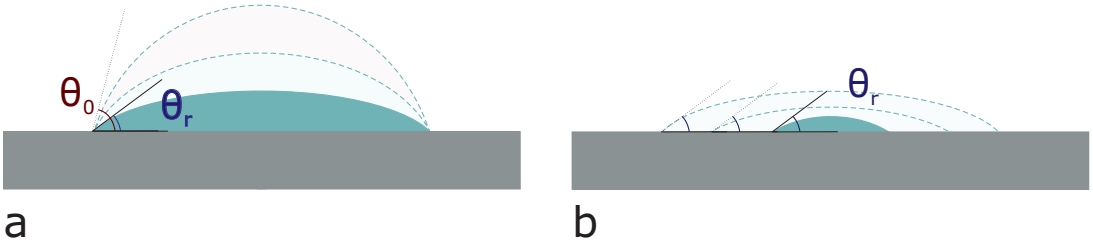

Figure 3.3: Example of evolution for a sessile droplet shape during its evaporation: (a) contact line pinning leads in the early stage to a constant area drop in volume; θ therefore decreases till the value of the receding contact angle. (b) A contraction of the liquid occurs with constant contact angle, till the evaporation of the droplet is complete.

3.2.2 Evaporation dynamics

Focusing now on the dynamics of the evaporation, a crucial point is found in the diffusion limited nature of the process. Indeed, the bottle neck is not passage of molecules from the liquid phase to the gaseous one, but rather the crossing of the vapour saturated environment. By modelling such crossing with diffusion laws we can draw the following:

$$\frac{dm}{dt} = -\,s\,D\,\rho_0 \tag{3.2.1}$$

where $\frac{dm}{dt}$ represents the rate of loss of weight of the drop, s is the shape factor of the gas film which surrounds the liquid, D is the diffusion coefficient for the specie considered and ρ_0 is the partial density of the vapour at the liquid-gas interface. Indeed, such equation reminds a Fick law, where $s\,\rho_0$ is related to the gradient of concentration within the vapour film.

Considering that the shape factor for a spherical shell is found to be

$$s = \frac{4\,\pi\,r\,l}{l - r} \tag{3.2.2}$$

where r is the radius of the circumference defined by the solid-liquid interface and l is an estimation of the average radius of the shell where the presence of vapour is not negligible. Moreover, from ordinary gas law, ρ_0 is found to be

$$\rho = \frac{p\,M}{R\,T} \tag{3.2.3}$$

with p the partial pressure of the gas at the interface, M the molecular weight, R the gas constant and T the absolute temperature. p is specific for each specie

and defines the tendency of the liquid phase to evaporate, namely its volatility. For this reason, it is called vapour pressure.

In conclusion, considering that l is normally much longer than r for small droplets, the evaporation rate can be written as

$$\frac{dm}{dt} = -\frac{4\,\pi\; D\,p\,M}{R\,T} \tag{3.2.4}$$

It is found surprisingly to depend linearly (not with square function) on the radius of the drop [26]. The influence of liquid properties are found to be decisive. In particular, since the vapour pressure depends on the energy of the molecules in the liquid available to "jump" into the gaseous phase, it introduces a further dominating dependence on temperature. In fact, from ClausiusClapeyron equation:

$$p \propto \exp\left(-\frac{\Delta H_{vap}}{R\,T}\right) \tag{3.2.5}$$

where $\Delta \mathrm{H}_{vap}$ is the molar enthalpy of vaporization, namely the energy involved in the liquid-gas phase transition of one mole of specie. Increasing temperature leads, therefore, to overall higher value of ρ_0 and to enhanced evaporation rate. At the boiling point of the liquid, p equals the atmospheric pressure, meaning that the equilibrium consists of a fully vapour phase. The transition occurs then not only at the interface but also in the bulk of the liquid.

Other implicit contributions comes from the value of the diffusion coefficient. In fact, it is found to depend on temperature through an Arrenhius law (similar to Equation 3.2.5 with specific attivation energy E_{att} instead of $\Delta \mathrm{H}_{vap}$) as well as to be inversely proportional to the vapour pressure.

3.2.3 Coffee ring effect

The previous calculation involved a averaged estimation in the evaporation rate. However, a fundamental information is hidden by considering a symmetrical behaviour all over the liquid-gas interface. In fact, diffusion limited processes are strongly affected by the geometry of the problem. A sessile drop can be consider a cylindrical symmetric system, nevertheless strong differences occur between the top and the borders of the liquid. In particular, a substantially higher amount of vapour is found in the regions where each point of the surface is surrounded by liquid. Conversely, in proximity of the contact line, a drop in the amount of

liquid which participate to the creation of the vapour film occurs. Together with an increase in the available free space (especially for contact angle values less than $\frac{\pi}{2}$), this results in an enhancement of the evaporation rate in such regions (Figure 3.4)

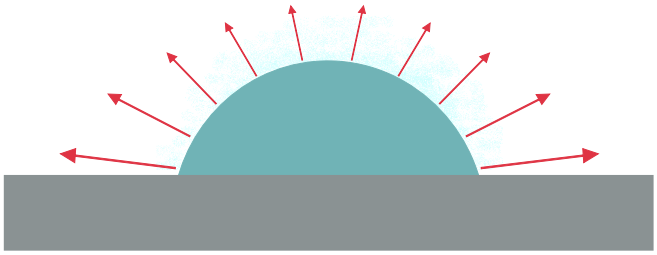

Figure 3.4: Evaporation rate over a drop surface. Since the process is diffusion limited in the gaseous environment, enhanced evaporation occurs close to the contact line, where the atmosphere is less saturated.

This conclusion leads to very important consequences. Indeed, by considering now the evaporation evolution with constant area previously discussed, fundamental mismatches occur between the amount of liquid which leaves the droplet and the local decrease in volume. Such balance finds opposite outcomes if calculated respectively on top and close to the contact line. Thus, the conservation of matter is valid by mean of resultant internal liquid fluxes which, as shown in Figure 3.5, supply the edges with molecules coming from the center of the drop.

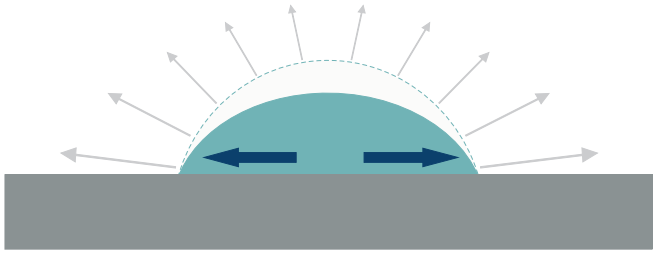

Figure 3.5: Pinning effect: the strong evaporation close to the contact line leads to a redistribution of the liquid within the drop, in order to keep a spherical cap shape. Resultant internal fluxes bring fluid at edges of the drop.

This is indeed a very important example showing how deep a complete study of the evaporation for even tiny drops should be. Nevertheless, so far in this section, no explicit interesting connection with the purposes of this work were discussed. By considering the same physical problem for a solution instead of a simple liquid, some fundamental information immediately arise. Indeed, the last effect involving internal fluxes, as well as any other phenomenon which underlies the fluid dynamics evolution within the liquid, is responsible of dragging both

solvent and solute molecules. The presence of these contributions explains the outcome of the deposition of a solid material from solution. The most famous effect, caused by the outward fluxes, is the so called coffee ring effect, shown in Figure 3.6. The pattern of a dried coffee drop on a flat surface involves evident accumulation of solute on the boundaries of the stain.

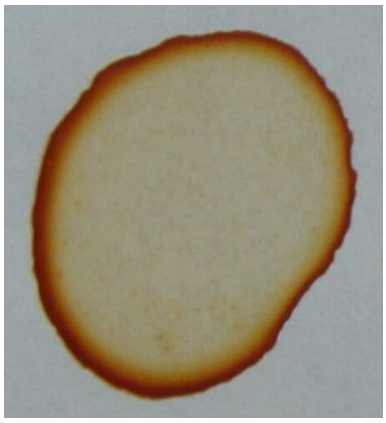

Figure 3.6: A dried drop of coffee shows significant accumulation of solute on the border of the stain. The phenomenon which underlies this outcome is found to be fundamental in solution processing deposition.

Such kind of pattern will be further discussed in the next chapter, where it will be found to affect the uniformity of layers deposited with spray coating technique. In fact, by extending the previous qualitative and mathematical treatments to the case of a liquid whose characteristic size is much higher than the capillary length, most of the conclusions will still be valid, including the coffee ring effect. A lot of investigations can be found in the literature on the modelling of the phenomenon [18] [17]. The accumulations of solute influences the evaporation evolution, changing the contact angle. In fact, an increase in the energetic barrier, which hinder the contact line to move, is involved. This results in an enhanced tendency to evaporate following a constant area regime. Such effect is usually called self-pinning of the contact line, and it can occur more than once during the liquid layer contraction.

3.3 Spray coating deposition

3.3.1 Sprayed solution on a substrate

As I mentioned in Chapter 2, spray deposition involves the atomization of the solution into $\sim$10 μm radius droplets. At the time of landing, such droplets assume a spherical cap shape. Their evaporation takes place in a very short scale

time, due to the limited size. The deposition of a very small amount of solution results in the situation shown in Figure 3.7.

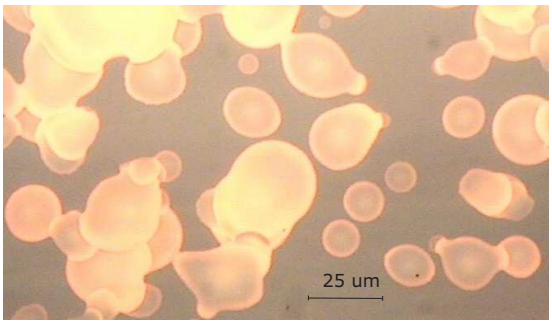

Figure 3.7: Atomized solution deposited on a substrate. The solute distribution gives information on the size of the original drops. Evident coffee ring effect affects the deposition within each circle.

From such image, information about the size of the droplets could be drawn. In particular radius values in the range of 10 to 50 μm are observed. Moreover, the presence of coffee ring effect is noticeable and it is found to affect the uniformity in the solute deposition within each drop. Interestingly, once a drop fell on a region where already some solute had been deposited, it did not dissolve the latter, but rather undertook a standard evaporation on such patterned substrate. This is ascribable to the very fast evaporation process which does not allow the solvent to interact with eventual underlying solute.

3.3.2 Spray deposition methods

According to the settings adopted in the spray deposition, two substantially different methods have been shown [20].

In particular I will refer to linear depositions, in which the nozzle covers a straight distance passing over the substrate, as shown in Figure 3.8. By doing so, the amount of solution deposited on the considered surface can be estimated with

$$V = \frac{R\,L}{v} \tag{3.3.1}$$

where R is the deposition rate, v the speed of the nozzle and L the length of the substrate along nozzle's path direction

Considering such elementary step, the two different deposition methods consist in:

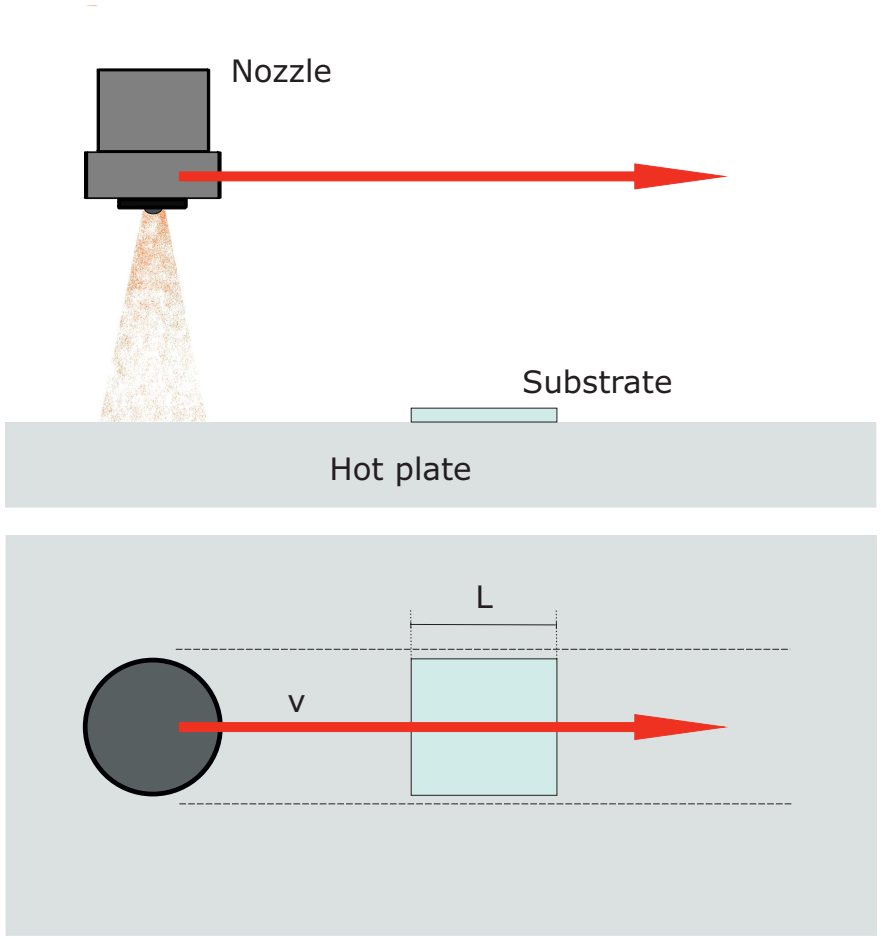

Figure 3.8: Deposition method: the nozzle travels over the substrate following a linear path. The amount of solution deposited depends on the speed of the nozzle and on the deposition rate (Equation 3.3.1).

- **Single Pass technique (SP)**: the nozzle makes only one travel over the substrate. The full coverage of the surface is guaranteed at high deposition rate by droplets merging.
- **Multiple Pass technique (MP)**: the nozzle makes more than one travel over the substrate. The layer is built by several sets of droplets which evaporate independently from each others.

The latter is found to be very suitable for the scaling of the process. Indeed, the investigation on the deposition concerns actually the deep understanding of one drop evolution. Relying on statistics, Multiple Pass method aims to uniform distribution of the solute over the surface. Considering a deposition performed with such technique, features as shown in Figure 3.9 can be observed.

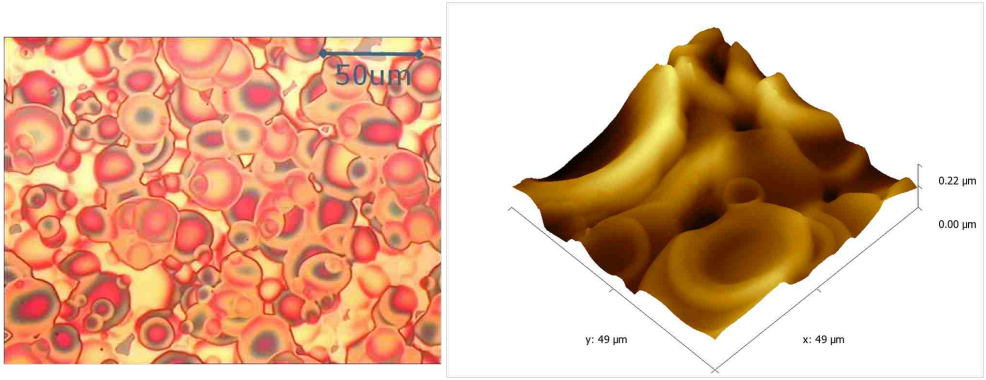

Figure 3.9: Assessement of an organic layer deposited via spray deposition with Multiple Pass technique. The picture on the left was taken by mean of microscope with a 100X magnifying. On the right the surface topography is shown (AFM scan) [14].

Indeed, in the picture taken with the microscope, the shape of single drops depositions are found to overlap one on top of each other. Furthermore, their random positions leads to an uniform distribution. But concerning the uniformity, a dramatic influence of coffee ring effect is observed for each drop solute deposition. From the AFM scan, over 200 nanometers peak to valley value arises, absolutely unacceptable for our purposes. Further investigation might have given improvements in terms of uniformity, but since the starting point was so far from reasonable levels of quality, we discarded this option.

The studies presented as state of the art in Chapter 1, pursued by other research groups, seemed to involve deposition techniques showing similarities to the Multiple Pass. As it can be observed in Figure 3.10, the independent and very fast drying of the droplets led to topography with low uniformity. Indeed, the roughness of such surfaces were found to be over 40 nanometers rms.

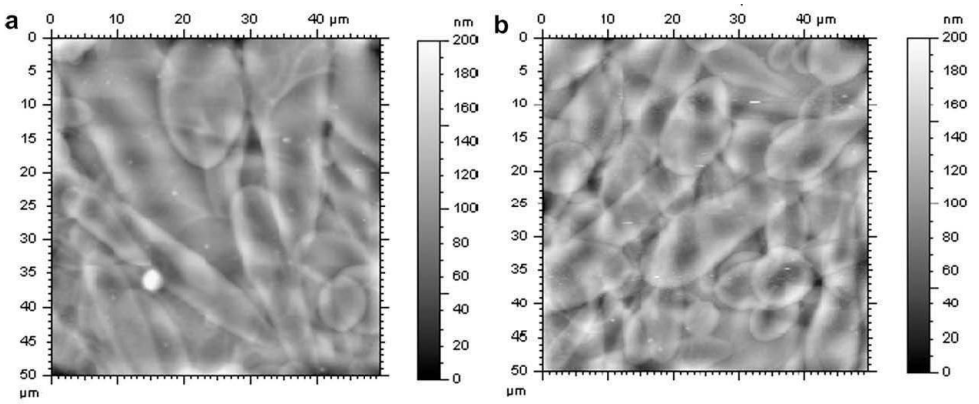

Figure 3.10: AFM measurement over a P3HT:PCBM layer deposited via spray deposition. The deposition of a monolayer (a) and of a bilayer (b) of droplets led respectively to 68 and 46 nanometers rms rough films [24].

The Single Pass method seemed to be a quite promising technique, since it does not involve independent droplets evaporation. In fact, the formation of a full single liquid layer is achievable. On the other hand, this means that the evolution of the process strongly depends on the geometry of the system, leading to a much less obvious scalability.

Nevertheless, by adopting the SP method, similar conditions as the one of other coating techniques can be reproduced. A fundamental difference distinguishes spray coating from for example spin coating or blade coating. In fact, the latter ones involve an external spreading force which permit to substantially thin the layer. This factor underlies the very good performance in uniformity achievable with such techniques. In SP spray coating, the absence of any external force acting on the deposited solution put even more in evidence how important is the understanding of the thermodynamics and fluid dynamics of an evaporating solution. Interestingly, it is worth to investigate such method, mainly because of this simplicity. The absence of external forces gives rise to the high potential of spray coating for large area high speed depositions.

Chapter 4

Spray coating deposition of organic materials

The deposition of organic layers, by mean of a spray process, represents first of all a matter of coating. Since such layers are eventually involved in electronic devices, their thickness settings are typically in the order of the hundreds or even the tens of nanometers. Spray coating does not involve any external force acting on the deposited solution in order to improve the uniformity of the final layer. Because of this, accuracy in the nanometer scale becomes a particularly challenging requirement. In a standard organic solar cell, two organic blends are found to implement the anode and the active layer of the device. In this chapter, my investigations on the spray deposition of such layers are presented.

4.1 PEDOT:PSS spray deposition

4.1.1 Introductive concepts

In the standard structure for solution processed organic solar cells, PEDOT:PSS blend is typically found to interface the active layer, fulfilling the harvest of photo-generated holes. The sheet resistance of the film is too high for an effective extraction of the charges to the external circuit. For this reason, a transparent conductive oxide, usually Indium Tin Oxide (ITO), is employed to accomplish this task. PEDOT:PSS remains a fundamental buffer layer which enables a correct working of the device.

The thickness setting of this layer has to be discussed. High enough value has to be chosen in order to assure a stable work function for the layer. Moreover, ITO

layer consists of big crystal grains structure arising root mean square (rms) values of roughness around 5 to 10 nanometers and especially spikes of several tens of nanometers which can cause shorts in thin film devices. Therefore, the insertion of PEDOT:PSS layer guarantees higher reliability, as long as the deposition of a uniform layer can be attained.

On the other hand, a decrease in cell's performance occurs when too high values for the thickness are chosen. Indeed, the presence of PEDOT:PSS layer leads to a reduction in the light intensity that reaches the active layer. Furthermore, it increases the distance that electrical carriers must cover in order to be harvested at the low-resistance electrodes. Therefore, it is important to keep its contribution to the series resistance negligible, compared with ITO and the metal contact.

In literature, thickness values around 30 nanometres are found to optimize standard structure solar cells. This represented the reference order of magnitude in the early stage of my work.

4.1.2 Provided material

The material is available in a commercial water-based dispersion (Baytron Clevios AI4083 purchased from H.C. Starck GmbH). The provider makes some chemical and physical properties of the solution available, but further information about the solvent are missing.

Nevertheless, from the data shown in Table 4.1 we could infer that a dominant amount of water underlies the composition of this product. Indeed, the values of vapour pressure, boiling point, density, surface tension match thoroughly water's features.

This solution is already suitable for the reference PEDOT:PSS spin coating deposition. By programming a time of spinning of 60 sec at the speed of 3000 rpm, a very smooth layer can be attained with average thickness of 36 nm.

4.1.3 Solvent analysis

The investigation of PEDOT:PSS spray deposition started from PEDOT:PSS Clevios water based solution. For brevity, I will name PEDOT:PSS-DIW, however referring to this product. According to spray coating requirement, an higher dilution level compared with spin coating was needed. Adopting (PEDOT:PSS-

Table 4.1: PEDOT:PSS Clevios water based solution.

Form	Liquid
Odour	Odourless
Colour	Darkblue
Surface resistance	max 1 MOhm
Conductivity	max 10 S/cm
Solid content	1.2 to 1.4 %
Na content	max 500 ppm
Sulfate content	max 80 ppm
Viscosity	60 to 100 mPas
ph value	1.5 to 2.5 at 20 C
Density	1 g/cm at 20 C
Mean particle size	d50 approximately 80 nm (swollen)
Refractive index	n 1.5228 at 589 nm (dried layer)
Surface tension	71 mN/m at 20 C
PEDT :PSS ratio	1 : 2.5 (by weight)
PEDT work function	approximately 5.2 eV
Boiling Point	approximately 100 C
Vapor pressure	23 mbar at 20 C

DIW) : additional solvent in a 1:10 ratio, I started the analysis of solvent influence. By adding only deionized water, good properties in regard to stability could be maintained. Unfortunately, due to the very high surface tension of such solution (71.9 mN/m), more than twofold higher than the values for other common solvents, the first trials resulted in very bad wetting properties (Young's formula for the contact angle Equation 3.1.6).

A different additional solvent had to be chosen in order to overcome this intrinsic limitation of water based solution. In particular, by focusing on a two solvents technique, it was possible to take advantage of a secondary solvent properties.

Our action consisted in adding isopropanol in order to improve the wetting properties of the solution. In fact, due to its very low surface tension (21 mN/m), improvements in the spreading of the solution over the substrate could be expected. On the other hand, isopropanol is not such a good solvent as water is for PEDOT:PSS blend, so that a degradation of the overall solution occurred.

Nevertheless, considering that the vapour pressure of the species is 6.04 and 2.3 kPa respectively for isopropanol and water at room temperature, we expected a significantly faster evaporation of the secondary solvent. If so, a dominant presence of water in the last moments before the evaporation ended could have been achieved.

The investigation of different ratio for the two solvents in the solution was

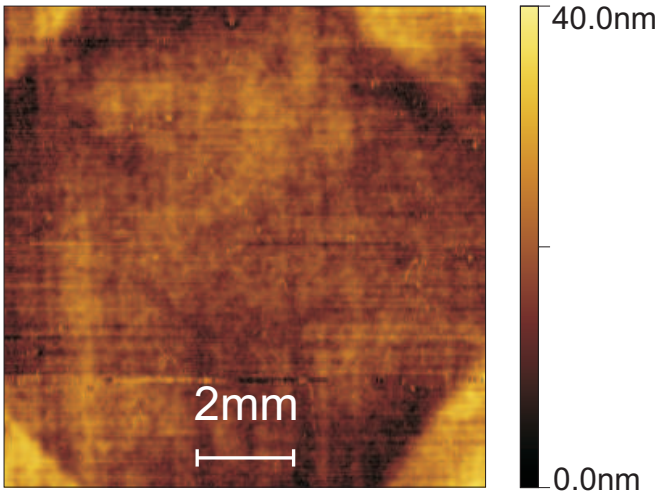

Figure 4.1: Dektak surface scan of PEDOT:PSS layer deposited with spin coating process. The film shows 3.5 nm rms and about 35 nm for the p-v values

pursued. We considered (PEDOT:PSS-DIW):DIW:IPA compositions, with a constant dilution level. Solutions with 1:5:5, 1:4:6, 1:3:7, 1:2:8, 1:1:9 proportions were tested.

- By depositing the 1:5:5 solution (6/5 ratio between water and isopropanol), accumulation of solute could be found on the sample, giving rise to over 1μm thick hills as shown in Figure 4.2. By observing the glass substrate, such accumulation appeared as bluish stripes noticeable even with naked-eye. Negligible amount of solute was deposited on the rest of the surface. In fact, the contraction of the liquid layer took place in the first time span after the deposition, when the solution showed a still very high dilution level.

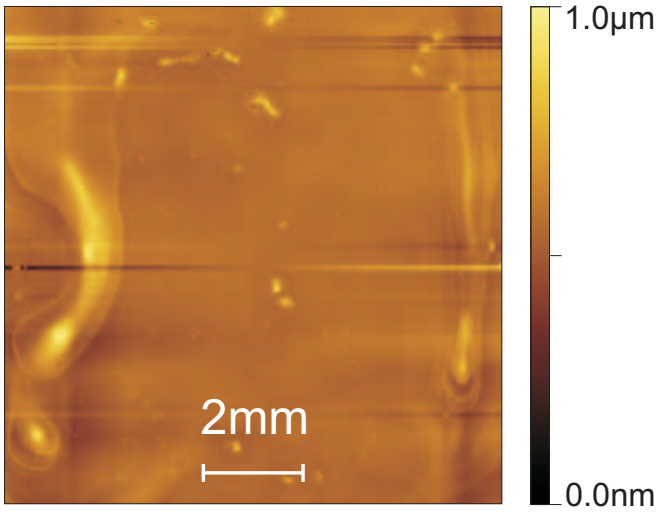

Figure 4.2: Dektak surface scans on PEDOT:PSS layer obtained from spray deposition. By adopting solutions with deionized water to isopropanol ratio of 6/5

Such phenomenon could be explained, by considering what Liu et al. claimed in [29] regarding water-ethanol sessile drops evaporation. Indeed, the first time span after the deposition involved a migration of isopropanol on the liquid-gas interface. Its lower surface tension in fact, permitted a lowering in the overall energy of the system. The following fast evaporation of such molecules left a thin film of water covering a certain amount of solution still roughly showing the original composition. Hence, an increase in the contact angle rapidly occurred. The slow diffusion of the remaining isopropanol towards the surface did not further affect the wetting behaviour, no advantage could be taken from its presence. The necessity to keep a more stable proportion between the two species on the liquid-gas interface during the evaporation arose. This suggested to move towards lower water to isopropanol ratio, in order to balance such proportion according to their different extents of transition to the gaseous phase.

- Conversely, by adopting the 1:1:9 solution a very anomalous behaviour was observed in the outcome of the deposition. The depositions on glass showed big clusters of solute and a low coverage of the surface. In Figure 4.3, such behaviour is shown. Since a big amount of pure solvent lay over the solution during its preparation, in the preliminary stage of this study we ascribed this result to the bad quality of the dispersion. Nevertheless, the presence of coffee ring effect around each cluster let me think that their formation was due to a contraction of the solvent rather than to the presence of particles in the solution.

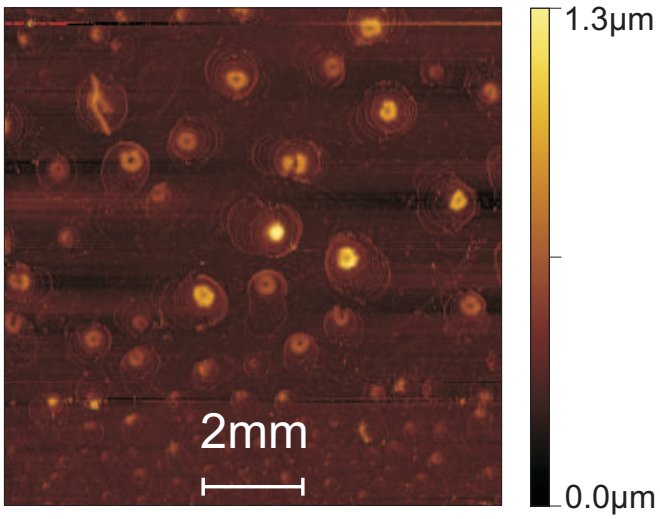

Figure 4.3: Dektak surface scans on PEDOT:PSS layer obtained from spray deposition. By adopting solutions with deionized water to isopropanol ratio of 2/9

Considering water-isopropanol mixture more into details, the vapour-liquid

equilibrium is found to show an azeotropic point, as shown in Figure 4.4. This means that, despite of its higher vapour pressure, the fraction of isopropanol in the vapour phase can be higher but also lower than in the liquid phase, according to its initial proportion and to such point. The azeotrope is in fact a particular ratio between the two components, which leads to a perfectly balanced passage of the two species in the vapour. In such conditions, the same composition is kept in the liquid phase and it is transferred to the gaseous phase.

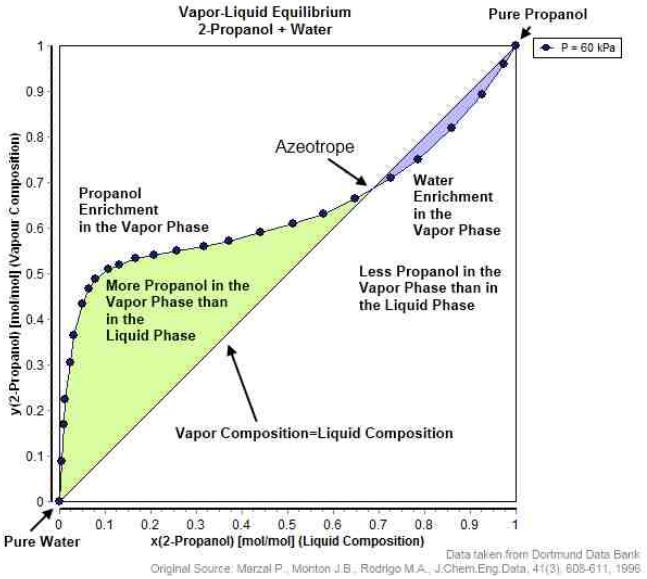

Figure 4.4: Trend for the vapour-liquid equilibrium of a water-isopropanol mixture in isobaric conditions. Such composition show an azeotropic point when a 67.7% molar fraction of isopropanol in the liquid is adopted.

For a water-isopropanol mixture, the azeotropic condition is reached when a 68.5% molar fraction of isopropanol is adopted, namely 90.2% volume fraction. The 1:1:9 composition previously discussed, which involved a 81.8% of isopropanol was apparently already too close to such condition. Indeed, the considered azeotrope is an unstable point. Slightly different shifts of compositions from such value can lead to evaporation processes evolving towards completely opposite direction. In a first case ("left" shift referring to Figure 4.4), a fast drop in the isopropanol would be observed in the liquid layer leaving a water-dominant composition; for a "right" shift, the system would evolve conversely. The presence of domains in the deposited solution, where the local composition was beyond the azeotropic point, would lead to a fast increase in the isopropanol proportion in those region. Such explanation can underlie the dramatic agglomeration of PEDOT:PSS.

A 1:2:8 composition, namely a 27% water 73% isopropanol, represented a good

estimation of the limit proportion, which could take advantage of isopropanol presence, without affecting the reproducibility of the deposition.

A similar approach was pursued by Chung et al. in the deposition of PEDOT:PSS by mean of gravure printing technique [16]. For such process, a substantially higher water to isopropanol ratio was found to be sufficient in order to achieve acceptable uniformity performance.

Solutions with 1:2:8, 2:1:8 and 3:0:8 compositions were tested in order to assess the influence of solute concentration variations. Notably, water and isopropanol remained for all such solutions in a 3:8 ratio, so that their wetting properties could be maintained in a first order approximation similar. In fact, by changing the amount of solute, variations in the properties of the overall solution could be expected. Particular attention had to be paid on surface tension and viscosity. Indeed, such parameters play important roles in the whole deposition process.

By mean of pendant drop method it was possible to assess the surface tension of the liquids we dealt with. The order of magnitude of surface tension for the mixture of the two solvents and the variations due to the presence of PEDOT:PSS were assessed. In Table 4.2we show the results for water, isopropanol, water:isopropanol 3:8 mixture and for the solution compositions considered in this work.

Table 4.2: Surface tension values from pendant drop method for solvent mixtures and PEDOT:PSS solutions.

Solution tested	γ [mN/m]	γ at 25°C (literature) [mN/m]
Pure DIW	65.0	71.9
Pure IPA	20.0	21.2
DIW:IPA 3:8	25.2	22.5
PEDOT solution 1:2:8	25.0	-
PEDOT solution 2:1:8	24.9	-
PEDOT solution 3:0:8	25.0	-

The values for water and isopropanol show strong inaccuracy, so that also the other measurements are probably not reliable. Nevertheless the outcomes from different measurements for the same liquid had low mean deviation so that these coarse evaluations of surface tension remain valuable for comparison. It is clear how the addition of isopropanol leads to a drop in surface tension that in turn gives rise to substantial improvement in wetting properties. By considering composition with PEDOT:PSS and changing its concentration in the solution no significant variations were observed.

Subsequently, we performed for the same mixtures some viscosity measure-

ments by mean of a micro-Ostwald viscometer (Schott Instruments GmbH) with an inner capillary diameter of 0.6 mm.

Table 4.3: Viscosity measurements on solvent mixtures and PEDOT:PSS solutions.

Solution tested	ρ [kg/m^3]	μ [cP]	μ literature [cP]
Pure DIW	1.0	0.961	0.894
Pure IPA	0.77	2.17	1.96
DIW:IPA 3:8	0.85	3.23	-
PEDOT solution 1:2:8	0.85	4.41	-
PEDOT solution 2:1:8	0.86	5.74	-
PEDOT solution 3:0:8	0.84	7.02	-

The data in Table 4.3show a very particular behaviour for the water-isopropanol solution, namely the viscosity of the mixture of the two solvents is higher than the viscosity of the liquids considered separately. Moreover it is evident how the addition the PEDOT:PSS dispersion leads to more viscous compositions. Such increase is directly proportional to the concentration of the blend. Viscosity plays an important role in the fluid dynamics during the evaporation evolution. Indeed it represents the main source of quenching for the fluxes in the liquid layer. We expected therefore a lowering coffee ring effect for higher concentration of PEDOT:PSS, but on the other hand also a worse uniformity due to the slowed settlement process (Marangoni number is inversely proportional to the viscosity).

4.1.4 Substrate temperature influence

The role of the hot plate temperature during the spray deposition was investigated. Indeed, high values of such parameter lead to a drop in surface tension for the deposited solution. On the other hand, it also controls the evaporation evolution of the solvents, affecting the time of drying. In Figure 4.5, very clear information on the effect of temperature values spanning from 75°C (close to the boiling point of isopropanol) to 30°C are noticeable. By adopting 75°C, it was evident how the evaporation of the solvent took place in a very short time (the drying took about 2 seconds), so that complete merging of the droplets was not possible. Indeed, the surface scan a) points out similarities with the spray droplets distribution at the time of landing expectable for a single pass deposition. A "freezing" of such situation is therefore achievable by choosing high temperature. This led inevitably to lacking coverage on the edges of the sample. Thus, while aiming to uniformity, the settlement of the liquid layer is found to be an essential factor.

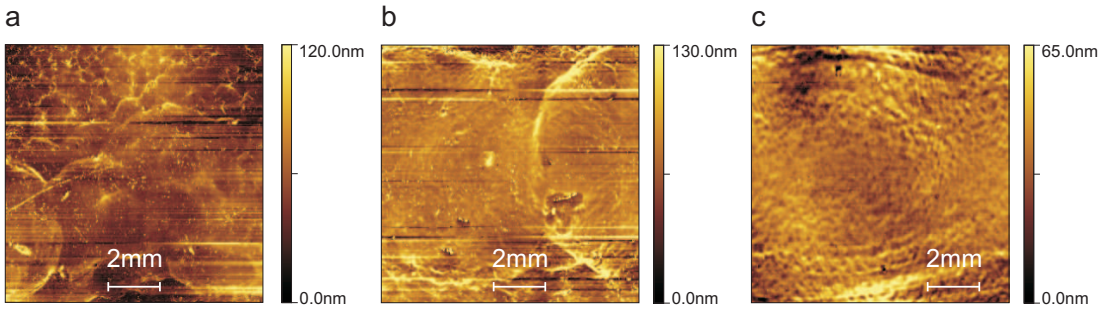

Figure 4.5: Dektak surface scan on PEDOT:PSS layer: influence of (a) 75, (b) 55, and (c) 30 °C temperature applied to the hot plate during the spray deposition

Another interesting detail is that every defined spot showed strong coffee ring effect. Hence, the adoption of temperature values close to the boiling point of the solvent was not a good choice for uniformity and not for quenching the internal fluxes either.

Considering lower temperature, uniformity improvements are observed. he effect of 55°C temperature is shown in figure b). It is evident that, when the contraction of the liquid film started, its settlement was not complete yet. Indeed, some details of such scan reminds wave-like features which characterize a perturbed liquid surface. Moreover, the merging took place but only in the central band where an high amount of solution was deposited. Nevertheless, the overall uniformity of the layer showed a significant improvement compared with the previous temperature setting.

Ultimately, PEDOT:PSS deposition at nearly room temperature were tested. In particular, 30°C was the lowest value which could be controlled with reproducibility. In such conditions, the evaporation was slow enough (time of drying around 40 seconds) so that a complete wetting of the whole surface was achieved. Furthermore, the longer time available for the settlement transient of the liquid layer resulted in solid films with surprising uniformity. As shown in Figure c), peak to valley values below 100 nanometers were finally achievable.

We could conclude that the contribution of isopropanol provides significant improvement to the wetting properties of the solution. Adopting higher temperature in order to achieve further decrease in surface tension is not necessary, but rather this choice reduces dramatically the time of drying and leads to incomplete settlement of the liquid layer. This is found to strongly affect the final uniformity of the solid film so that lower temperature and consequent higher evaporation time are required.

Nearly room temperature were therefore adopted. In particular, only 30 and

40°C temperature values were assessed in the following investigations. Depositions of PEDOT:PSS were performed and filmed in order to evaluate the evaporation evolution of the solvent. Subsequently, we made an estimation for the time of drying for each film by timing the time span between the crossing of the nozzle on the substrate and the completion of the liquid layer contraction.

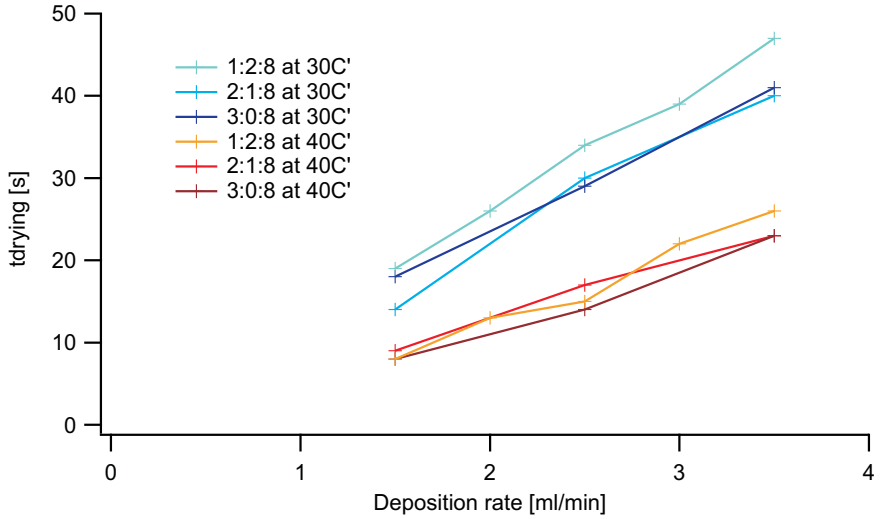

Figure 4.6: Time of drying for PEDOT:PSS solutions estimated from the films of the depositions

In Figure 4.6 such data are plotted, depending on the deposition rate for all three the solution compositions and temperature values tested. The time of drying followed a linear trend by varying the deposition rate, namely the volume of liquid involved in the evaporation. Moreover, it is clear how the slope of such curves is related to the temperature of the substrate and show how warmer environments leads to higher rate of evaporation.

4.1.5 Thickness control

In a first order approximation, the thickness of a deposited layer is proportional to the amount of material that "falls" on the substrate and that eventually forms the solid film. This is in turn proportional to both the amount of solution deposited and to the solute concentration. Such statements are true as long as the average value of the thickness is considered.

We adopted 100 millimeters per second as value for the speed of the nozzle so that the amount of solution deposited on the substrate could be easily controlled by tuning the deposition rate. In order to make the solution covering the surface with a full merged collection of droplets, a 1.5 ml/min minimum value for the deposition rate was needed. Higher values could guarantee the coverage of the

whole surface also along the borders of the sample. By changing the deposition rate from 1.5 ml/min to 3.5 ml/min, the thickness of the layer showed small changes.

Conversely, a linear dependence of the thickness from the solute concentration was found for the different compositions at the same deposition rate.

In Figure 4.7 these trends are shown. The markers show the average thickness values, measured for samples where the amount of PEDOT:PSS was controlled with either the deposition rate or the solute concentration.

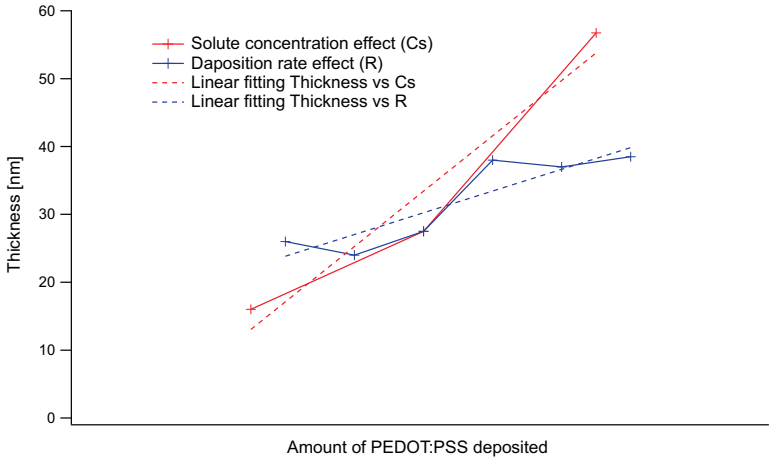

Figure 4.7: Trends of PEDOT:PSS layer thickness in the active area of the substrate. The x-axis refers to the amount of material which is varied by changing either (red line) the solute concentration in the sprayed solution or (blue line) the deposition rate.

The blue curve refers to layers obtained by adopting the solution composition 2:1:8 and varying the deposition rate from 1.5 to 4 ml/min. The red curve shows the dependence of the thickness from the solute concentration; the 1:2:8, 2:1:8 and 3:0:8 compositions and a constant 2.5 ml/min deposition rate were chosen. The dashed lines represent fittings of such data. The ratio between the slopes of the two lines is 2.55. Indeed, the thickness of the layer is much more sensitive to variations in the solute concentration than in the deposition rate. Moreover the thickness axis intercept coefficients for the two lines are respectively -7.4 and 14.23 nanometers. Since when either the solute concentration or the deposition rate is set to zero the thickness has to be necessarily zero as well, we observe that solute concentration variations lead to more linear trend. In fact, by depositing the same amount of solution, we expected that the wetting behaviour does not change significantly if different solute concentrations are adopted. Evaporation evolutions resulting in solid layers whose thickness values are proportional to the amount of solute deposited is a reasonable outcome. Conversely, by changing the deposition rate we change the initial amount of liquid on the substrate as

well as its initial distribution. This represents a much stronger variation in the boundary conditions. Indeed, we expect the evolution after the deposition and the time of drying to change so that a linear dependence on the thickness is no longer straightforward. By increasing the deposition rate, the fraction of the substrate surface whose coverage is guaranteed increases. This entails the solute to be arranged on larger area and can explain a quenching in the thickness sensitivity at low deposition rate. But this behaviour does not explain such quenching at higher deposition rate values which permit a full coverage of the substrate. Another important point is that the tendency of the solute to move towards the borders. This phenomenon affect the amount of material which contributes to the layer formation in the central part of the surface. From the study of the evaporation we observed that the higher is the amount of liquid on the substrate, the higher is the time of drying. So that a possible explanation for the thickness-deposition rate trend can be that the internal fluxes responsible of the coffee ring effect lead to enhanced migration of the solute towards the border according to the time span during which they effectively act. Hence, by changing the amount of solution deposited on the substrate the variation of the central thickness is not linearly sensitive.

From UV-vis measurements we could assess the absorbance contribution of PEDOT:PSS layers as well as their thickness estimation. In fact, in a first order approximation, the absorbance of a layer is proportional to the thickness of the layer itself.

The measurements were performed in the range of wavelength between 300 and 900 nanometers. As we already argued PEDOT:PSS layer needs to show absorbtion the lowest possible. The order of magnitude of the absorbance referred to few tens of nanometers of such film is around 10^{-2}. Since at low wavelength glass and the organic layer showed comparable absorbance, the profiles are traced between 450 and 900 nanometers.

In Figure 4.8, the absorbance profiles depending on the solute concentration, the deposition rate and the temperature are shown.

These measurements confirmed the difference in sensitivity that the solute concentration and the deposition rate showed in regard to the thickness of the layer. By changing the amount of PEDOT:PSS in the solution, a linear influence is observed on the thickness. Conversely, a less important effect is obtained when the amount of solution deposited is changed. Considering the values of absorbance at 700 nanometers (close to sun photon flux peak) for each measurements it is possible to evaluate such trends. For the depositions performed at 30

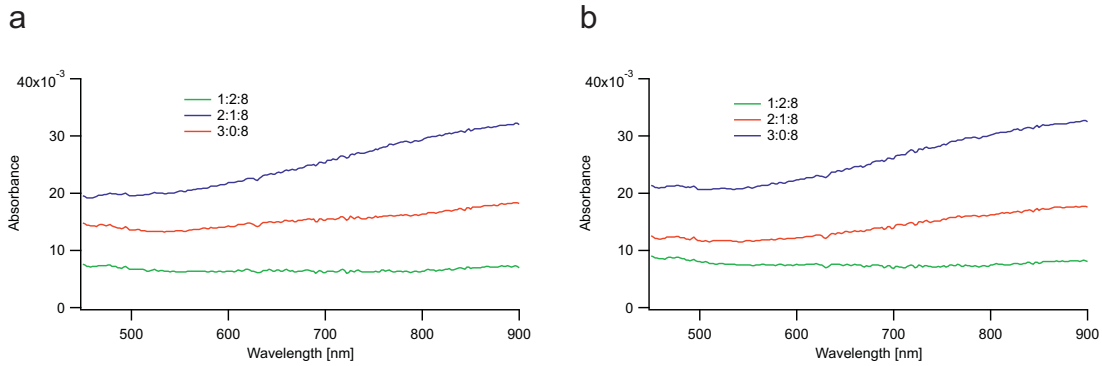

Figure 4.8: UV-vis absorbance measurements for PEDOT:PSS layers deposited from solutions with different solute concentrations at the same deposition rate. The temperature of deposition was (a) 30 and (b) 40 degrees.

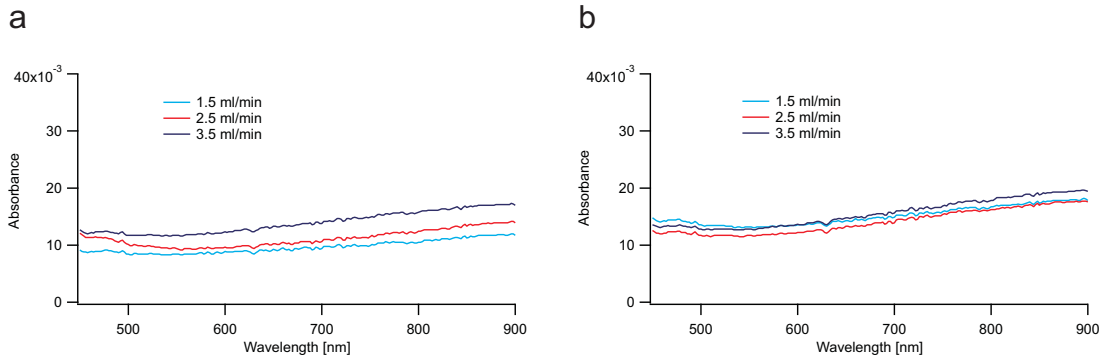

Figure 4.9: UV-vis absorbance measurements for PEDOT:PSS layers deposited from the same solution composition with different settings for the deposition rate. The temperature of the hot plate during the process was (a) 30 and (b) 40 degrees.

degrees the data fitted thorougly in a linear approximation. The ratio between the approximated slopes was found to be around 3.41, even higher than the value obtained from Dektak thickness measurements (2.55). The increase in temperature from 30 to 40 degrees led to a slight increase in the thickness of the film, but the extent of such tendency is negligible compared with the other parameters' influences.

4.1.6 Macroscopic uniformity assessment

Starting from the one square centimeter scans of surface profiles, we assessed the macroscopic uniformity of the layers. The measurements showed a overall good uniformity in the central band. The important issue we could notice in this stage was the coffee ring effect. In fact, solution fluxes towards the contact line due to enhanced evaporation rate in proximity of the edges, lead to accumulation of solute along the perimeter of the sample, but also in intermediate positions. Especially the latter represents a significant concern for uniformity degradation

in the active area of the device.

In Figure 4.10 we show the scan for three deposition at 30°C where only the solute concentration was changed. A clear rise in roughness is observed by passing from the 1:2:8 to the 2:1:8 and the 3:0:8 compositions.

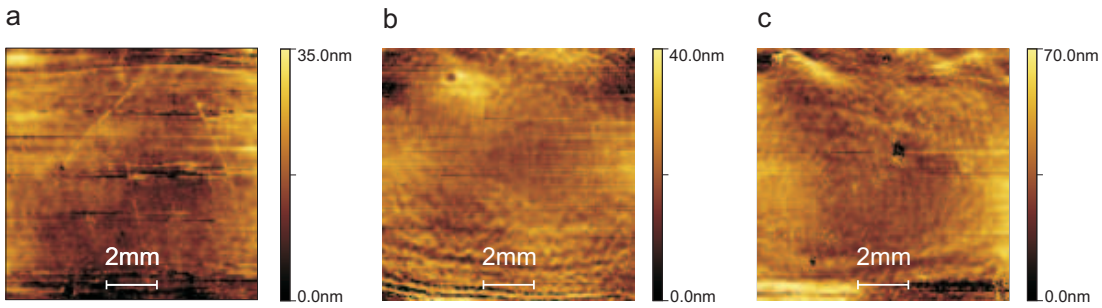

Figure 4.10: Dektak surface scan of PEDOT:PSS layers deposited at 30 °C. The compositions adopted for the solution (PEDOT:PSS-DIW):DIW:IPA were (a) 1:2:8, (b) 2:1:8 and (c) 3:0:8. The influence of the solute concentration consists in a clear increase for both the rms and the p-v values.

Deposition with 1:2:8 solution led too very low thickness around 15 nanometers. A correct evaluation of the scan was hard to draw. The average value of the profile referred to the lower value was in fact around 15 nanometers. This means that probably part of the surface was not covered, namely the deposition could not be considered reliable. Conversely, interesting features in the depositions with higher solute concentration could be observed. Both these scans show acceptable uniformity in the center of the samples, but also some over 100 nanometers "hills" were observed.

Less significant variations were observed when deposition rate was changed as shown in Figure 4.11. Layer thicknesses and rms values for the roughness showed only small increase by raising the amount of deposited liquid.

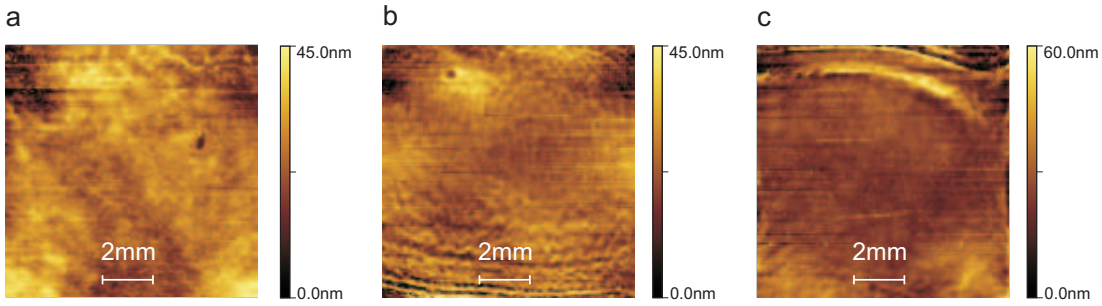

Figure 4.11: Dektak surface scan of PEDOT:PSS layers deposited at 30 °C with the solution (PEDOT:PSS-DIW):DIW:IPA 2:1:8. The influence of (a) 1.5, (b) 2.5 and (c) 3.5 ml/min deposition rate values were tested. A slight increase is found for the rms and the p-v values by increasing the amount of solution deposited.

Ultimately, by raising temperature to 40 degrees, the time of drying was nearly halved. This impacted on the evaporation evolution which got further from a quasistatic process so that less uniformity was observed.

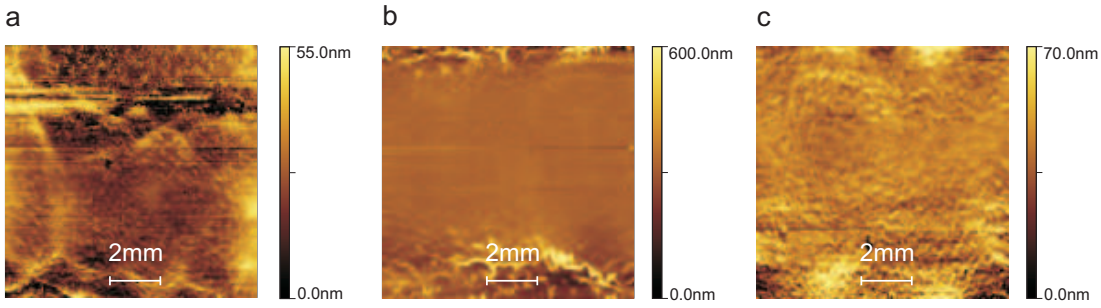

Figure 4.12: Dektak surface scan of PEDOT:PSS layers deposited at 40 °C. An overall increase in the roughness of the layers is noticeable compared with depositions at 30°C. At 1.5 ml/min deposition rate (a) no full coverage could be achieved. Anyway, by using higher values the deposition was not reproducible. In both (b) and (c), a 3.5 ml/min deposition rate and 3:0:8 solution were adopted. Nevertheless, the liquid showed substantially different wetting.

In Figure 4.12 (a), the adoption of a 1.5 ml/min turned in a significant lack of coverage on the surface. The strongest coffee ring effect was then revealed, close to the center of the sample. (b and (c) refer to the same deposition settings, and show how different outcomes can arise from variations in the first wetting of the substrate. The reliability of the deposition seemed overall to degrade even if only a 10°C increase in the temperature was considered.

In table 4.4 the rms values of roughness for PEDOT:PSS layers for all the settings that we tested are shown. From such data, it was possible to find a confirmation for what we argued about so far. Especially the solute concentration and the temperature of the hot plate during the depositions were found to be very influential parameters for the quality of the film.

Table 4.4: Root mean square values of roughness [nm] for PEDOT:PSS deposition.

	1.5ml/min		2.5ml/min		3.5ml/min	
	30°C	40°C	30°C	40°C	30°C	40°C
1:2:8	3.6	5.2	3.9	9.6	5.6	4.4
2:1:8	6.7	10.6	6.6	13.5	7.4	10.9
3:0:8	8.8	44.0	11.0	13.3	9.2	10.0

Considering that the thickness of the layer is a linear function of the solute concentration, an increasing roughness was observed for thicker layers. The temperature determined, together with the deposition rate, the time of drying of the

deposition, which in turn influenced the eventual uniformity. As we already discussed, a slow evaporation of the liquid layer led to better settlement and higher homogeneity in the thickness.

4.1.7 Morphology analysis

In the early stage of this study our attention was focused on the coating effectiveness of the spray process. Anyway, further investigations had to assure that by worsening the solution quality, no critical morphology changing affected the electrical properties of the layer. In fact, isopropanol is found not to be a good solvent for PEDOT:PSS. Therefore, we wanted to assess whether anomalous aggregations of the particles took place in the micrometer scale during the evaporation of the DIW:IPA mixture. By performing atomic force microscopy measurements, quite smooth and detailed surface profiles were observed.

Very small variations could be noticed by changing the deposition parameters in the ranges previously discussed. The roughness of the film showed rms values in the range between 1 and 4 nanometers, while the peak to valley values were found not to exceed 50 nanometers.

Similarly to the dektak scans, the parameters which affected the roughness seemed to be the thickness of the layer itself and the time of drying. Especially the rms values seemed to increase when the PEDOT:PSS concentration was increased.

In Figure 4.13, couples of depositions whose settings differ from each others only for the solution composition are shown. Some differences could be noticed on the characteristic length which the variations in the profile referred to. In particular it seemed that high concentrated solution and fast dried films led to rougher and bigger domains structures. The topography of the films seemed anyway to keep similar features by spanning the deposition parameters in the ranges that we assessed.

4.2 P3HT:PCBM spray deposition

4.2.1 Introductive concepts

As mentioned in Chapter 2, our choice was to adopt P3HT:PCBM bulk heterojunction as active layer of the reference solar cell structure. The materials adopted in the early stage of this work were PCBM purchased from Solenne and

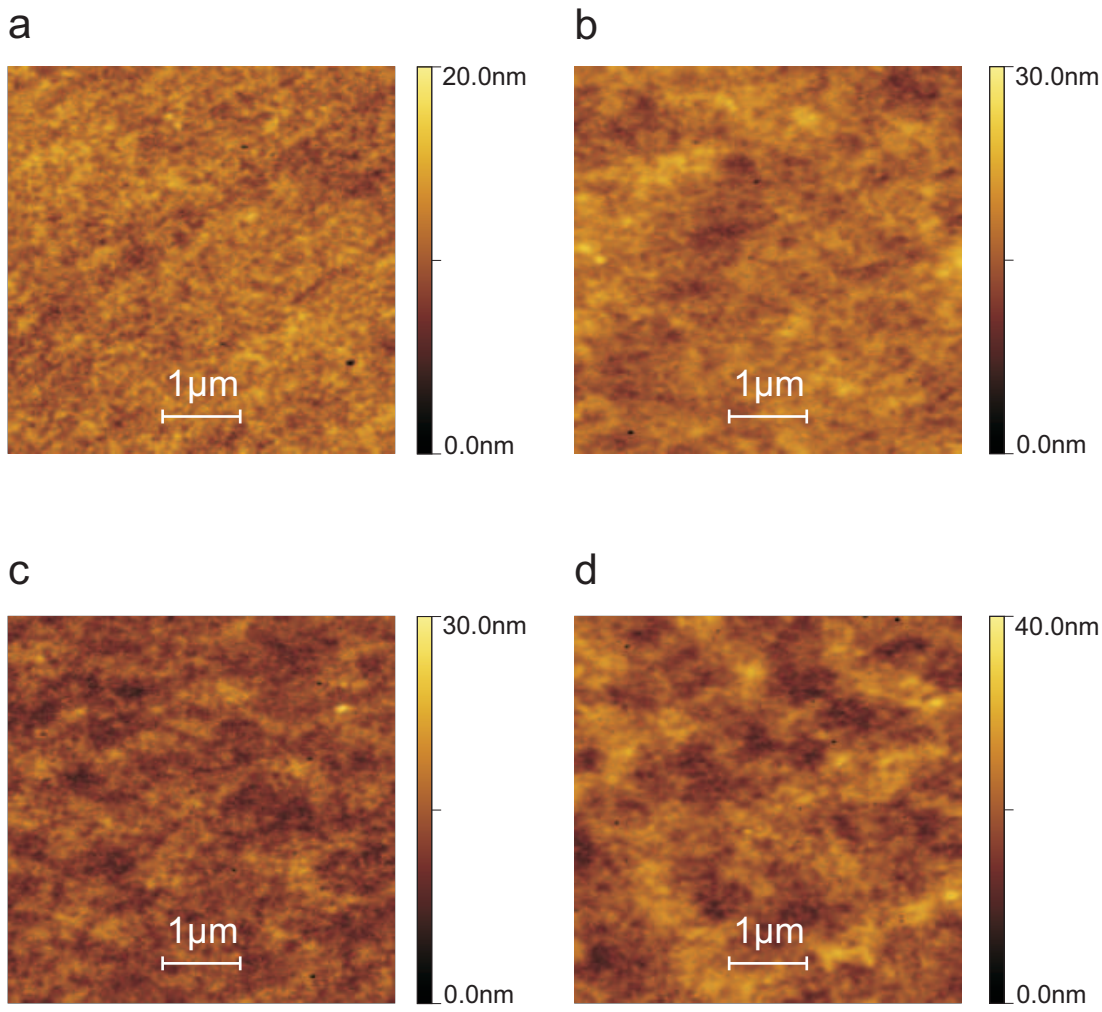

Figure 4.13: Morphology analysis on PEDOT:PSS layers with Atomic Force Microscopy. Layers processed at 30 degrees adopting (a) 1:2:8 and (b) 2:1:8 solutions are shown, as well as depositions at 40 degrees using (c) 1:2:8 and (d) 2:1:8 compositions. By increasing the solute concentration, the rms values of the scans increases from (a) 1.77 to (b) 2.44 nanometers and from (c) 2.09 to (d) 3.77 nanometers.

P3HT Sepiolid P100 purchased from Rieke Metals Inc.

In literature, a thickness setting between 200 and 250 nanometers is found to optimize the performance of spin coated devices adopting P3HT:PCBM as active layer. Such order of magnitude was considered as reference in the early stage of my study, although a deep investigation on such parameter was needed. In fact, by considering P3HT:PCBM bulk heterojunction more into details (Chapter 2), the role of its morphology is found to be decisive. Morphology, in turn strongly depends on the processes involved during the fabrication of the layer, so that extremely different trends might be expected by dealing with spray coating.

A correct analysis of the physical properties of the layer and their optimization are possible only once the layer itself shows acceptable uniformity. Therefore,

analogously to PEDOT:PSS deposition study, our main concern was to achieve a reproducible method to deposit P3HT:PCBM and to control its thickness by mean of spray coating technique. In this section, I will show all the investigations which concerned the coating problem. A deeper study of the physical properties of the layer is presented in Chapter 5, where an evaluation of such features is performed together with devices testing.

4.2.2 Solvent analysis

Both the materials P3HT and PCBM can be dissolved in several liquids, especially chlorinated are found to be very good solvents for such molecules.

A dramatic improvement has been shown in the literature when a high boiling point solvent is chosen for the spin coating process of the active layer. Indeed, the emloyment of ortho-dichlorobenzene (oDCB)(boiling point 180°C) instead of chlorobenzene (CB)(boiling point 131°C) led to better performance for P3HT:PCBM based solar cells [32]. A significantly different morphology of the final layer is observed by changing the solvent specie and especially the time available for the solute to build a ordered structure is found to be a fundamental parameter for the eventual quality of the network. Thus, such result can be ascribed to the slow drying process involved by using high boiling point solvents.

Therefore, we chose to start our investigations adopting dichlorobenzene as solvent for the P3HT:PCBM blend. This solvent shows a relatively low value for the surface tension, so that acceptable wetting performances were expected. Starting from a solution composition P3HT:PCBM:oDCB 10%wt, we analyzed spray depositions on glass at different temperature values adopting the single pass technique. Temperature higher than 90°C led to uniformity issues due to a too fast evaporation evolution. Lower temperature seemed anyway not to solve such problem, resulting in a highly inhomogeneous solid layers as shown in Figure 4.14.

Such phenomenon is related to the evaporation evolution of the liquid layer. The pyramid-like shape of the film could be explained considering the gradual contraction of the liquid during the evaporation and the fact that the precipitation of the solute strongly depends on the level of dilution. Moreover, a sequence of self-pinning phenomena during the contraction of the liquid led to the collection of concentric accumulations of solute. A marvellous depiction which epitomizes the coffee ring effect is the outcome of such deposition.

Since no acceptable uniformity could be achieved with a single solvent solution, we decided to apply the two solvents technique also in this case. A solvent

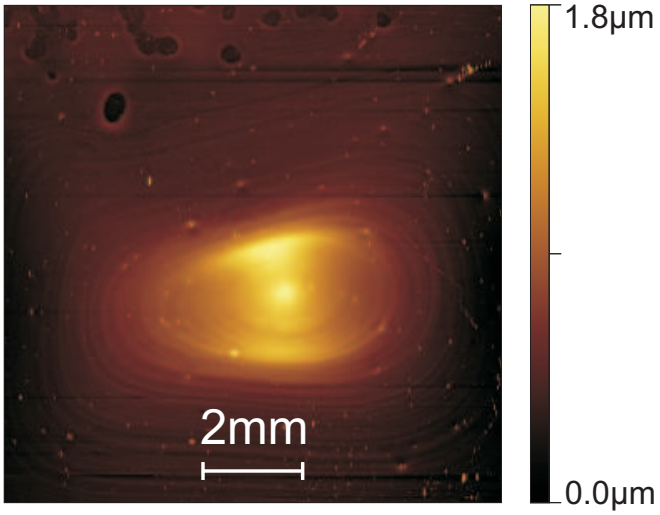

Figure 4.14: Dektak surface scan on P3HT:PCBM layer deposited from a solution of ortho-dichlorobenzene.

with lower surface tension and lower boiling point compared with dichlorobenzene had to be chosen.

Mesitylene is a solvent for the P3HT:PCBM blend, not as good as chlorinated, but its surface tension and boiling point seemed to be in tune with the requirements for a good "second solvent". By adding Mesitylene, an improvement in the wetting properties could be expected, but also a significant change in the chemical environment which swelled the organic molecules had to be considered. Therefore, the proportion between the two solvent is affected from a trade-off.

In [23] a oDCB:Mesitylene mixture was found to optimize the performances of ink-jet printing deposition of P3HT:PCBM. A proportion of 68:32 for such composition was claimed to optimize the trade-off previously mentioned, improving the spreading properties of the solution as well as conserving the stability of the solution.

Starting our investigation with a 7:3 oDCB:Mesitylene ratio the outcome of the deposition showed a dramatic improvement in the quality of the layer. Indeed a uniform surface was observed in an extent that can be appreciated in Figure 4.15.

Analogously to the case of PEDOT:PSS, the temperature of the hot plate was found to play a fundamental role in the determination of the quality of the layer. Acceptable uniformity of the layer could be achieved only in the range of values between 45 and 65°C. Higher temperature led to uniformity issues due to the too fast evaporation affecting the settlement of the liquid film. Temperature values lower than 45°C showed anomalous behaviour in the first time span after

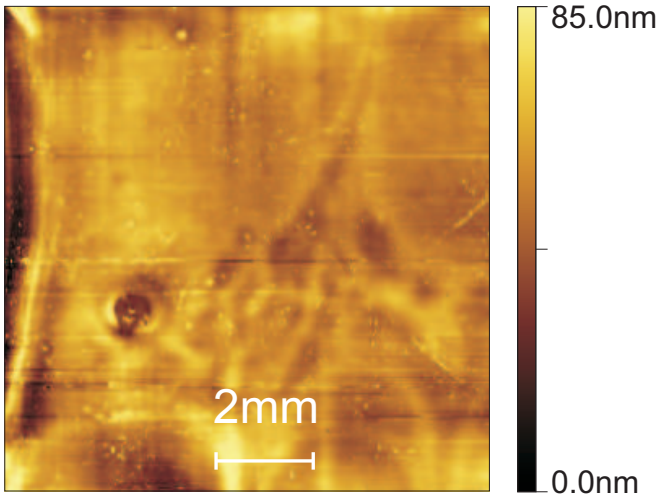

Figure 4.15: Dektak surface scan on P3HT:PCBM layer deposited from a solution of ortho-dichlorobenzene and mesitylene in a 7:3 ratio.

the deposition. An initial contraction of the deposited solution apparently compromised the uniformity in the central region of the sample as well as the full coverage of the substrate.

From the first deposition attempts we could observe how the amount of solution needed for a proper coverage of the sample was in the same order of magnitude than the one adopted for the PEDOT:PSS study. Thus we considered deposition settings which led to similar volume of liquid deposited on the surface. In such conditions, thickness values around 240 nanometers, found to be optimal for spin coated cells, could be obtained by using a 8 mg/ml solute concentration for both P3HT and PCBM.

The adoption of the two solvents technique represented also for the spray deposition of the active layer an important turning point. Furthermore, even higher levels of uniformity could be achieved by controlling the time of drying of the solvent. Such technique consists basically in forcing a slowdown of the evaporation evolution, by placing the substrate in a vapour saturated environment. This choice leads to substantially better morphology of the film and, therefore, it will be treated with more details in chapter5. Regarding the uniformity of the layer, a significant improvement in the macroscopic flatness was observed by using the slow drying technique.

In Figure 4.16 a decisive picture of the scan of a slow dried P3HT:PCBM layer is shown. Indeed, an outstanding quality with less than 10 nanometers rms rough and 240 nanometers thick film could be achieved by mean of spray deposition.

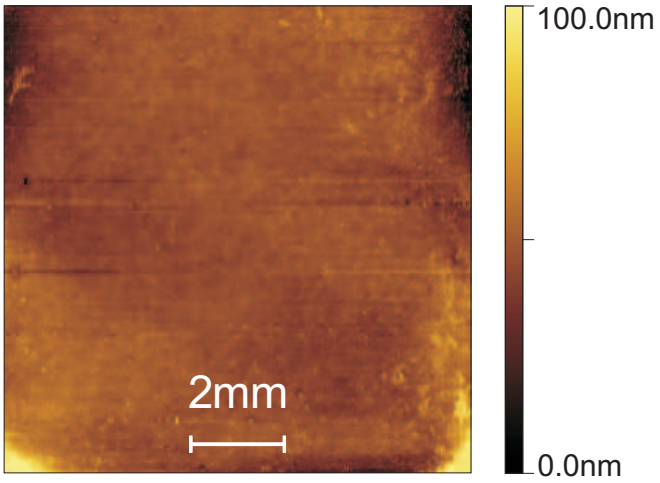

Figure 4.16: Dektak surface scan on P3HT:PCBM layer deposited from a solution of ortho-dichlorobenzene and mesitylene in a 7:3 ratio by using the slow drying technique. By covering the sample with a petri dish right after the deposition, a vapour saturated environment was created. The quasi-static evaporation led to remarkable uniformity.

4.2.3 Thickness control

Ultimately, the influence of the deposition rate, namely the amount of solution deposited on the surface, was investigated. Surprisingly, a quite linear dependence of the thickness from the deposition rate was found, differently from what observed in the PEDOT:PSS layer study. The extent of this trend was assessed with both thickness measurements, which gave local information, and UVvis measurements (shown in Figure 4.17), referred to an integral evaluation of the thickness.

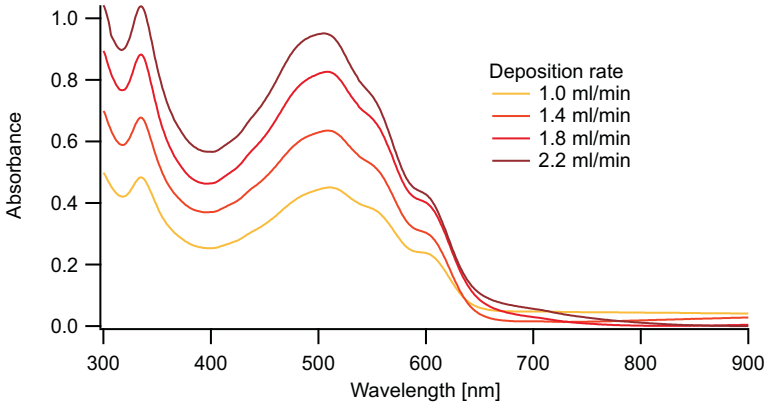

Figure 4.17: UVvis spectra for P3HT:PCBM depositions performed with a 8+8 mg/ml concentrated solution at different deposition rates. The estimation for the thickness of the layers followed a linear trend.

The span of the deposition rate in the range 1 to over 2.2 ml/min led to a variation in the thickness of the layer in the window between roughly 120 and 280 nanometers. Moreover, by considering lower solute concentrations, layers

with acceptable uniformity and thickness below 100 nanometers could be attained (see Table 4.5).

Table 4.5: Average thickness of P3HT:PCBM layers depending on the solute concentration and the deposition rate.

Solute concentration	4 mg/ml			8 mg/ml			
Deposition rate [ml/min]	1.2	2	2.8	1.0	1.4	1.8	2.2
Thickness [nm]	63	136	166	130	175	232	281

4.3 Marangoni effect in two solvents depositions

In this section, a deeper evaluation of the results achieved will be shown. Indeed the first concern of this work was the analysis of coating properties for sprayed solutions. The uniformity of the organic layer formed after the solvent evaporation was therefore the main figure of merit.

In this context, the adoption of mixtures consisting of two suitable solvents was found to be decisive for both the cases of the materials that we analysed. Indeed, outstanding improvements in the spreading of the solution as well as in the flatness of the final films compared with the outcomes of single solvent depositions were observed. We already mentioned that such mixtures had to be carefully chosen. In particular:

- the two solvents had to be miscible, so that an homogeneous solution could be obtained.

- A proper primary solvent had to be chosen. In our case, we referred to solvents already adopted for the spin coating deposition of the specific organic materials. In general, the primary solvent has to well dissolve the solute as well as guarantee a good morphology in the eventual film.

- The secondary solvent was supposed to decrease the contact angle of the overall solution on the considered substrate, namely leading to better wetting. Hence, its surface tension had to be lower than the primary solvent's one. Moreover, since we wanted the primary solvent to determine the final morphology of the layer, it needed the secondary solvent to evaporate faster right after the wetting enhancement was accomplished. This turned in a constraint on the vapour pressures of the solvents.

Although the drop in surface tension is definitely an important source of improvement in the wetting behaviour of the solutions, we assumed that the significant results arising from the introduction of the secondary solvent were not completely ascribable to such factor.

Especially, the failure of depositions where a relatively low surface tension solvent was adopted suggested that another phenomenon underlay the fluid dynamics of the problem. In particular, we ascribed the enhancement in the uniformity of the layer to the intervention of Marangoni flows which pulled the solution towards the borders of the sample. The evolution we expected consisted in (Figure 4.18):

- During the deposited solution settlement, the regime of diffusion limited evaporation was reached all over the liquid-gas interface. In particular, the lower vapour saturation in proximity of the border of the sample turned in enhanced evaporation (a).
- Furthermore, in such regions, the higher vapour pressure of the secondary solvent caused a significant rapid change in the composition of the solution. On the other hand, in the central part of the sample, slighter variations were induced due the milder evaporation rate. The situation as described involved a gradient in composition, hence a gradient in surface tension (b).
- Such gradient represented the driving force for Marangoni flows. The solution migrated, from the center of the sample, towards the borders (c).
- A "swelling" of the liquid layer occurred in proximity of the contact line, leading to an increase in the contact angle and preventing the solution to contract (d).
- Finally, the liquid layer dried by shrinking from the border to the center of the substrate.

The contraction of the liquid was in fact the main failure cause in single solvent spray depositions. Such problem does not affect other coating techniques, like spin coating and blade coating. Indeed, by applying a suitable external force to the liquid layer, such processes end up with a very thin and highly concentrated solution. Then, the evaporation of the solvent does not involve significant perturbation in the material distribution, namely the solute "freezes" because of the high viscosity of the solution.

Since no external forces could be exploited in spray coating deposition, the introduction of an internal force was found to be promising. Indeed, the pull of

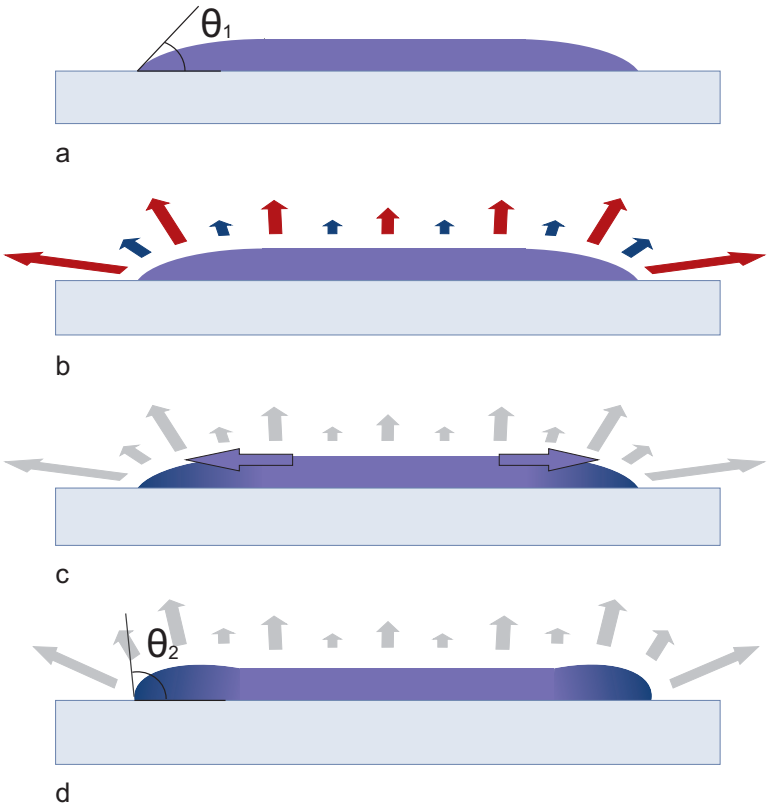

Figure 4.18: Mechanism underlying the wetting improvement coming from the adoption of two solvents. After the deposition (a), the enhanced evaporation of the secondary solvent close to the contact line (b) leads to a gradient in surface tension. Such gradient becomes the driving force (Marangoni effect) which pulls the solution on the edges of the solution (c). The increasing contact angle (d) represents the tendency of the liquid to spread.

the liquid towards the borders of the substrate led to a delay in the contraction of the solution. Such time span, when the Marangoni flows were effective, permitted to achieve an high level of viscosity. A sufficient "freezing" of the solute permitted the attainment of uniform depositions.

Marangoni flows were analysed by Fanton et al. [19]. Referring to a two solvents mixture on a substrate, considering z as one of the horizontal axis coordinate, neglecting the influence of gravity and of gradients in temperature, the velocity due to Marangoni effect can be written as

$$v(z) = \frac{h}{2\,\eta}\frac{d\gamma}{d\phi}\frac{d\phi}{dz} \tag{4.3.1}$$

where $h = h(z)$ is the thickness of the liquid layer, η=$\eta(\phi)$ is the dynamic viscosity, γ=$\gamma(\phi)$ is the surface tension and ϕ=ϕ(z) is the volume fraction of the secondary solvent along the liquid layer. Since the contraction of the liquid layer always started from the borders of the sample, an end of the Marangoni effect necessarily occurred. From Equation 4.3.1, two factors have to be considered: the decreasing $\frac{d\phi}{dz}$, indeed the flows try to compensate the gradient in composition; the increase in viscosity of the solution due to solvent evaporation.

Another important consequence of the evolution previously discussed is the strong coffee ring effect affecting the deposition. Indeed, the internal fluxes, which supplied the loss of solvent on the borders of the sample, were effective for a significant time span during the evaporation. In Figure 4.19, the profile of the surface in such region, for a PEDOT:PSS sprayed film, is shown (optical scan measurement).

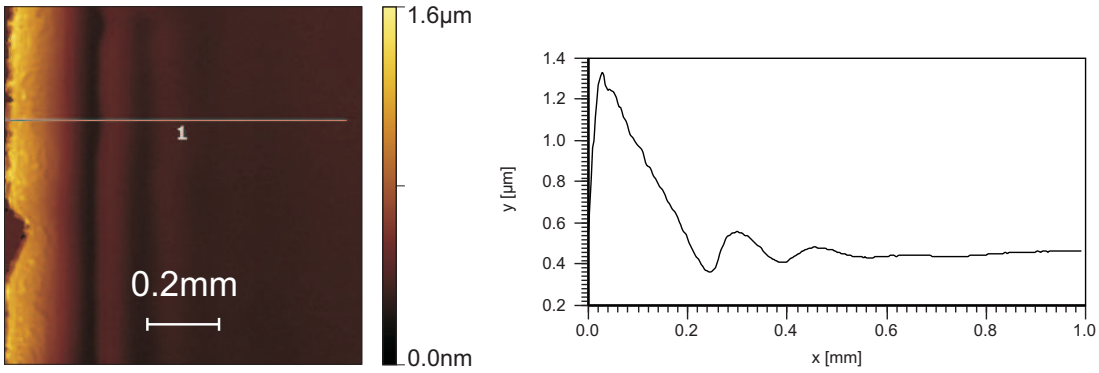

Figure 4.19: PEDOT:PSS deposition on glass: optical scan of the solute accumulation on the edge of the sample. Peak over 1 µm are observed for a 30 nanometers thick layer

Despite a substantially flat topography in the center of the substrate, an over 1 μm high accumulation was observed close to the edge of the sample. A further

source of delay in the liquid contraction could be found in the eventual self-pinning contribution due to such deposited material.

As long as such phenomenon can be confined far from the active area, no significant drawbacks are involved (apart from the waste of material). Nevertheless, further experiments will have to verify the effectiveness of the technique on up-scaled substrates.

Chapter 5

Spray processing of organic solar cells

Considering the progresses shown in Chapter 4, the insertion of sprayed organic layers in full devices could be implemented. In fact, by adopting proper settings for the solutions and the deposition parameters, acceptable uniformity and thickness control became possible. The last and crucial step was therefore to test the physical properties of the layers, aiming to solar cells optimization.

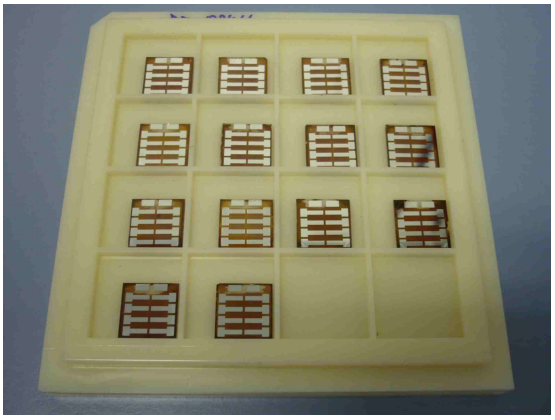

Figure 5.1: Sample holder with organic solar cells. The experiments often consisted in the comparison among several devices fabricated through different process steps.

Referring to the standard structure presented in Chapter 2, the performance of devices where one of the organic layer was processed via spray coating instead of spin coating will be discussed.

5.1 Sprayed PEDOT:PSS layer in organic solar cells

Spray coated PEDOT:PSS was inserted in organic solar cells. The layer was processed on samples with ITO, and the influence of the deposition parameters was investigated. The device structure was completed by spin coating P3HT:PCBM Rieke 4002 on top of each PEDOT:PSS film and by evaporating Yetterbium/Aluminum metal cathode. For the active layer, spin coating was chosen in order to let the experiment being as much reproducible as possible. This permitted to accurately assess the influence of PEDOT:PSS layer on device performance.

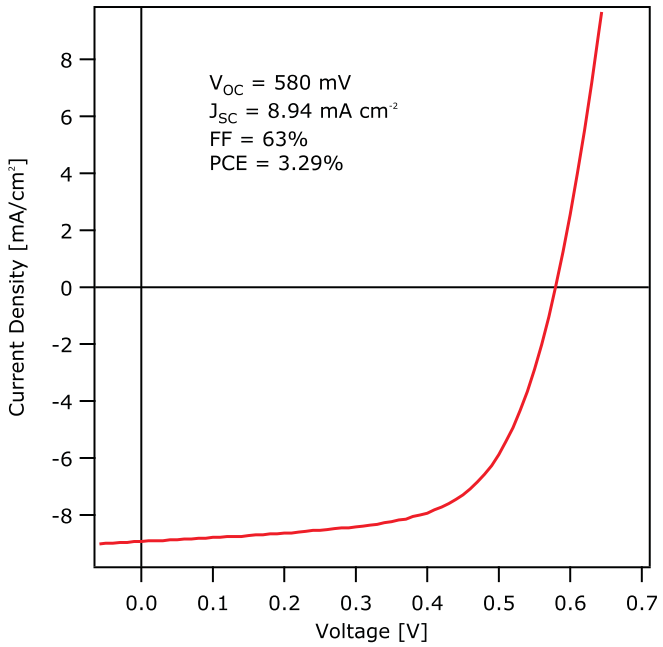

Figure 5.2: Current-Voltage characteristic for a full spin coated solar cell.

First of all we show the reference, obtained with the standard procedure for spin coating process. The thickness of the active layer was found to be slightly lower than the optimum value, nevertheless good performances were measured for almost all the devices on the sample. The fourth quadrant of the I-V measurement for one of the cells is shown in Figure 5.2.

The quality of spin coated PEDOT:PSS could be appreciated by considering the low series resistance of the cell. Moreover, the open circuit voltage was around 590 mV, hence the layer made sure that a proper energetic level faced the active layer in order to collect photo-generated holes without further losses. An overall 3.3% efficiency could be achieved.

Focusing on devices where PEDOT:PSS was spray coated the influence of

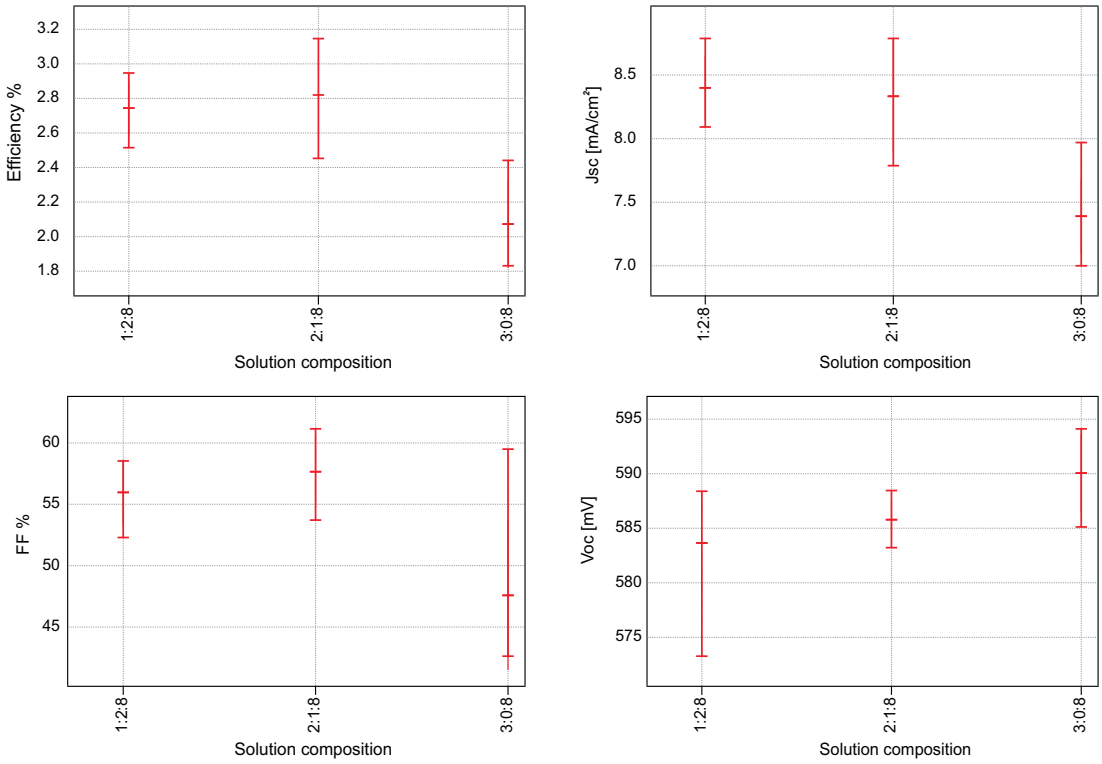

Figure 5.3: Trends for the efficiency, the J_{sc}, the FF and the V_{oc} depending on the solute concentration of PEDOT:PSS solution.

variations in each deposition parameter was assessed. For what concern the solute concentration, all depositions were made at 30°C and adopting 2.5 ml/min as deposition rate. In this conditions, the 1:2:8, 2:1:8 and 3:0:8 solutions had been tested.

We already pointed how this parameter is strongly connected to the final thickness of the solid layer. From the fitting with the Shokley's formula for a p-n junction of the I-V curves, an increase could be noticed in the series resistance for high concentrated solutions. Compared with 2 ohms/cm^2 for spin coated layer, values in the range of 2 and 4, but also up to 7 ohms/cm^2 were observed. In particular, the 3:0:8 composition led to solar cells with lower efficiency due to very low fill factor and short circuit current. We could ascribe such degradation in performance either to the higher thickness or to the rougher surface of the layer. Nevertheless, it was not clear whether such a little variation in the solute concentration and in the final layer's features could impact so intensely on device performance.

On the other hand, very thin layers achievable with the 1:2:8 composition did not lead to better results, meaning that, indeed, a minimum value for the thickness of the layer is required. In particular, some devices on this sample showed a significant lower V_{oc}, ascribable to a lacking coverage of the ITO contact. Since

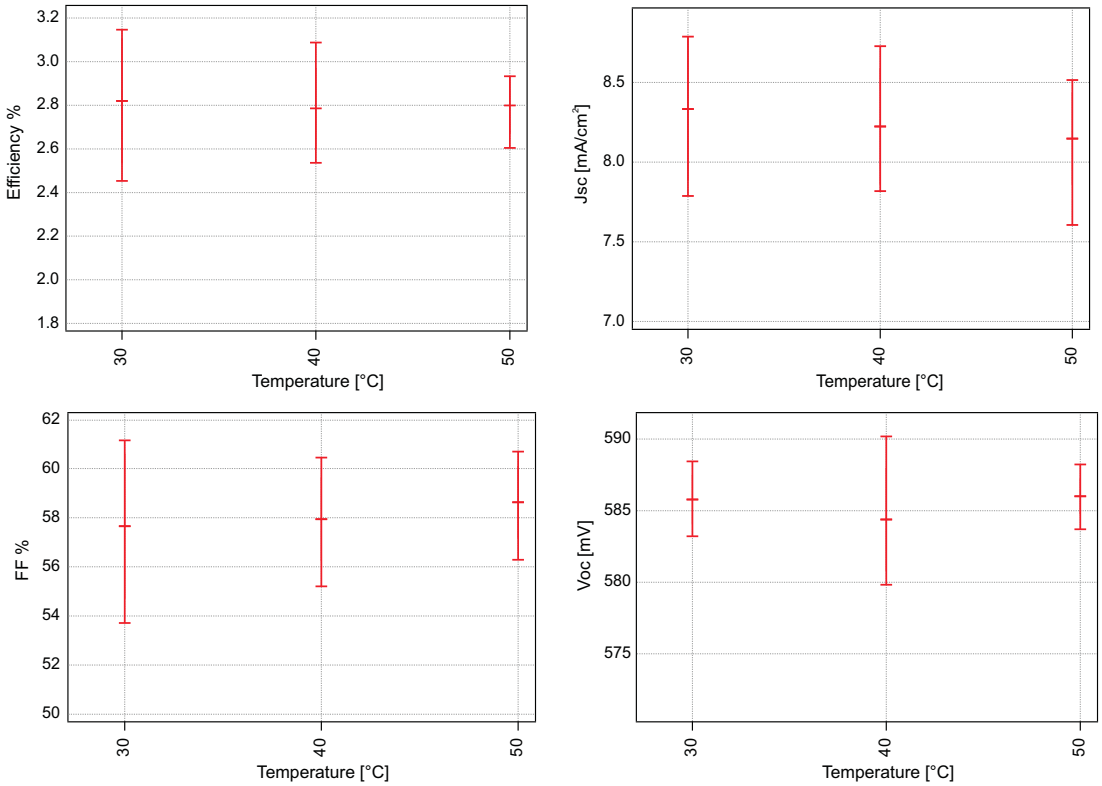

Figure 5.4: Trends for the efficiency, the J_{sc}, the FF and the V_{oc} depending on the hot plate temperature during PEDOT:PSS deposition.

the best performances were achieved with the 2:1:8 composition we could draw the conclusion that thickness values around 40 nanometers for the PEDOT:PSS layer do not affect cell performance, moreover they assure a full coverage of the ITO contact.

Regarding the temperature of the hot plate during the spray deposition, we already pointed out that lower values of such parameter determines a slower drying of the solution and leads to more uniform layers. Therefore, we wanted to assess whether an increase of few degrees could significantly improve the electrical properties of the layer. Temperature of 30, 40 and 50°C were tested. We chose not to assess higher values because of uniformity issues.

From the analysis of solar cells parameters, no significant variations could be noticed. Apparently, the rougher surface of the layers deposited at higher temperature did not affect the efficiency of the devices. On the other hand, faster drying seemed not to change the electrical properties of the film. Indeed, the efficiency and the fill factor were found to be quite stable. Since the coverage of the surface improves by decreasing the temperature, the lowest value in the range we tested represented the best candidate for PEDOT:PSS spray deposition recipe.

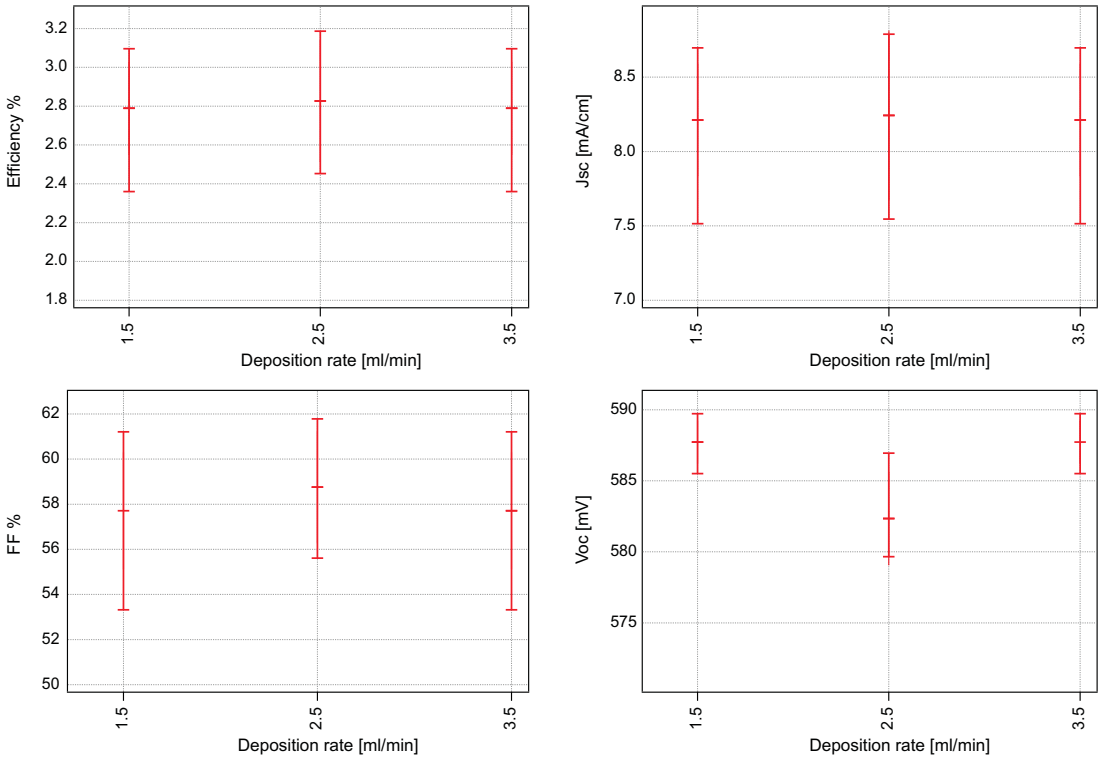

Figure 5.5: Trends for the efficiency, the J_{sc}, the FF and the V_{oc} depending on the spray deposition rate of PEDOT:PSS solution

Ultimately, considering a 2:1:8 solution composition and 30°C temperature, we studied the influence of different deposition rate. From this comparison no evident trends arose and all devices showed comparable performance.

From this investigation we could draw the conclusion that for PEDOT:PSS spray deposition, a 2:1:8 for the (DIW-PEDOT:PSS):DIW:IPA composition optimizes the thickness of the film. Moreover, a nearly room temperature of hot plate during the deposition leads to reliable coverage of the substrate, as well as good electrical properties. By using deposition rate setting in the range between 1.5 and 3.5 ml/min, layers with similar electrical features can be achieved.

5.2 Sprayed P3HT:PCBM layer in solar cell

5.2.1 Slow drying technique

The first investigation we assessed was made in order to further improve the morphology of the layer by slowing the evaporation process of the solvent after the deposition on the substrate [28]. This effect could be attained by considering a saturated vapour environment. In chapter 2 we already mentioned that the evap-

oration of a liquid is in most of cases a diffusion limited process. Its effectiveness is therefore mainly affected by the capability of the gaseous specie to "escape" from the saturated atmosphere which surrounds the liquid-gas interface. Thus, by hindering the diffusion of the vapour in the free space, a significant drop in the evaporation rate could be achieved.

Such condition could be concretely attained by covering the sample right after the deposition with a few milliliters volume petri dish. Such confinement prevented the vapour to diffuse towards region with lower concentration. A collection of small droplets was observed to attach on the internal surface of the petri dish few seconds after the coverage of the sample. The presence of a vapour saturated environment was therefore confirmed. We expected the drying of the liquid layer to take place in a more quasi-static regime.

The adoption of such technique resulted in a dramatic variation of the features of P3HT:PCBM layer. The color of the sample was red-purple, whereas the fast drying deposition always led to orange films. This is ascribable to a red shift in the peak of absorption of P3HT. Furthermore the slow drying causes a better organization of the polymer chains within P3HT domains. A higher level of crystallinity is the outcome of the quasi static assembling process. Notably, this gives rise to a widening in the window of absorption spectra as well as to a significant improvement in the hole mobility throughout the P3HT phase.

Confirmation of the red shift and enhanced optical absorption spectrum could be observed from the UV-vis measurement in Figure 5.6 where a fast and a slow dried layers are compared. The appearing of the "shoulders" in the absorbance profile is a clear sign of higher crystallinity.

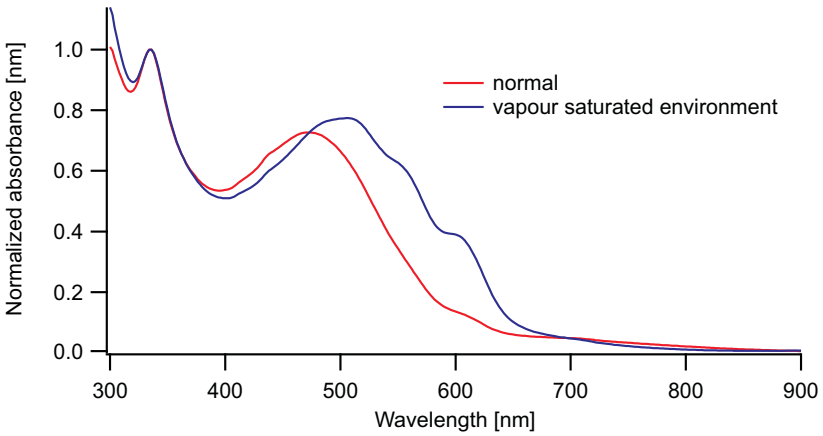

Figure 5.6: The enhancement in the absorbance spctrum due to the slow drying of the solvent is shown. A higher lever of crystallinity in the P3HT:PCBM networks underlies such improvement.

Further analysis showed how the temperature of the hot plate during the deposition permitted to control the evaporation evolution of the layer. From a two and a half minutes for a fast dried layer, the duration of the evaporation was observed to be 18, 8 and 5 minutes from the adoption of respectively 45, 55 and 65°C temperature. The optical properties of such layers showed mild variations which anyway confirmed that higher times of drying lead to enhanced crystallinity. Indeed the lower was the temperature of the hot plate and the more the absorption shoulders were pronounced.

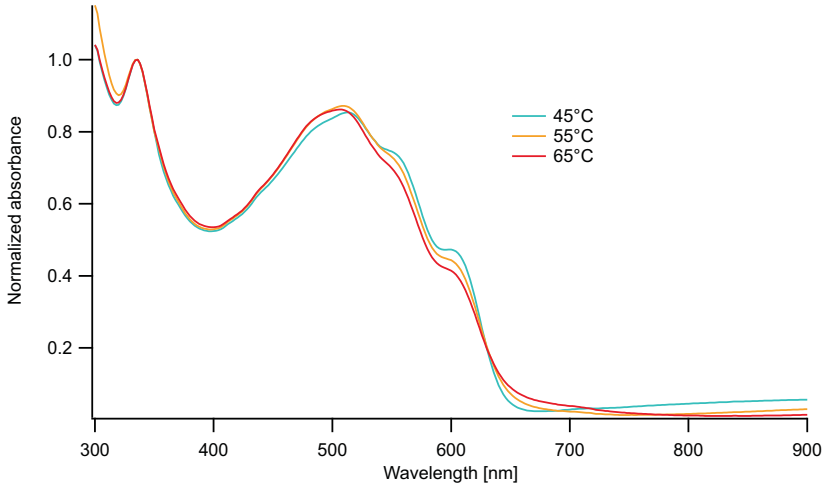

Figure 5.7: Influence on the UVvis absorbance spectrum of the hot plate temperature during the deposition. The most crystalline structure of P3HT:PCBM was achieved by adopting the lowest temperature, namely with the slowest drying of the solution.

Significant signs of different microscopic features were suggested by AFM analysis of spray coated P3HT:PCBM layers fabricated in different conditions. Indeed, a strong relation between the roughness of the layer at the micrometer scale and the degree of development in the morphology of the networks of the two species was observed.

A dramatic variation in the topography of the scans takes place when, from the fast drying deposition shown in Figure 5.8, the slow drying technique is introduced (Figure 5.9). A more detailed surface is observed resulting in higher peak to valley and roughness rms values. The extent of this effect seems to be therefore well related to the time of drying of the layer as demonstrated in the comparison of depositions made at 45 and 55°C.

The fabrication of solar cells with standard structure, where the PEDOT:PSS layers were spin coated to permit a better comparison among different spray coated active layers, showed a trend which confirmed the previous assessments. Depositions of P3HT:PCBM blend with the longest time of drying resulted in

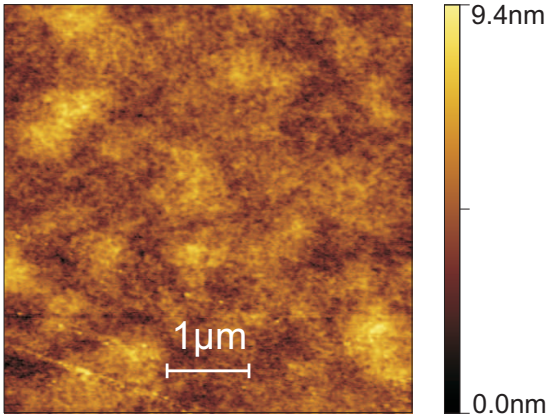

Figure 5.8: AFM measurment on P3HT:PCBM layer deposited from a solution of ortho-dichlorobenzene and mesitylene in a 7:3 ratio at 55 °C. The fast drying turns in a poor morphology development.

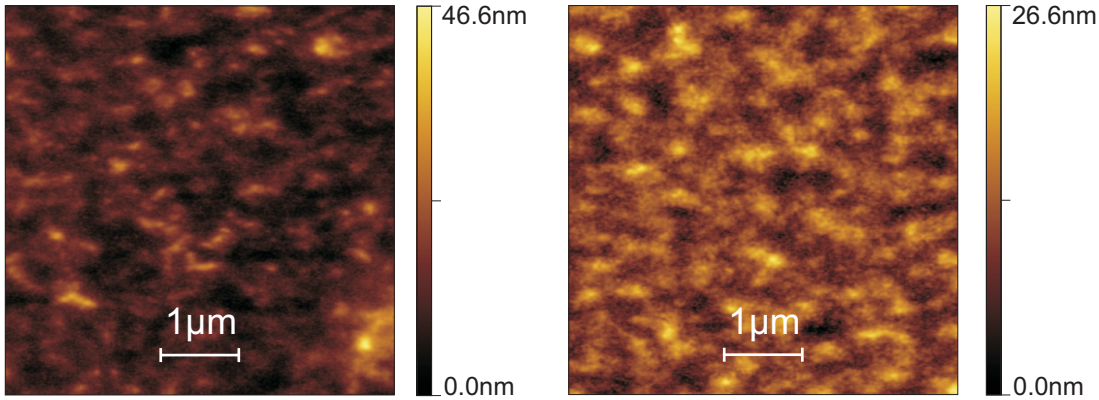

Figure 5.9: AFM P3HT:PCBM layer deposited from a solution of ortho-dichlorobenzene and mesitylene in a 7:3 ratio at (a) 45 and (b) 55 °C. The slow drying technique led to more detailed topography. The significant roughness of the layers ((a)4.7 nm and (b) 3.3 nm rms values) is due to a enhanced phase separation. Both the rms and the p-v values increased by slowing down the evaporation evolution.

solar cells with efficiency as high as 3.24%. By raising the temperature of the hot plate during the deposition a slight decrease in the performance was observed. Remarkably, the active layer fabricated at 45°C showed the highest values for the short circuit current, due to the improved absorption and transport properties of such more crystalline morphology. Conversely the open circuit voltage was slightly lower, having a negligible effect on the overall performance though. This effect can be ascribed again to the larger extent of the regio-regularity of the P3HT which leads to a shift in the energy levels and therefore in the LUMO acceptor to HOMO donor energetic difference.

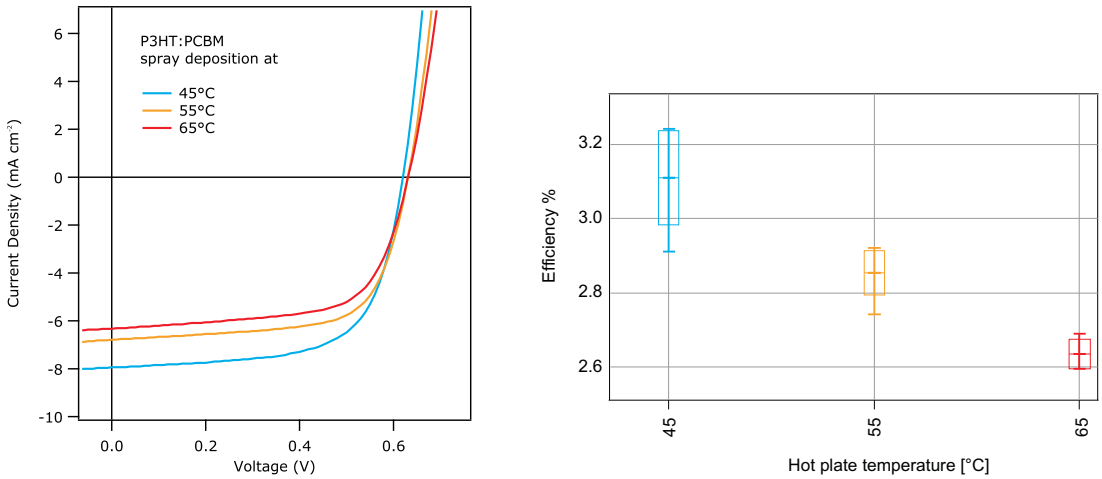

Figure 5.10: The influence of different morphologies arising form different hot plate temperature on OSC performance is shown. Deposition at lower temperature led to better morphology and therefore to higher efficiency devices.

Regarding the macroscopic quality of the films, depositions at 45°C gave often rise to contractions of the liquid in the first time of the evaporation, affecting the final uniformity of the layer. At 55°C the process showed much higher reliability resulting in full coverage and high uniformity(see Figure 4.16). My choice was to continue the investigations adopting 55°C as hot plate temperature during the deposition, since it was the minimum value which led to full and reliable coverage of the substrate.

An assessment of the active layer thickness influence was consequently implemented. The control of such parameter could be achieved, as already mentioned, by varying either of the deposition rate and the solute concentration. By using two different concentrations for the P3HT:PCBM solution and different deposition rates, we could fabricate active layer whose thickness values covered the range between 50 and 300 nanometers.

In Figure 5.11 the profile obtained from the experimental data of the short circuit current for different devices is shown. A not very clear trend arises from

the plot, but nevertheless we could notice the presence of two peaks around 80 and 240 nanometers.

A possible explanation of such result is found in the optical analysis of a solar cell. In fact the thickness of the active layer is a parameter which has a not obvious influence on the photogenerated charges. In an infinite medium the absorption of a electromagnetic wave takes place with a exponential quenching of the optical power according to the distance of the region considered from the surface and to the absorption coefficient of the medium itself. Since the values of the wavelengths involved in the solar spectrum profile are higher than the order of magnitude of the characteristic length of the device along the axis perpendicular to the layers' planes, diffractive optics calculations have to be considered. The stack of layers one on top of the other gives rise to a microcavity structure, where optical interference effects determine the actual electric field function of the depth. The integration of the square magnitude of such profile in the active layer is reasonably related to the amount of electron-hole pairs generated per time unit, and which are involved in the photoconversion.

From the simulation of this optical problem, a non monotonic profile is found to describe the influence of the active layer thickness on the total amount of photogenerated charges. Indeed, it is possible to point out two relative maximums around the values of 80 and 240 nanometers. By merging such result with short circuit current trend, the peaks of the curves seemed to roughly match.

The estimation of the active layer thickness from two measurements on both sides of each device was clearly a very coarse estimation of the actual average thickness. Indeed such assessments often showed over 20 nanometers variations over a distance in the millimeter scale. Moreover, the non linearity of the phenomenon considered actually introduces a further unpredictable fluctuation even if a correct average thickness could be estimate.

By comparing these curves we also neglected the contribution of transport efficiency in the determination of the short circuit current. In fact, a decreasing dependence from the path which the charges have to cover quenches the amount of electrons and holes able to reach the contacts. In the simulation the total amount of photogenerated charges are shown, and the outcoming profile is expected to stray when higher thickness of the active layer are considered.

Such effect was found not to be compromising for spin coated solar cells analysis up to 250 nanometers thick layers. It was instead decisive by considering thicker films, where the lowering in the built-in electric field and the increase in the average distance from the electrodes led to a drop in the short circuit current

as well as in the fill factor. The overall effect is therefore that the maximum in the J_{sc} profile around 240 nanometers represented in principle the target for the active layer thickness. The fulfilment of such constraint optimizes the performance of spin coated devices.

By relying on Figure 5.11, since the maximum in efficiency of the cells with spray coated active layer matched the maximum in J_{sc}, an analogous conclusion could be drawn for our study. Nevertheless, the most important information arising from this investigation was that thickness of spray coated active layer cannot be thoroughly optimized as in the case of spin coating. Indeed, variations in the order of 40 nanometers along the film surface give rise to inaccurate reproducibility within the sample itself as well as the impossibility to clearly define a optimal thickness.

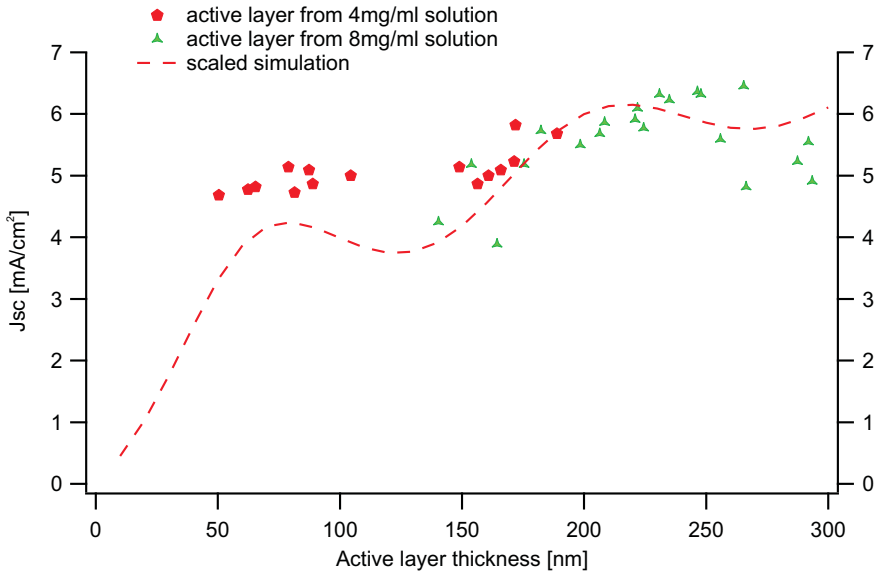

Figure 5.11: Experimental data for the J_{sc} of solar cells with different active layer thickness values. The trend is compared with a scaled version of the optical simulation outcome.

5.2.2 Thermal treatment

Although the slow drying technique already led to a significant improvement in the morphology of the layer, we wanted to assess the effect of an annealing step. Many studies demonstrated the effectiveness of such post process treatment to reach higher efficiency values [30] [32]. Furthermore, in this early stage, we wanted to investigate the effect of annealing performed either right after the deposition of the active layer or after the evaporation of the metal contact. By focusing on the most common annealing temperature for P3HT:PCBM solar cells, we could point

out that a termal treatment does improve the electrical parameters of the device. In particular, such effect was observed only when the annealing was performed before the metal evaporation, whereas when it was made afterwards, the devices showed equal or even worse performance (Figure 5.12). Focusing therefore on the pre-annealing step a very interesting increase in efficiency could be attained from an average 2.3% to a 2.9% value. Notably, the short circuit current showed a mild improvement, while the increase in the fill factor up to over 70 % values was found to be the most significant source of this enhancement.

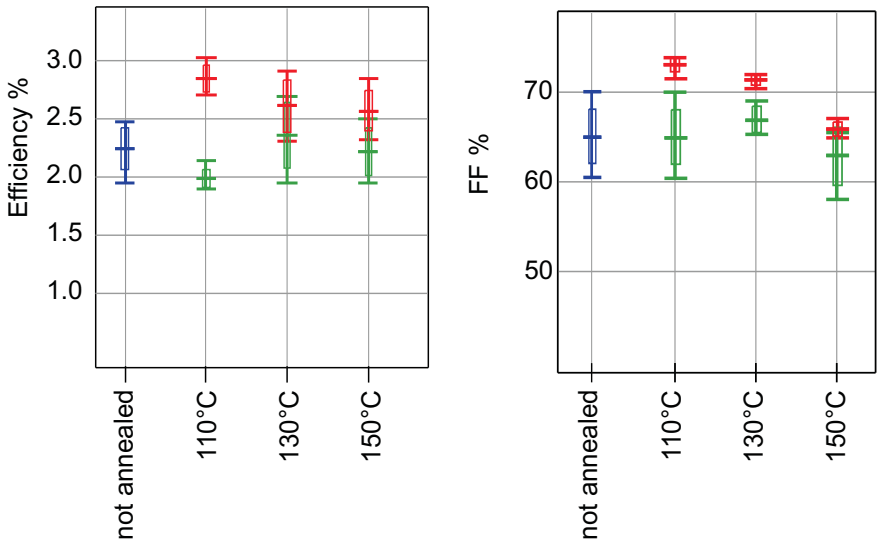

Figure 5.12: Effect of the annealing step for samples which underwent such treatment either before or after the metal evaporation.

Subsequently the effect of the annealing temperature (T_a) was more accurately investigated, and a wider range of temperature was considered. After the spray deposition of P3HT:PCBM on spin coated PEDOT:PSS, a set of equally processed samples were placed on a hot plate for 10 minutes at different temperature of 80, 100, 110, 120, 130 and 150°C. In Figure 5.14 the dependence of the efficiency, the short circuit current, the fill factor and the open circuit voltage from T_a are shown.

Clear trends could be observed from such study. Indeed, a significant and rather constant improvement in the J_{sc} was achieved when T_a was in the range between 80 and 130°C. The resulting fill factor was found to be more sensitive in this window of values. A bell-shape trend, which also impacted on the profile of the efficiency, defined 110°C as optimal T_a best candidate. When the active layer underwent an annealing step at 150°C, no improvement in the J_{sc} could be observed. The efficiency of the solar cell was rather low, although a very high fill factor could be achieved also in this case. The open circuit voltage showed a neat profile which was substantially contrasting with the trend in the fill factor.

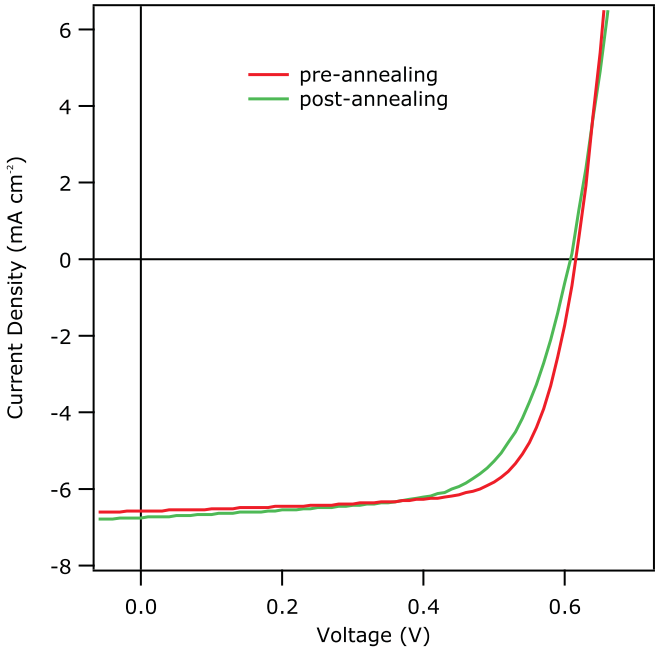

Figure 5.13: Effect of a pre-annealing or post-annealing step on the I-V curve. The thermal treatment performed before the metal evaporation led to better fill factors.

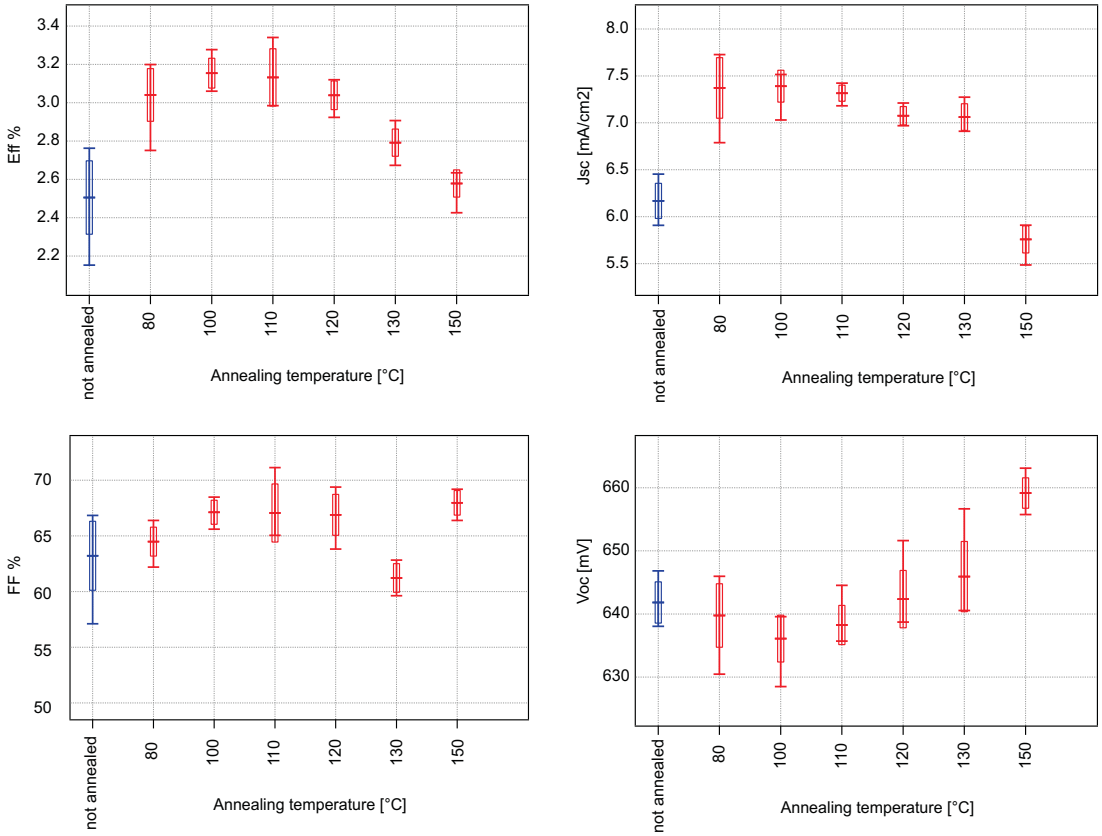

Figure 5.14: Trends for the efficiency, the J_{sc}, the FF and the V_{oc} depending on the pre-annealing temperature. A maximum in performance was noticeable when 110 °C was adopted. A remarkable boost in the fill factor underlay the improved efficiency of the solar cells.

Since few tens of millivolts variations were involved, such effect was found to be negligible in the determination of the overall efficiency. Again, this trend could be explained by considering that higher levels of order in the P3HT domains lead to better absorption and transport properties but to lower V_{oc}. Thus, we had a further confirmation that the improvement in the device performance which arose from the adoption of annealing temperature in the range between 80 and 130°C could be ascribed to the improved morphology of the active layer.

Further reasonable conclusions can be drawn by considering the effect of phase separation. Indeed, thermal treatments enhance the process of accumulation of P3HT and PCBM in larger domains. This effect is often beneficial for the transport of the charges, since they can take advantage of wider and longer paths. On the other hand, when the domains' size exceeds the diffusion length of the exciton, the amount of photogenerated electron-hole pairs which reach the donor-acceptor interface drops significantly, leading to an increased recombination and lower J_{sc}.

Thus, the contribution to the phase separation followed up a 80 to 130°C annealing leads to improvement in charge transport, but does not affect the charge transfer process, resulting in an overall better solar cell. Furthermore in this case, the P3HT ended up in a more ordered structure within the polymer phase, so that the optical absorption was found to be improved as shown in Figure 5.15.

Such enhancement was not observed instead for P3HT:PCBM layers annealed at 150°C, which showed identical optical absorbance as the sample before the treatment. This means that the pronounced migration of the species and their gathering in big domains did not lead to better morphology though. The significant drop in the J_{sc} let us rather infer that the phase separation played a degrading role. In fact, a quenching in the charge transfer between the donor and the acceptor phase due to the too big size of the domains could underlie such effect.

The extent of the annealing effect on the morphology of the layer can be partially assessed by mean of AFM measurement. In Figure 5.16 we show the scans of layers which underwent a thermal treatment. The topography are found to differ from the same measurement performed to a slow dried P3HT:PCBM layer (see Figure 5.9), consisting in a rougher surface. Moreover, it is evident how, while a 80°C annealing did not change the detailed features of the slow dried layer, at 150°C a substantially different reorganization took place. We can interpret such more coarse morphology showing bigger grains as sign of a too pronounced phase separation.

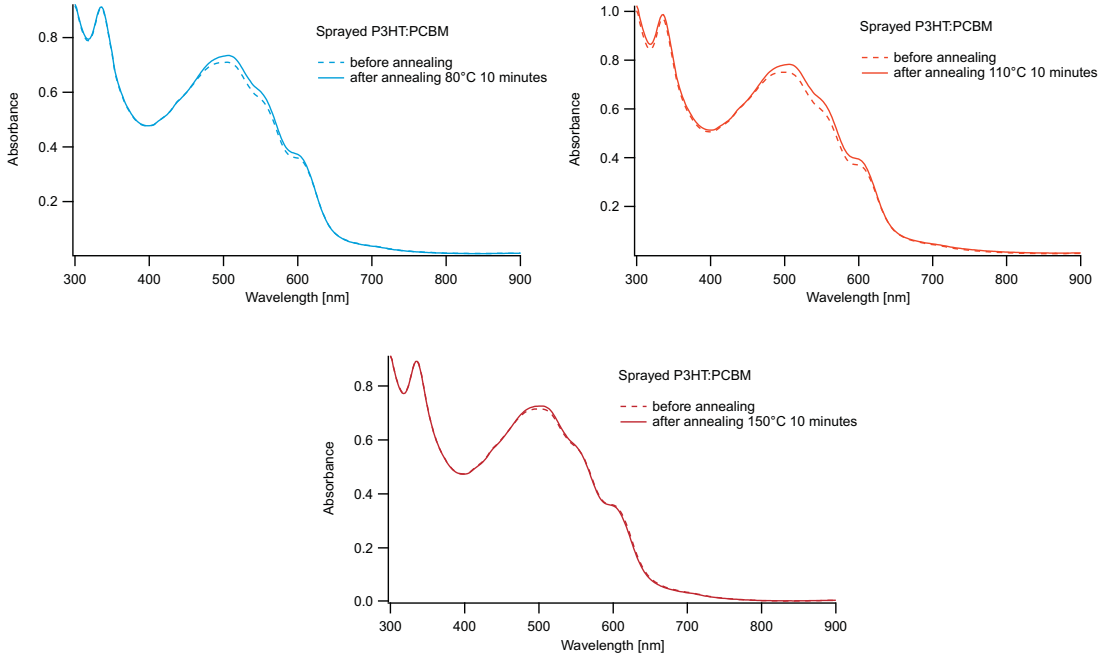

Figure 5.15: UVvis measurements of P3HT:PCBM optical absorbance improvement depending on the annealing temperature.

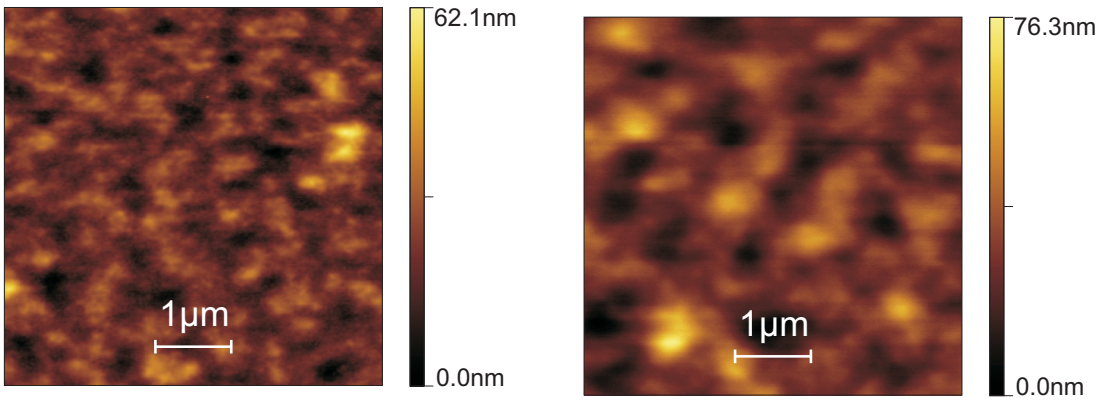

Figure 5.16: AFM measurements performed on P3HT:PCBM layers which underwent an annealing step at (a) 80 and at (b) 150°C.

A second stage of optimization consisted in the investigation of the annealing time influence. By choosing 110°C as temperature of the hot plate, a set of samples, fabricated as previously discussed, underwent a thermal treatment lasting different time spans before the evaporation of the metal.

The comparison among the efficiency values of the devices did not give rise to any clear trend. All the solar cells which were annealed for more than 4 minutes showed similar performance in terms of efficiency and J_{sc}. Only the dependence of the fill factor from the annealing time showed a trend. As it is shown in Figure 5.17 A first increase of its value was followed by a mild drop for time longer than 15 minutes.

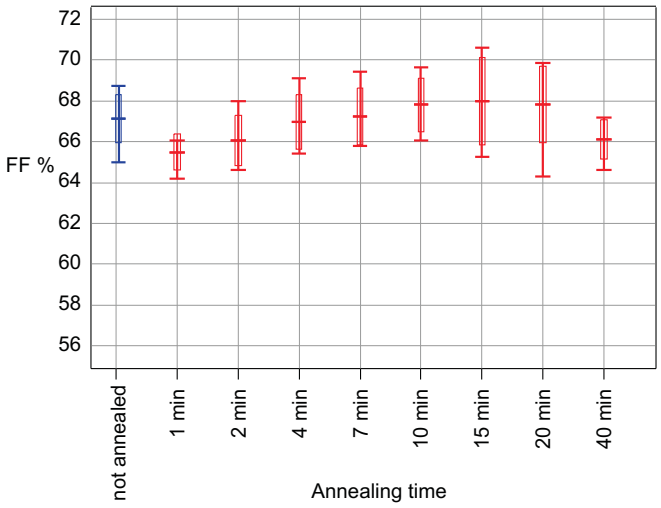

Figure 5.17: Trend of the fill factor for organic solar cells which underwent a pre-annealing step at 110 °C lasting different time spans.

Such dependence did not find a complete explanation. In fact, the initial improvement can be ascribed to the transient involving the movement of the species within the phases and the arrangement in a new morphology. It is reasonable that, once a certain extent in the crystallization had been reached, the mobility of the molecules in the network would have been no more sufficient for a further change in the structure. A substantial freezing of the organization was therefore what we expected.

The actual trend showed instead that a too long annealing step was not beneficial, namely other competing processes took place and affected the transport properties in the film. This was anyway hard to justify since, from the UVvis absorbance measurements (Figure 5.18), we assessed a evident increasing improvement of the optical properties by lengthening the annealing time.

Such result let us infer that the process of cross-linking in the P3HT continued significantly also with time longer than 15 minutes, which therefore does not

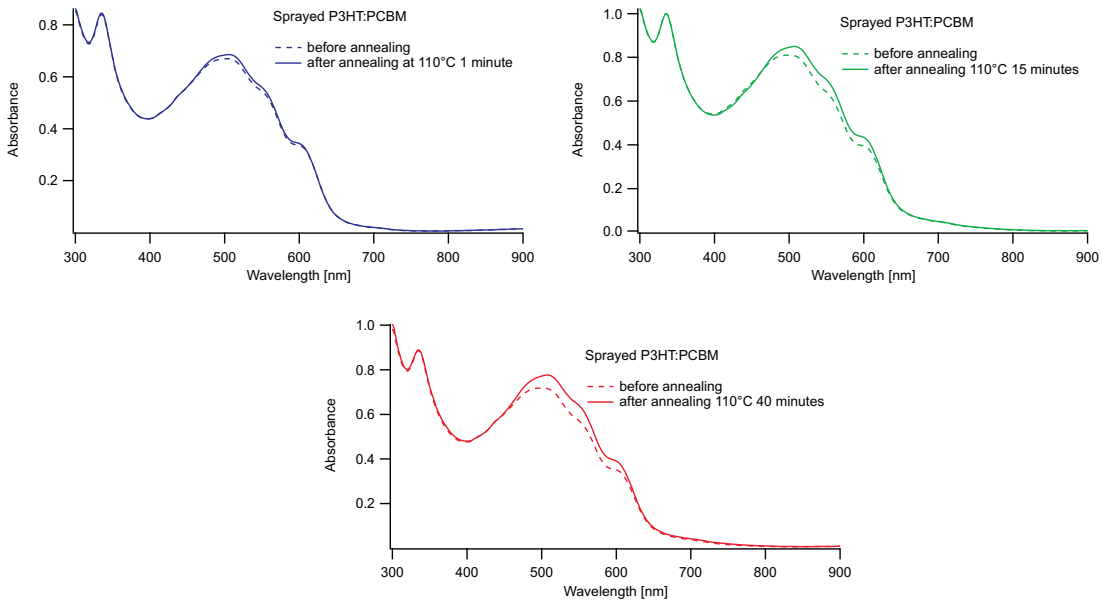

Figure 5.18: UVvis measurements of P3HT:PCBM optical absorbance improvement depending on the annealing time.

represent a saturation threshold. The drawback of this phenomenon could be a too pronounced phase separation. But since the short circuit current in the devices showed only a slight increase with the annealing time, it is unlikely this to have taken place.

Based on these results, we could only infer that the annealing step at 110°C for 15 minutes of spray coated P3HT:PCBM layer could significantly improve the performance of the final device. Hence, we considered this as final step of the recipe for the active layer spray deposition.

In literature, several P3HT and PCBM morphology optimization can be found. Especially when different procedure are involved, the optimal settings for the processes can sensitively vary. Nevertheless, it is interesting to mention that the highest efficiency published for spin coated P3HT:PCBM involved an annealing step at 110°C for 10 minutes [27]. A decrease in performance was in fact assessed by Li et al. when annealing time as long as 20 minutes were adopted.

5.2.3 Test on different P3HT materials

In order to get more meaningful comparison between spray coating and spin coating processes and to assess more deeply the potential of spray deposition, we involved in our investigation higher performance polymers. In particular we had available four different P3HT materials. In fact, according to the chemical process which implements the synthesis of the polymer, a wide range of physical

properties can be changed. Referring especially to the regio-regularity of the chains as well as to their molecular weight, noticeable variations can be induced in the optical and electrical features (different absorption windows, different hole mobilities).

Moreover, by varying the solute of the solution, all the physical parameters of the fluid, such as surface tension and (especially in case of polymers) viscosity, undergo a deep change. Therefore, it was not easy to predict the dynamic of the deposition process involving solutions which differ of even tiny variations.

The materials which we had available were:

- P3HT Rieke material P100: it is found to be suitable for organic transistors applications. Low absorption spectrum, good hole mobility.
- P3HT Rieke material 4002: it represents the reference P3HT Rieke for solar cells. Good performance and affordable price.
- P3HT Rieke material P200: polymer with high regio-regularity and high molecular weight. Its wide absorption window and high hole mobility value lead to high performance in solar cells. It is found to be very expensive though.
- P3HT Plextronics material: it shows similar features to Rieke P200, very effective but also expensive material.

The solutions were prepared according to the following recipe:

- Solvent: ortho-dichlorobenzene:mesitylene with a 7:3 proportion;
- Solute concentrations: 8 mg/ml of P3HT, 8 mg/ml of PCBM;
- The solution was stirred and heated at 80°C for 1 hour, then was let cooling down to room temperature with continuous stirring;
- Right before the usage, the filtering of particles up to 5μm size was performed.

The heating of the solution was introduced because of the slow dissolution of Rieke P200 and Plextronics material. Indeed, these polymers show the highest molecular weight within the set of materials that we tested. This factor probably underlies their strong tendency to aggregate despite the stirring.

The four solutions were sprayed on glass substrates with ITO where PEDOT:PSS was previously spin coated. By following the procedure that has been defined in this chapter, layers with different features could be achieved. By using P3HT Rieke 4002, the quality of the film was very similar to the case of P3HT Rieke P100. P3HT Rieke P200 showed wetting problems when deposited at 55°C. A full coverage and very uniform deposition could be attained by raising the temperature. Therefore, for such material, the active layer was processed with spray coating with 75°C hot plate. Ultimately, the solution with P3HT Plextronics material showed full coverage of the substrate, but 100 nanometers steps affected the uniformity of the surface. Thus, although the settings for the spray deposition of the active layer were formulated with P3HT Rieke P100, the process led to acceptable quality of the films even when different materials were tested.

The I-V curve of the best cell for each sample is shown in Figure 5.19, while in Figure 5.20 the electrical performances of the four devices are compared. Indeed, all the "new" P3HT materials led to more efficient solar cells. Notably, efficiency as high as 3.75% could be achieved. Such value represents an outstanding result, since it parallels typical spin coated P3HT based solar cells performance.

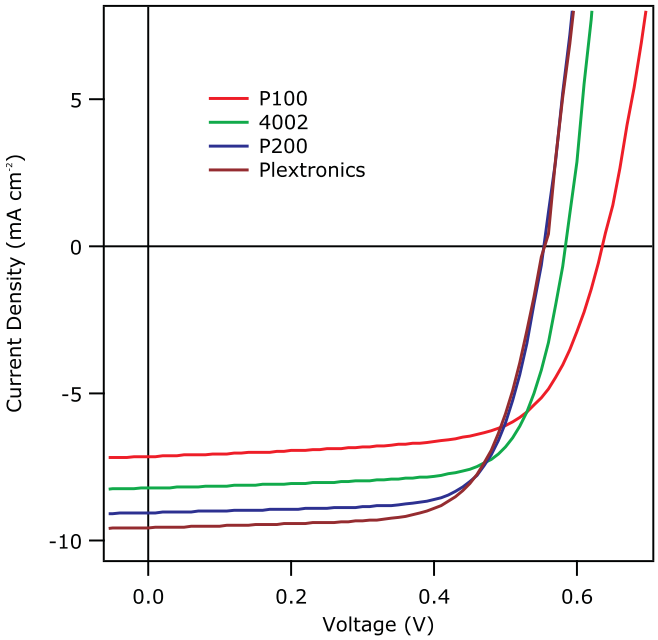

Figure 5.19: I-V curves for solar cells fabricated with different P3HT materials.

Even more remarkable, all devices showed over 70% fill factor values (peak at 73%). The higher regio-regularity of Rieke P200 and Plextronics materials turned in a substantially lower V_{oc}. Due to the very high short circuit current (up to 9.2 and 9.7 mA/cm^2 respectively), the solar cells which referred to these polymers reached the maximum efficiency values.

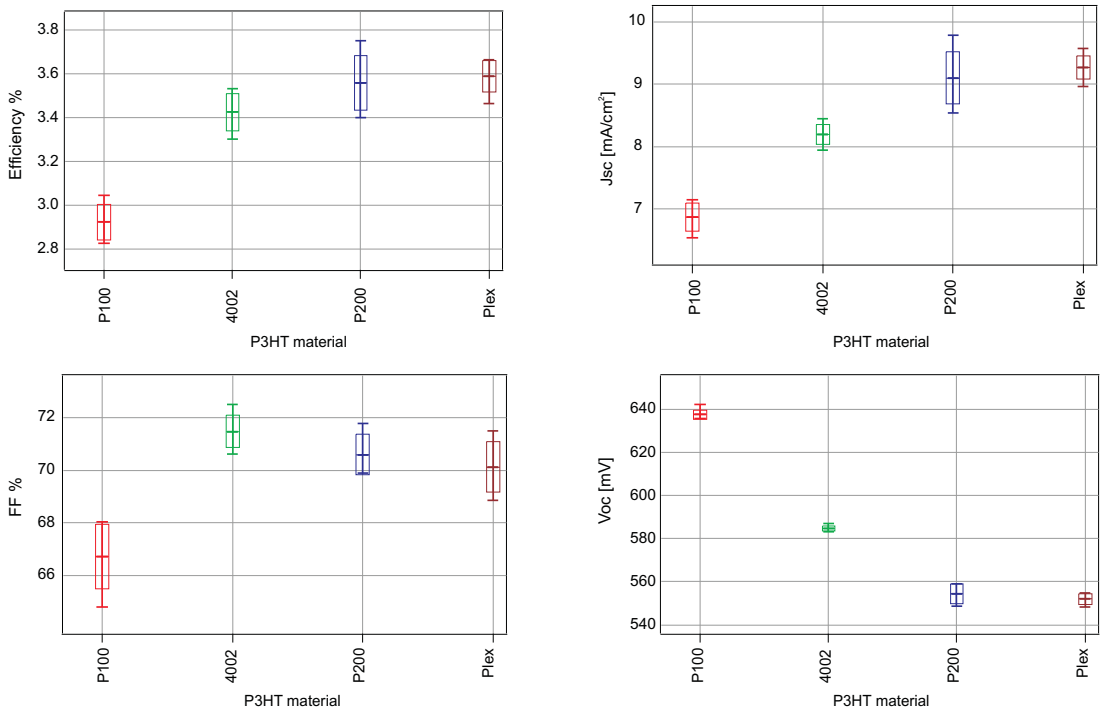

Figure 5.20: Trends for the efficiency, the J_{sc}, the FF and the V_{oc} depending on the P3HT material used in the active layer.

The extent of such more powerful photo-generation properties could be further assessed by analysing the spectral response of all the devices. In fact, from the measurement of the External Quantum Efficiency (EQE), information on the electrical charges extraction depending on the wavelength of the absorbed photons could be drawn.

The features of the optical absorption of the active layers were found to dramatically change by changing the P3HT material. In order to well interpret the measurements, the thickness of the layers had to be taken into account. The assessment of such parameter led to results which are resumed in Table 5.1.

Table 5.1: Average thickness of P3HT:PCBM layers depending on the solute concentration and the deposition rate.

	P3HT material			
	Rieke P100	Rieke 4002	Rieke P200	Plextronics
Active layer thickness [nm]	230	215	335	310-400

First of all the width of the main absorption window was clearly dependent on the polymer, namely it was found to be broader for the Rieke P200 and especially for the Plextronics material. Since by integrating the EQE function an estimation of short circuit current is supposed to be drawn, such profiles were clearly in agreement with the trend coming from the measurement of the I-V

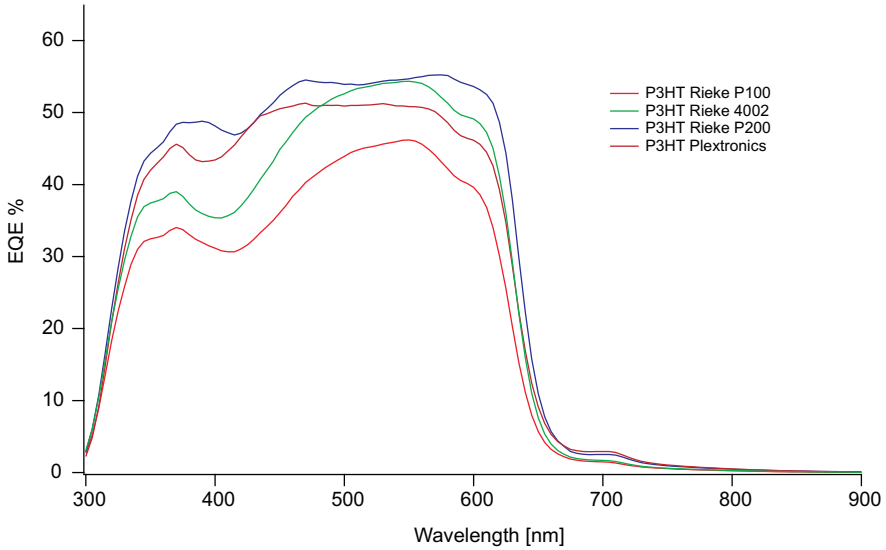

Figure 5.21: External Quantum Efficiency measurement performed on organic solar cells fabricated with different P3HT material.

curve.

Moreover, the typical profile of P3HT could be observed in the measurements for the cells referred to Rieke P100 and Rieke 4002 materials. Conversely, the curves for the solar cells fabricated with P3HT Rieke P200 and Plextronics showed a saturation in the absorption of photons in the 450-580 nanometers wavelength range. Thus, the roughly 50 and 55% respectively peak values of the EQE measurements represented estimations for the transport efficiency in those layers under short circuit conditions. A peak value around 55% was reached also in the profile of Rieke 4002, but no evident signs of saturation were observed. Together with the very high fill factor, this suggested that a possible more effective charge transport characterized the layer properties. It is also true that the significantly higher electric field, due to the lower thickness of the film, enhanced the carriers extraction.

I chose to adopt Rieke 4002 for the further investigations since it led to both good coating and to high performance when processed in solar cells. Moreover, the standard procedure which we referred for spin coated devices was formulated by using such material, therefore a reliable comparison between spray coating and spin coating could have been assessed.

A deeper understanding of the role of the active layer thickness seemed to be necessary. Indeed, the very high values reached in the fill factor suggested that, by adopting 200-250 nanometers thick films, no transport issues were noticeable. Actually, over 70% fill factors could be achieved with thickness up to 400 nanometers with Plextronics material. Thus, the maximum in efficiency could be

expected by using thicker layers which lead to higher short circuit current.

Therefore, we fabricated solar cells P3HT Rieke 4002 based with different thickness for the active layer. The range between 200 and 500 nanometers could be spanned by adopting different solute concentration. Although by doing this the viscosity of the solution was expected to change significantly, we could rely on a linear variation of the thickness as well as on a equal evaporation evolutions for all the depositions.

Furthermore, the role of annealing had to be clarified. Therefore, two sets of devices were processed and only on one of them the thermal treatment was performed. In Table 5.2 the thickness of all the devices that we tested is shown.

Table 5.2: Average thickness of P3HT:PCBM layers depending on the solute concentration.

	P3HT concentration [mg/ml]				
	8	10	12	14	16
Active layer thickness (not annealed) [nm]	214	242	331	391	559
Active layer thickness (annealed) [nm]	204	272	298	442	492

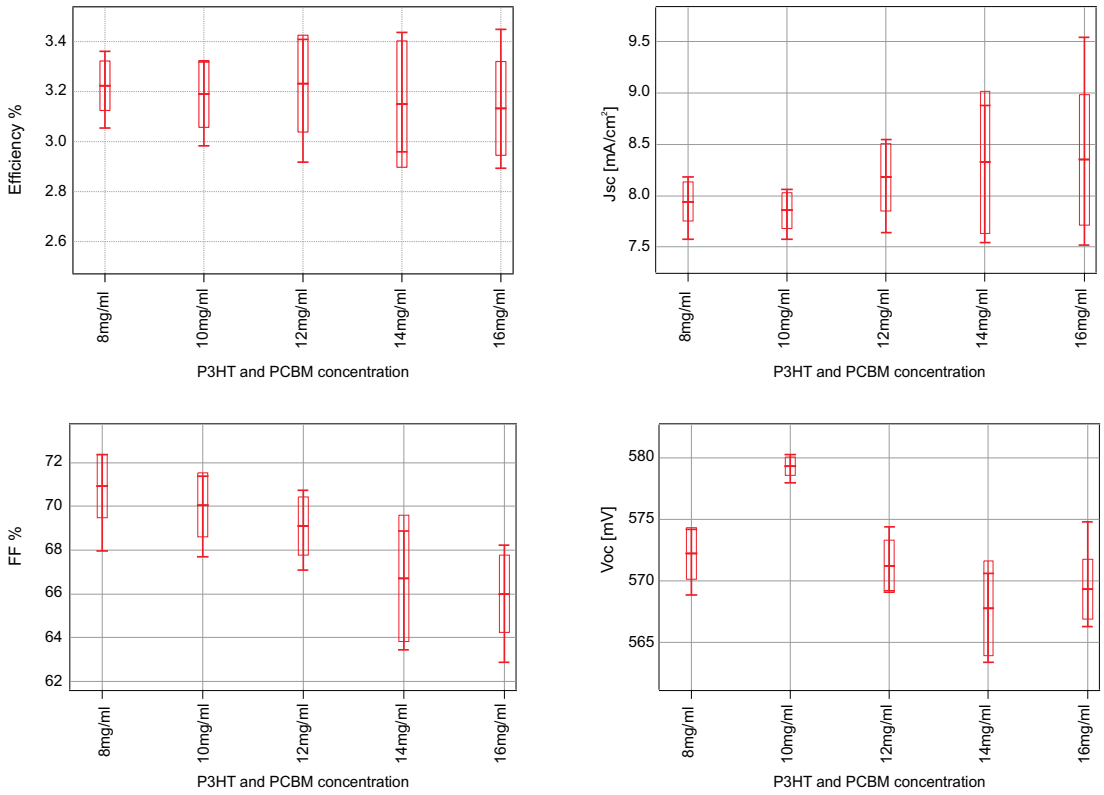

Figure 5.22: Trends for the efficiency, the J_{sc}, the FF and the V_{oc} of solar cells whose active layer was fabricated from solutions with different P3HT:PCBM concentrations.

Considering the devices which underwent only the slow drying, surprisingly

the efficiency remained rather constant over the whole span of thickness. Average values slightly higher than 3.2% could be reached for all the samples but also peaks over 3.4% were observed with the highest concentrations. The increasing thickness apparently did not affect the carriers extraction, turning in a rising short circuit current. Moreover, the effect of such increase was not quenched by the fill factor which showed only a moderate drop from 71 to 66% value.

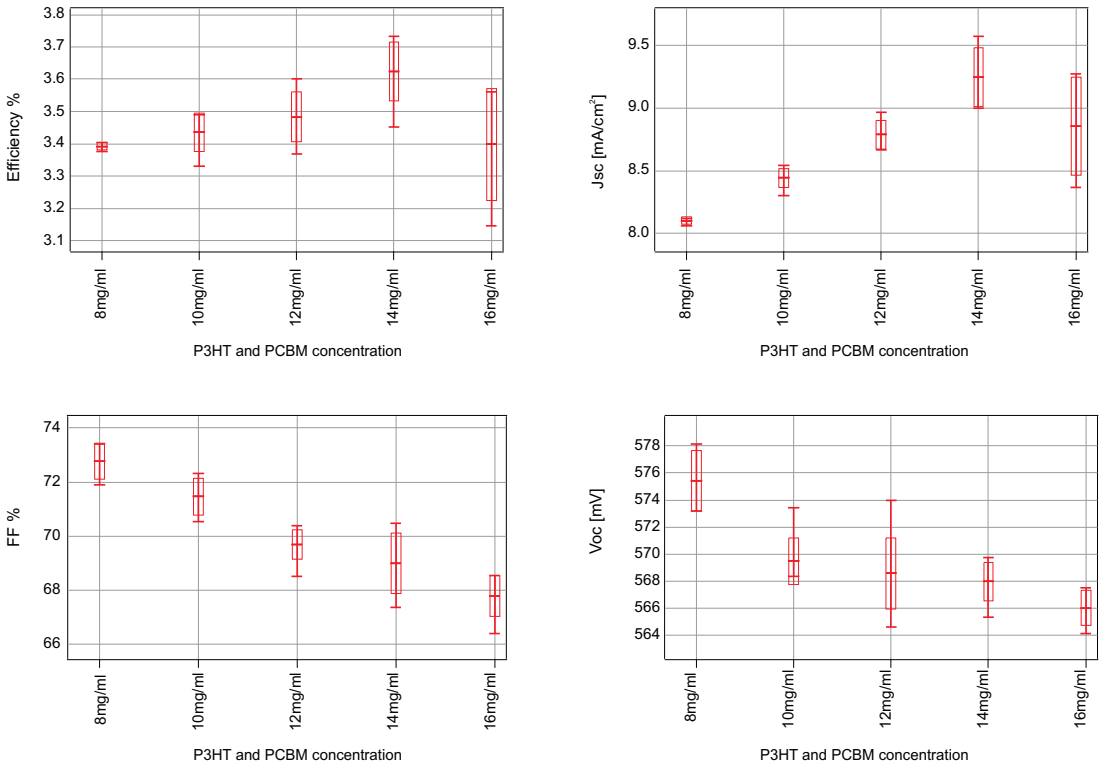

Figure 5.23: Trends for the efficiency, the J_{sc}, the FF and the V_{oc} of solar cells which underwent a pre-annealing step, and whose active layer was fabricated from solutions with different P3HT:PCBM concentrations.

From the analysis of the annealed samples, even more interesting trends could be observed. Indeed, higher efficiency could be reached with average values over 3.4%. But in this case, a significant improvement in the performance could be assessed by raising the thickness of the active layer, and a peak as high as 3.73% was reached by adopting a P3HT and PCBM concentration of 14 mg/ml. Again, the fill factor showed a mild drop which basically seemed to follow the same profile already discussed for the not annealed samples, but with an up-shift of about 2 per cent. The more significant increase in the short circuit current, which notably reached values up to 9.6 mA/cm^2, underlay the higher efficiency values obtained. Such peak, which also represented the maximum in efficiency, referred unbelievably to a 440 nanometers thick active layer.

All the performance of the devices suggested that the processing of P3HT:PCBM

via spray coating, in the way discussed in this chapter, leads to morphology within the film which substantially differs from any other one shown in the literature so far. The bulk heterojunction network attainable is clearly prone to enhanced transport properties, leading to very good performance even when half a micrometer thick active layers were used.

Chapter 6

Spray/spin coating comparison

In the conclusive stage of this work, I will discuss and evaluate the results achieved and shown in the previous sections. The best way how to do this consists in comparing such results to the state of the art, so that all the lacking points but also the innovative sides of the method can be underlined.

The following assessment will focus on coating performance and electrical properties of spray coated layers. From these points of view, spin coating is found to be the most suitable reference for organic solar cells technology. In fact, although the insurmountable intrinsic problems in the run towards large area production, it still represents the reference for nowadays research. Indeed, spin coated films show outstanding uniformity as well as the highest effectiveness, when involved in solar cell devices.

6.1 Spray and spin coated PEDOT:PSS layers

Considering PEDOT:PSS layer deposition, the features of films processed with spray and spin coating are shown in Figure 6.1 and Figure 6.2.

From the AFM scans, no significant differences could be noticed. The arrangement of gel particles in the layer kept in both depositions a quite smooth morphology. No degradation effects occurred for spray coated PEDOT:PSS, despite of the insertion of isopropanol in the solution.
Conversely, the measurements of the macroscopic uniformity of the samples showed some important differences. An overall rougher spray coated layer reminds the picture of a viscous liquid surface profile during its settlement. Indeed, close to the time of drying, a freezing of such condition occurs, witnessed by the solute

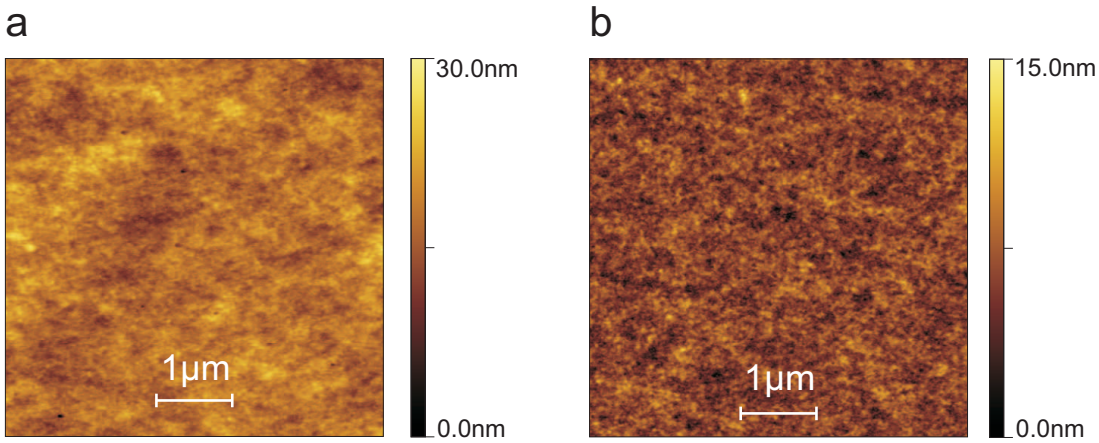

Figure 6.1: AFM measurements for (a) spray and (b) spin coated PEDOT:PSS layer. The rms and p-v values were found to be respectively (a) 2.4 nm and 26.7 nm for, (b) 1.5 nm and 15.1 nm.

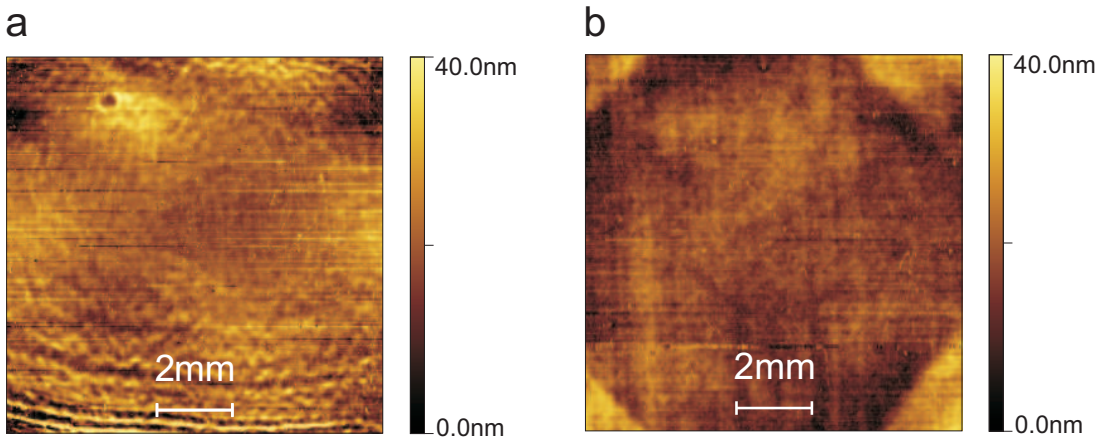

Figure 6.2: Dektak surface scan measurements for (a) spray and (b) spin coated PEDOT:PSS layer. The rms and p-v values were found to be respectively (a) 6.6 nm and 191 nm, (b) 3.5 nm and 35 nm.

distribution on the substrate. Over 100 nanometers high accumulation of PEDOT:PSS confined on the borders of the sample could be observed, ascribable to coffee ring effect. As long as such phenomenon takes place as edge effect and the active area remains exempt, only the waste of material is found to be concerning. In fact, as mentioned in Chapter 4, this is a direct consequence of the two solvents technique that we adopted in this work which, on the other hand, enabled the achievement of remarkable uniformity.
Notably, a similar trade off is found to affect spin coating with a much more critical extent. Indeed, the much higher level of uniformity shown in Figure 6.2(b) is reached by mean of a very inefficient process. Less than 10% of the solution deposited on the substrate is involved in the formation of the eventual layer.

By adopting a suitable solute concentration, average thickness between 30 and 40 nanometers could be achieved for spray deposition of PEDOT:PSS. Such order of magnitude was found to optimize cell performance, analogously to the case of spin coating. In Figure 6.3, the UVvis measurements of an optimal sprayed PEDOT:PSS layer and of a spin coated one are compared. Indeed, from the similar profiles, nearly equal average thickness values are expected.

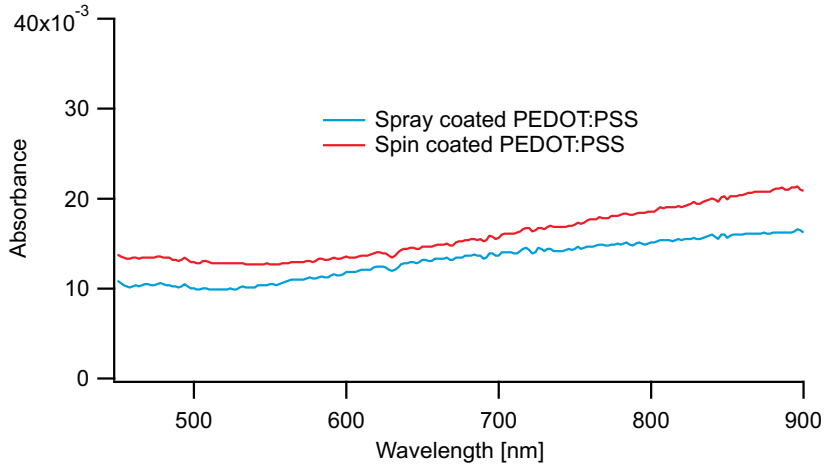

Figure 6.3: UVvis absorbance measurements for spray and spin coated PEDOT:PSS. The comparison shows similar thickness for the layers.

6.2 Spray and spin coated P3HT:PCBM layers

Concerning the spray deposition of P3HT:PCBM layer, more interesting points arose in this work. The uniformity of the layer could achieve very good levels, especially by adopting a slow drying technique as shown previously in Figure 4.16. The investigation in the morphology led to the most important results regarding device's efficiency. In the early stage, P3HT Rieke P100 was adopted. For such

material, the contributions of optimized slow drying technique and annealing step could be appreciated from AFM measurement as well as from UVvis spectra assessment.

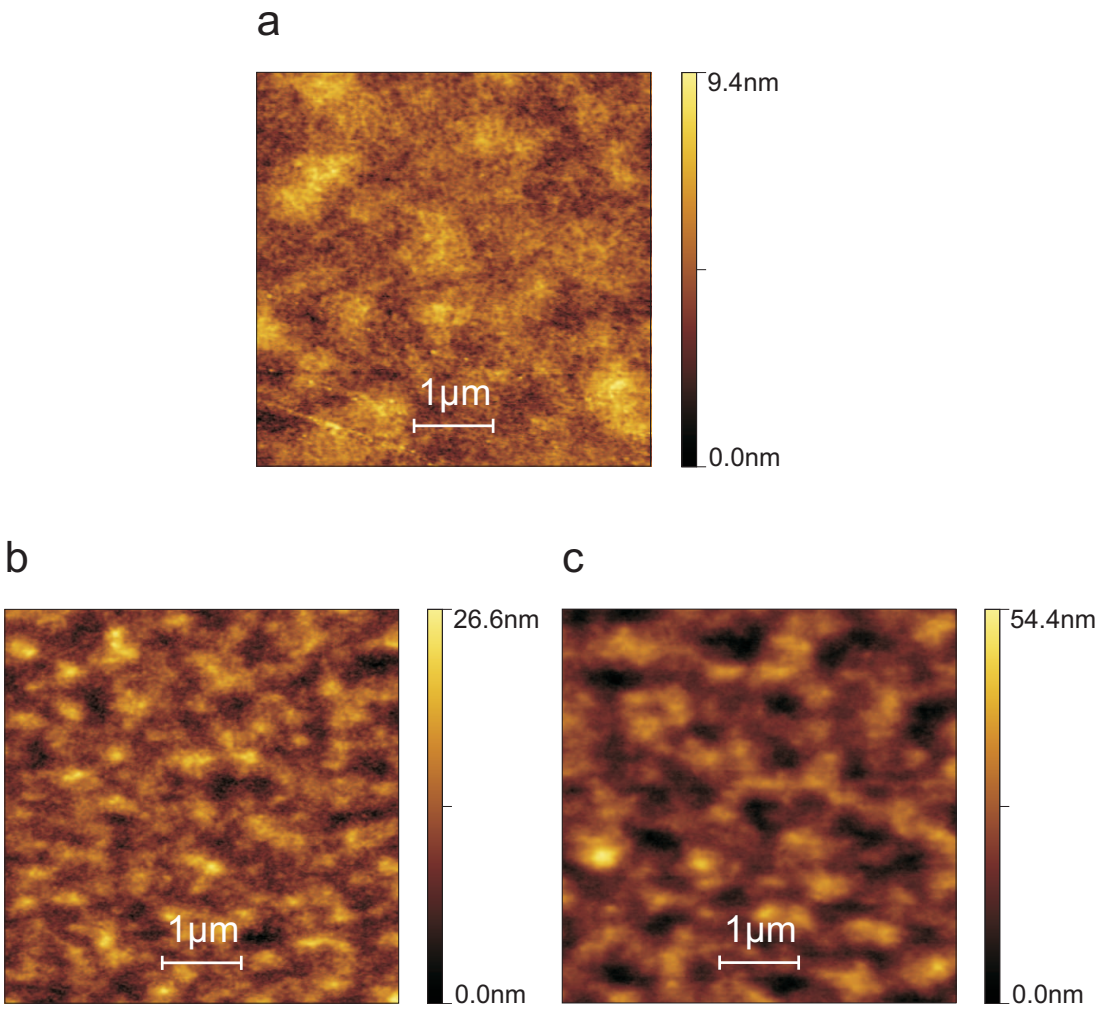

Figure 6.4: AFM measurements on spray coated P3HT:PCBM layers surface. The assessment was performed on films fast dried (a), deposited by mean of slow drying technique (b) and annealed at 110°C for 15 minutes after slow drying. An increase in the rms value is noticeable, from (a) 1.1 nm to (b) 3.3 and (c) 6.9 nanometers.

In Figure 6.4, a noticeable gradual morphology development for spray coated P3HT:PCBM can be observed. In particular, by applying the procedure discussed in Chapter 5, the topography did not lose the detailed nature, possible sign of a well sized phase separation.
Such improvement was further confirmed by mean of UVvis measurement, shown in Figure 6.5. The shape of the absorbance spectrum underwent an enhancement in magnitude as well as a red shift. The crystallinity of the layer was found to increase, thanks to both the slow drying technique and the thermal treatment.

The same assessments for spin coated P3HT:PCBM showed some important

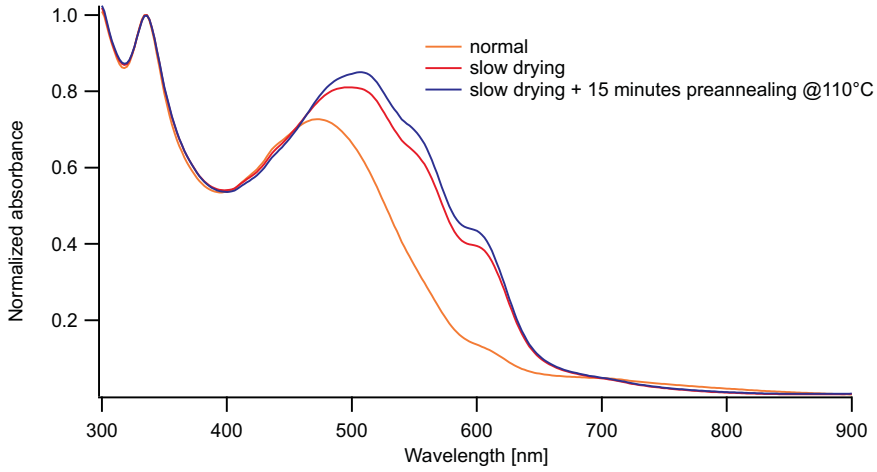

Figure 6.5: UVvis measurements of P3HT:PCBM optical absorbance improvements. The layers assessed were processed with fast drying, slow drying and annealing at 110 °C for 15 minutes after slow drying.

differences. First of all, the adoption of a slow drying technique was found to be much less effective. Indeed, since the covering of the sample occurred at the end of the spinning, the solvent which took part to the evaporation process was orders of magnitude less than in spray coating. This turned in a substantially different morphology of the layer.

Ultimately, the thermal treatment adopted for spin coated layers was found not to improve the performance of the layer. In fact, such process step was optimized during the investigation of spin coated P3HT Rieke 4002. Due to the intrinsic differences with such polymer, Rieke P100 gave rise to poor optical and electrical performance after annealing.

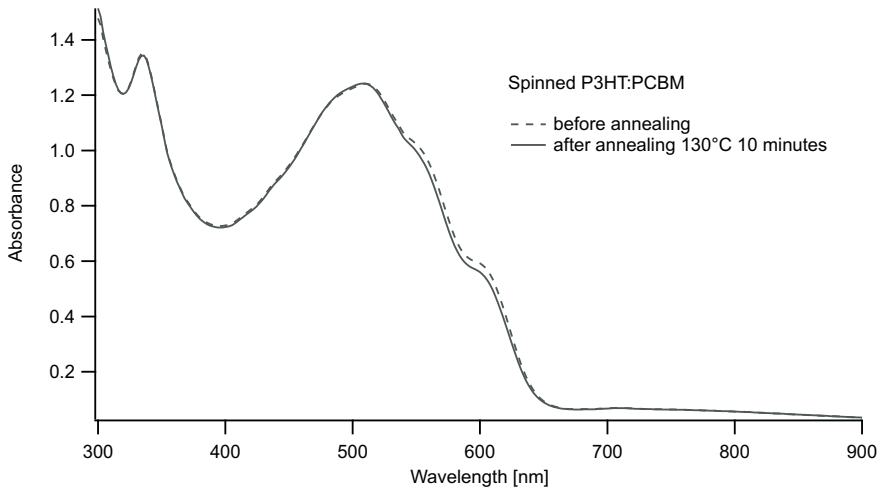

Figure 6.6: UVvis measurements of spin coated P3HT:PCBM optical absorbance. The layers assessed were processed with slow drying and annealing at 130 °C for 10 minutes after slow drying. A not suitable thermal treatment did not lead to morphological improvements.

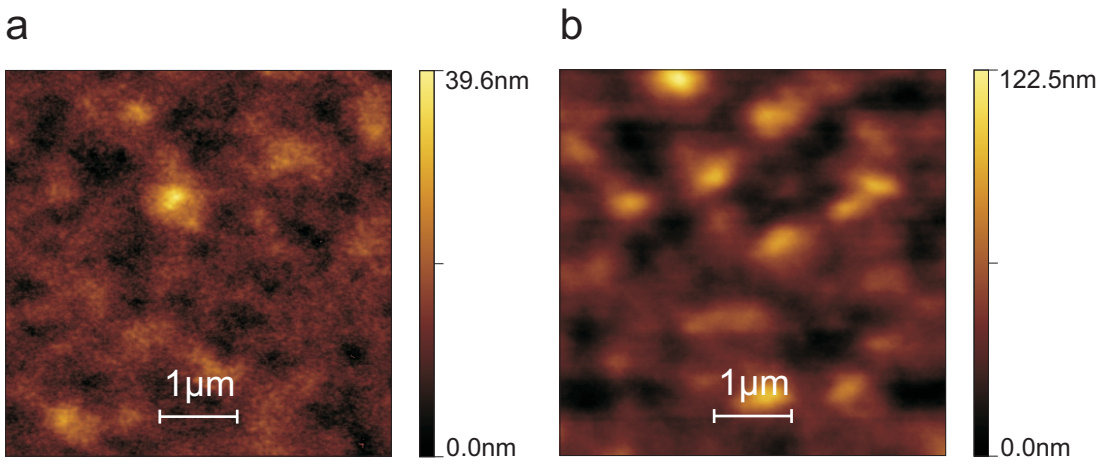

Figure 6.7: AFM measurements on spin coated P3HT:PCBM layers surface. The assessment was performed on films slow dried (a), and annealed at 130 °C for 10 minutes after slow drying. An very significant increase in the rms value is noticeable, from (a) 3.9 to (b) 15.0 nanometers.

Indeed, as shown in Figure 6.6, the optical absorbance of the layer got even worse after the thermal treatment. From the AFM scan, shown in Figure 6.7 a very coarse morphology was assessed. The characteristic length of the surface profile remained constant after the annealing, but a more than twofold increase in the peak to valley and in the rms values was observed. Such dramatic change apparently did not benefit the arrangement of the species within the domains.

A comparison between solar cells whose active layer was fabricated with either spray or spin coating is shown in Table 6.1. Although a lower value for the short circuit current, the significant difference in fill factor led to overall higher efficiency for the device with spray coated P3HT:PCBM.

Table 6.1: Solar cells parameters comparison for spray and spin coated active layer (P3HT Rieke P100).

	PCE %	J_{sc} [mA/cm^2]	FF %	V_{oc} [mV]
Sprayed active layer	3.0	6.8	71	626
Spinned active layer	2.8	7.8	58	617

6.3 Fully spray coated solar cell

By adopting P3HT Rieke 4002 material, a more meaningful comparison between spray and spin coated active layers could be drawn. In fact, as discussed in Chapter 5, such polymer is found to be more suitable for solar cells application. Moreover, the standard procedure for a fully spin coated device optimizes the

performance of this material. Based on a more reliable reference, we could better evaluate the potential of spray coating technique.

In order to make a direct comparison, fully spray coated and fully spin coated devices were fabricated. Moreover, a further assessment of the changes in performance due to the processing of each layer was needed. Therefore, "mixed" solar cells with spray coated PEDOT:PSS /spin coated P3HT:PCBM and vice versa were considered as well.

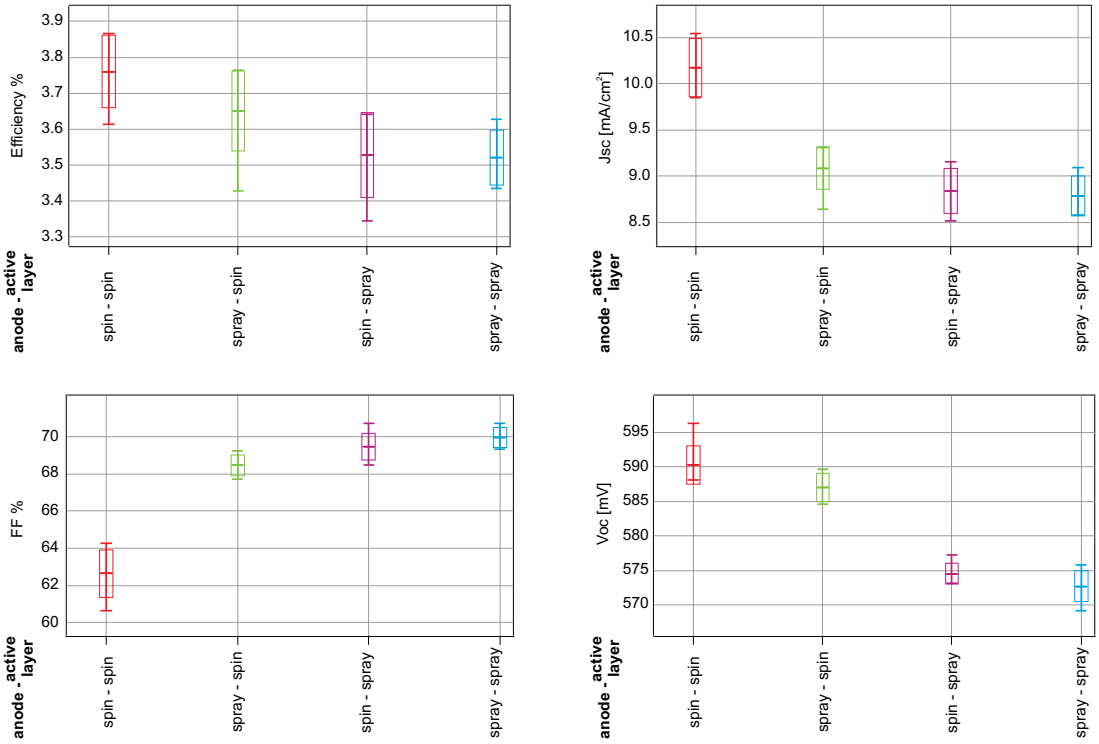

Figure 6.8: Electrical parameters of standard structure organic solar cells, whose anode and active layer were processed either with spray coating or with spin coating. All the combinations have been considered in order to better draw a comparison between the two deposition techniques.

The performances of such devices are shown in Figure 6.8.

- **Spray-spin coated anode** (Figure 6.9): the insertion of spray coated PEDOT:PSS did not lead to any substantial worsening of the performance. The V_{oc} of the devices thoroughly correspond and the profile in forward bias conditions are found to be identical. Only a significant higher J_{sc} (over 10% more) was observed for the reference device, although the processing of the active layer followed the same procedure for both samples and led to very similar thickness (around 290 nanometers). Nevertheless, a higher fill factor in the cell with sprayed PEDOT:PSS (69 against 63%) partially compensated such gap, so that the final PCE were found to be similar

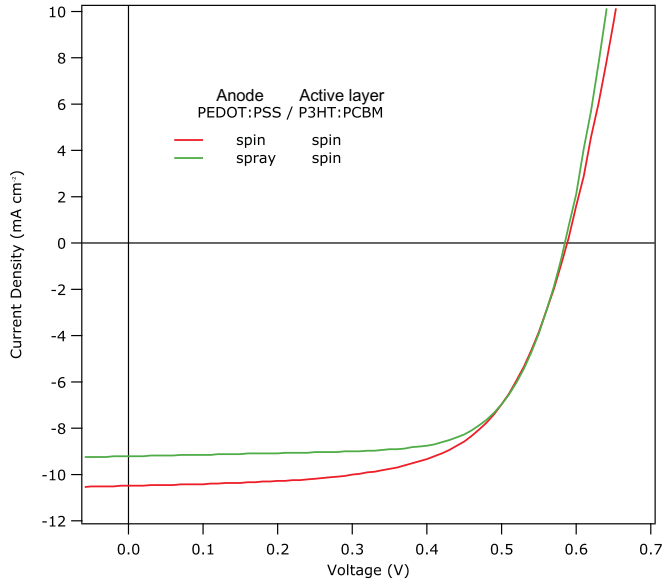

Figure 6.9: Comparison between the I-V curves of the fully spin coated reference and device whose anode was fabricated with spray coating.

within a 0.1% efficiency difference.

- **Spray-spin coated active layer** (Figure 6.10): the comparison between spray and spin coated P3HT:PCBM resulted in some expected conclusions. First of all, a difference of about 20 mV was found in the V_{oc}s. Such phenomenon suggested that the morphology of the active layer achievable with spray coating process showed an even advanced crystallization of the species, if compared with the optimized spin coated film. This hypothesis was confirmed from the higher fill factor observed in the former device. Indeed, referring to Figure 6.10, a more square-like shape is observed for the purple line than for the red one, index of enhanced transport properties.

  We ascribed this effect to the higher amount of solvent which participate to the slow evaporation after the deposition process and that probably enables the formation of bigger crystal domains. As already mentioned, the whole solvent sprayed on the substrate contributes to the arrangement of the organic species, so that higher levels of dilution are needed compared to spin coating. The latter involves only a very little portion of the solution cast in the formation of the active layer. P3HT polymer chains and PCBM molecules are found to settle in a less diluted environment giving rise to a substantially different morphology. Nevertheless, spin coated active layer led to very high values for the J_{sc} (up to 10.2 mA/cm^2), resulting in a overall higher efficiency. Eventual smaller size of its domains might explain this trend, giving rise to slightly worse transport properties, but to a more efficient exciton dissociation.

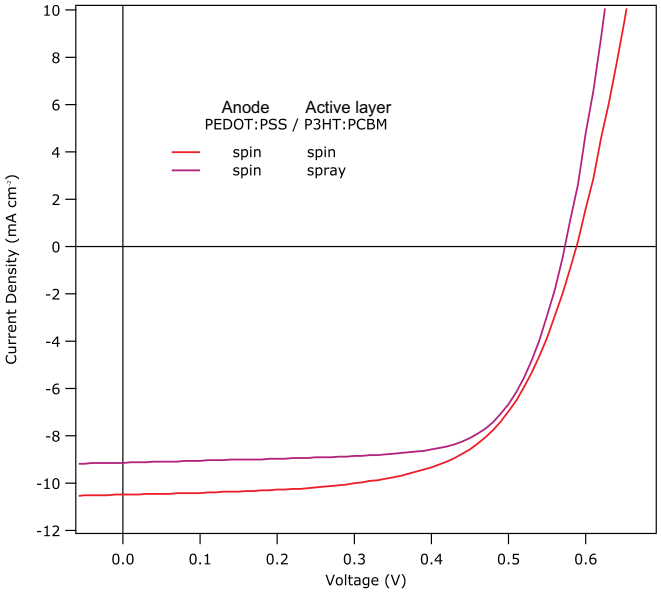

Figure 6.10: Comparison between the I-V curves of the fully spin coated reference and devices whose active layer was fabricated with spray coating.

- **Fully spray coated solar cell** (Figure 6.11): ultimately, the final investigation concerned a fully spray coated solar cell. The performance of the device was found to be very similar to the previous cells where only one layer was processed via spray coating. We discussed previously that the introduction of spray coated PEDOT:PSS led to a slight decrease in performance (losses in J_{sc}). This could be explained considering an high sensitivity in the formation of the P3HT:PCBM layer to the roughness of the underlying surface. Such limitation was not found to affect the processing of the active layer via spray coating, which in fact led to identical results when the substrate was coated either with spin coating or with spray coating.

In Figure 6.12, the comparison among four devices processed with different procedures is shown. Despite of the evident difference between the reference and the other cells, the maximum power points are found to be very close to each others. The gap in efficiency is therefore very limited, mainly due to the outstanding performance of spray coated P3HT:PCBM in terms of fill factor.

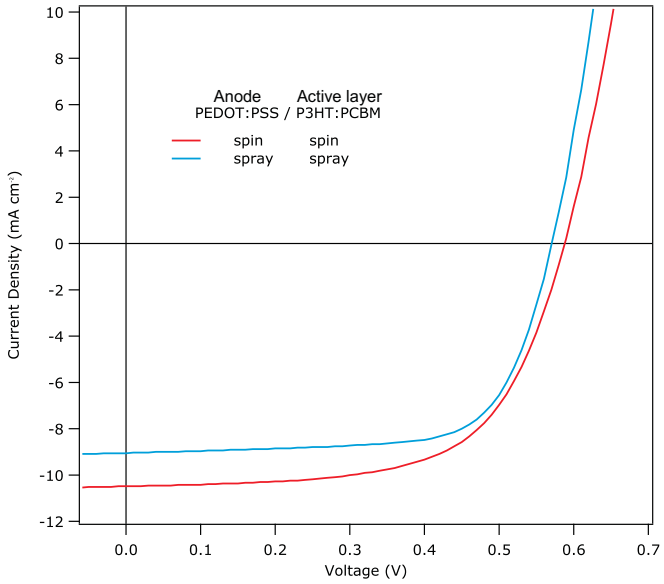

Figure 6.11: Comparison between the I-V curves of the fully spin coated reference and a fully spray coated solar cell.

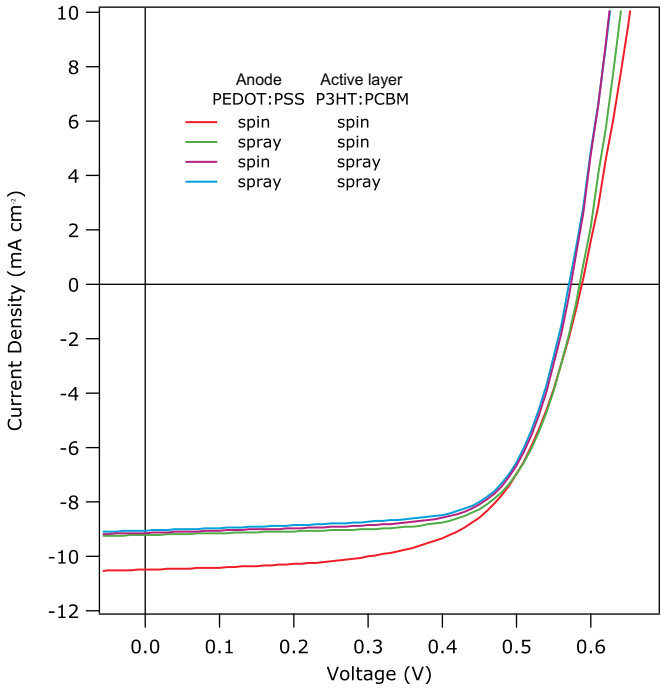

Figure 6.12: I-V curves already shown in Figures 6.9-6.10-6.11 merged in the same graphic.

Conclusions

My investigations on spray coating technique have been shown in this work. The attention has been focused on the capability of the method to coat a substrate depositing organic layers, as well as to the electrical performance of such layers within a solar cell device. The following conclusions arose:

- In regard to the coating, spray deposition has shown the possibility to attain full coverage with acceptable uniformity even for layer thickness down to few tens of nanometers. In particular, the adoption of the Single Pass method has been found to be a very promising way how to overcome the intrinsic uniformity issues arisen from independent evaporation of single droplets. Considering the formation and the controlled evaporation of a full single liquid layer has been a key point for the achievement of smooth organic films.

- It has been shown how the adoption of a two solvents technique gave rise to Marangoni flows of the deposited solution towards the borders of the sample, consisting in an internal spreading driving force which compensated the lack of control involved in spray coating.

- The optimization of the physical properties of the layers has been found to fulfil the basic requirements for their employment in solar cells. In particular for the active layer, a suitable morphology of the blend could be achieved by mean of a slow drying technique, together with a well-sized annealing step. Furthermore, it has been shown that spray deposition of P3HT:PCBM clearly involves especially effective electrical properties, leading to favourable charge transport in the blend. Indeed, the characterization of solar cells adopting such layer showed outstanding values for the fill factor of the device, up to 73%.

- Solar cells, whose both organic layers were spray coated, showed efficiency values as high as 3.52%. This demonstrated that no substantial differences

occur, in terms of overall performance, when comparison with spin coated reference is made.

Future work

The effectiveness of spray coating technique in the deposition of 1.25 by 1.25 cm^2 area organic layers has been studied. The next step consists, therefore, in the investigation in the up-scaling of the technique. Indeed, the Single Pass method has been found to be very promising in the achievement of smooth layers, but it involves the evaporation evolution of the whole deposited liquid. Thus, dependence of such evolution from the geometry of the system can be expected. Especially, the contribution of the Marangoni flows in the wetting of the substrate has to be verified on larger size surfaces, where the edge effects might play less decisive roles.

As remark, during our investigation, a successful processing of the active layer on a 5 by 5 cm^2 organic solar cell was implemented by mean of a sequence of 5 adjacent Single Pass depositions. This first result let us infer that the up-scaling might, indeed, lead to positive results. A possible extension of the process to a roll-to-roll production should involve the deposition of the solutions on a significantly wide substrate, by mean of arrays of nozzles. As long as the effectiveness of the two solvents technique is demonstrated on up-scaled substrate, such high symmetrical system will definitely further improve the reliability of the process, leading to more uniform distribution of the solute.

The adoption of spray coating for solar cells fabrication would be complete, if such process was able to implement the deposition of the top metal contact. Indeed, in view of a roll-to-roll extension, the thermal evaporation of the cathode would represent one of the main limitations to the throughput, as well as one of the most expensive parts of the process. A very important result was achieved by Girotto et al. [21], who demonstrated the possibility to fabricate a solution-processed top electrode, by mean of a silver nano-particles solution. The spray coating of such solution was performed directly on top of an inverted structure (ITO / Zinc Oxide / P3HT:PCBM / PEDOT:PSS) bulk-heterojunction organic solar cell through a shadow mask. The performances of such device were found to be comparable to those of references with evaporated top-contacts. The op-

timization of this process, together with the development of the deposition of a suitable transparent cathode would, indeed, lead to the fabrication of a fully spray coated organic solar cell.

Appendix A

Substrate cleaning procedure

The investigations of spray coating technique involved in this work the usage of two different kind substrates. For organic solar cells processing, 1.25 by 1.25 cm^2 area glass substrates with two Indium Tin Oxide stripes crossing the surface were adopted. For such substrates the cleaning procedure consisted in the following sequence:

- 10 minutes washing in soap;
- 10 minutes rinsing in deionized water (DIW);
- 10 minutes washing in acetone (ACE);
- 10 minutes washing in isopropanol (IPA).

All the steps were performed in ultrasonic bath.

For preliminary studies on organic layers deposition, glass substrate with 1.25 by 1.25 cm^2 area were adopted. Such substrates were obtained by cleaning old substrates on which other layers had been deposited in a H_2O_2:H_2SO_4 bath. Such treatment is found to be very aggressive, so that only acetone and isopropanol cleaning steps in ultrasonic bath were performed before the deposition.

Ultimately, the substrates were exposed to UVOCS T10X10/OES Ultraviolet Ozone Cleaning treatment for 15 minutes in order to further remove all the impurities and to increase the surface energy of the surface. Such step improved significantly the wetting properties of the solutions.

Appendix B

Standard procedure

The fabrication organic solar cells with standard structure is found to be optimized by adopting spin coating process for organic layers deposition. The procedure which permitted to achieve the best performance by adopting 1.25 by 1.25 cm^2 area substrates involves the following steps:

- Cleaning of the substrate according to the procedure shown in Appendix A;
- Spin coating of PEDOT:PSS water based solution at 3000 rpm for 60 seconds. A layer 35 nanometers thick is obtained in this way.
- Annealing in glove box for 10 minutes at 130°C, in order to remove eventual water molecules in the film.
- Spin coating of P3HT Rieke 4002 material PCBM Solenne material in orthodichlorobenzene. The solution has a 30 mg/ml concentration for both the components. A spinning at 800 rpm for 60 seconds leads to a 290 nanometers thick layer.
- Annealing of the sample at 130°Cfor ten minutes.
- Evaporation of 40 nanometers of Ytterbium and 100 nanometers of aluminium in vacuum conditions (below 10^{-6} torr).

The average performance achievable by adopting such procedure are shown in Table B.1.

Table B.1: Average solar cells parameters for organic solar cells fabricated following the standard procedure.

PCE %	J_{sc} [mA/cm^2]	FF %	V_{oc} [mV]
3.5	9.3	64	585

Appendix C

Surface tension measurement

Since the software we had available (OCA-20 contact angle measurement system) did not provide any automatic calculation of the volume, we tried to estimate these values by considering the ellipsoid whose cross section better approximated the shape of the drop. This led to underestimations of the actual volume of the liquid. The operation was made manually so that the accuracy of the method was further affected. Despite of the inaccuracy, the reproducibility of the measurement was acceptable. Therefore, we could rely on the comparison among measurement of different composition.

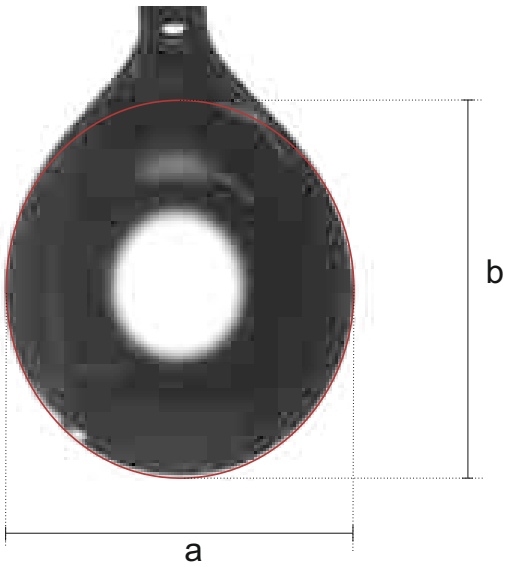

Figure C.1: Picture taken during surface tension measurement. The pendant drop method is one of the easiest and common way how to assess such parameter.

In Figure C.1 a picture of the way how I estimated the volume of the drop is

shown. The volume of the ellipsoid considered is

$$V = \frac{4}{3}\,\pi\,a\,b^2 \tag{C.0.1}$$

The following balance is valid right before the drop falls

$$\rho\,V\,g \;=\; \pi\,d\,\gamma \tag{C.0.2}$$

where g is the gravity acceleration, d is the diameter of the dispensing needle and γ the surface tension of the liquid. The meaning of such equation is thus that the limit in volume sustainable is the one referred to such a weight of the drop that equals the maximum cohesion force which the most critical region offers. Namely, the pulling force applied on the virtual line with diameter d close to the needle has to be considered. From C.0.2 is therefore possible to estimate the value of the surface tension γ.

The resolution of the measurement was limited by the resolution of the picture. In fact, the estimations of a, b and therefore of V were made by counting the pixels. Considering therefore the equation:

$$\gamma \;=\; \frac{4\,a\,b^2\,\rho\,g}{3\,d} \tag{C.0.3}$$

It is possible to estimate the relative uncertainty on the result with

$$\frac{d\gamma}{\gamma} = \sqrt{9\left(\frac{d\,n_d}{n_d}\right)^2 \;+\; 2\left(\frac{d\,n_a}{n_a}\right)^2 \;+\; \left(\frac{d\,n_b}{n_b}\right)^2} \tag{C.0.4}$$

where n_i is the number of pixels referred to the measurement of i. The term due to the diameter of the needle is indeed the most critical (it is the shortest length). Considering a reasonable error (dn) of 2 pixels for each length estimation, it results that

$$\frac{d\gamma}{\gamma} \;\approx\; 9\left(\frac{d\,n_d}{n_d}\right) \tag{C.0.5}$$

For the measurements that I performed, the outcome of such relative uncertainty calculation is 12%.

Appendix D

Spin coating process

Spin coating has been used for several decades for the application of thin films. The complete process consists of a dispense stage in which a fluid is deposited onto the substrate surface, an acceleration stage that spread the liquid and remove the exceeding part of it, a high speed spin stage to thin the fluid, and a drying stage to eliminate excess solvents from the resulting film. Stage Three (flow controlled) and Stage Four (evaporation controlled) are the two stages that have the most impact on final coating thickness.

Stage One The first stage is the deposition of the coating fluid onto the wafer or substrate. It can be done using a nozzle that pours the coating solution out, or it could be sprayed onto the surface. Usually this dispense stage provides a substantial excess of coating solution compared to the amount that will ultimately be required in the final coating thickness, resulting in a big quantity of wasted liquid. For many solutions it is often beneficial to dispense through a sub micron sized filter to eliminate particles that could lead to flaws. Another potentially important issue is whether the solution wets the surface completely during this dispense stage. If not, then incomplete coverage can result.

Stage Two The second stage is when the substrate is accelerated up to its final, desired, rotation speed. This stage is usually characterized by aggressive fluid expulsion from the wafer surface by the rotational motion. Because of the initial depth of fluid on the wafer surface, spiral vortices may briefly be present during this stage; these would form as a result of the twisting motion caused by the inertia that the top of the fluid layer exerts while the wafer below rotates faster and faster. Eventually, the fluid is thin enough to be completely co-rotating with the wafer and any evidence of fluid thickness

differences is gone. Ultimately, the wafer reaches its desired speed and the fluid is thin enough that the viscous shear drag exactly balances the rotational accelerations.

Stage Three The third stage is when the substrate is spinning at a constant rate and fluid viscous forces dominate fluid thinning behaviour. This stage is characterized by gradual fluid thinning. Edge effects are often seen because the fluid flows uniformly outward, but must form droplets at the edge to be flung off. Thus, depending on the surface tension, viscosity, rotation rate, etc., there may be a small bead of coating thickness difference around the rim of the final wafer. Mathematical treatments of the flow behaviour show that if the liquid exhibits Newtonian viscosity (i.e. is linear) and if the fluid thickness is initially uniform across the wafer (albeit rather thick), then the fluid thickness profile at any following time will also be uniform—leading to a uniform final coating (under ideal circumstances).

Stage Four The fourth stage is when the substrate is spinning at a constant rate and solvent evaporation dominates the coating thinning behaviour. As the prior stage advances, the fluid thickness reaches a point where the viscosity effects yield only rather minor net fluid flow. At this point, the evaporation of any volatile solvent species will become the dominant process occurring in the coating. In fact, at this point the coating effectively "gels" because as these solvents are removed the viscosity of the remaining solution will likely rise—effectively freezing the coating in place.

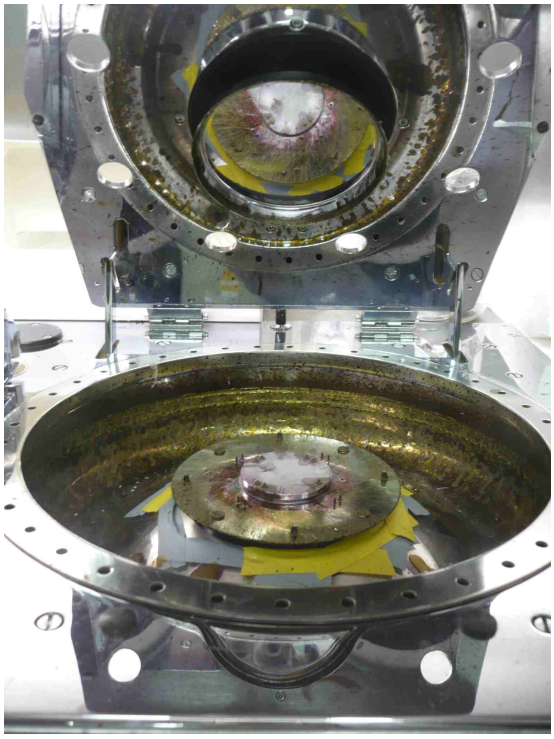

Figure D.1: Spin coater in glove box. The tool permits the processing for different sizes of the substrate. A automatic coverage of the sample during the spinning can be included in the program in order to better control the viscous forces-evaporation regimes.

Bibliography

[1] http://ec.europa.eu/environment/climat/climate_action.htm.

[2] Christoph J. Brabec and James R. Durrant. Solution-Processed Organic Solar Cells, 2008, MRS Bulletin.

[3] Wolfgang Bruetting. Physics of Organic Semiconductors, 2005, Wiley-VCH.

[4] http://www.sony.net/SonyInfo/News/Press/200710/07-1001E/.

[5] Peet, J. Kim, J. Y. Coates, N. E. Ma, W. L. Moses, D. Heeger, A. J. Bazan, G. C. Efficiency enhancement in low-bandgap polymer solar cells by processing with alkane dithiols, 2007 Nature Materials.

[6] www.solarmer.com.

[7] C. Klepek, S.A. Choulis, P. Schilinsky, C.J. Brabec, Adv. Mater. 19, 3973 (2007).

[8] M. Tuomikoski, P. Kopola, Technologies for Polymer Electronics TPE 06, Rudolstadt, Germany, 1618 May 2006.

[9] http://www.konarka.com/.

[10] F. Padinger, C.J. Brabec, T. Fromherz, J.C. Hummelen, N.S. Sariciftci, Optoelectron. Rev. 8 (4), 280 (2000).

[11] Christoph Brabec, Vladimir Dyakonov, Ullrich Scherf. Organic Photovoltaics, 2008, Wiley-VCH.

[12] Adam, Neil Kensington. The Physics and Chemistry of Surfaces, 3rd ed. 1941 Oxford University Press.

[13] Tharwat F. Tadros, Th. F. Tadros 0 Recensioni. Applied surfactants, 2008, Wiley-VCH.

[14] C. Girotto et al., MRS Fall meeting 2007.

[15] Y.-H. Chang, S.-R. Tseng, C.-Y. Chen, H.-F. Meng, E.-C. Chen, S.-F. Horng, and C.-S. Hsu. Polymer solar cell by blade coating. *Organic Electronics*, 10(5):741 – 746, 2009.

[16] D.-Y. Chung, J. Huang, D. D. C. Bradley, and A. J. Campbell. High performance, flexible polymer light-emitting diodes (pleds) with gravure contact printed hole injection and light emitting layers. *Organic Electronics*, In Press, Accept, 2010.

[17] R. D. Deegan, O. Bakajin, T. F. Dupont, G. Huber, S. R. Nagel, and T. A. Witten. Capillary flow as the cause of ring stains from dried liquid drops. *Nature*, 389:827–829, 1997.

[18] R. D. Deegan, O. Bakajin, T. F. Dupont, G. Huber, S. R. Nagel, and T. A. Witten. Contact line deposits in an evaporating drop. *Phys. Rev. E*, 62(1):756–765, July 2000.

[19] X. Fanton and A. M. Cazabat. Spreading and instabilities induced by a solutal marangoni effect. *Langmuir*, 14(9):2554–2561, April 1998.

[20] C. Girotto, B. P. Rand, J. Genoe, and P. Heremans. Exploring spray coating as a deposition technique for the fabrication of solution-processed solar cells. *Solar Energy Materials and Solar Cells*, 93(4):454–458, 2009. Processing and Preparation of Polymer and Organic Solar Cells.

[21] C. Girotto, B. P. Rand, S. Steudel, J. Genoe, and P. Heremans. Nanoparticle-based, spray-coated silver top contacts for efficient polymer solar cells. *Organic Electronics*, 10(4):735–740, July 2009.

[22] R. Green, A. Morfa, A. J. Ferguson, N. Kopidakis, G. Rumbles, and S. E. Shaheen. Performance of bulk heterojunction photovoltaic devices prepared by airbrush spray deposition. *Applied Physics Letters*, 92(3):033301, 2008.

[23] C. N. Hoth, S. A. Choulis, P. Schilinsky, and C. J. Brabec. High photovoltaic performance of inkjet printed polymer:fullerene blends. *Advanced Materials*, 19(22):3973–3978, 2007.

[24] C. N. Hoth, R. Steim, P. Schilinsky, S. A. Choulis, S. F. Tedde, O. Hayden, and C. J. Brabec. Topographical and morphological aspects of spray coated organic photovoltaics. *Organic Electronics*, 10(4):587–593, 2009.

[25] H. Hu and R. G. Larson. Analysis of the effects of marangoni stresses on the microflow in an evaporating sessile droplet. *Langmuir*, 21(9):3972–3980, March 2005.

[26] I. Langmuir. The evaporation of small spheres. *Physical Review*, 12(5):368–370, November 1918.

[27] G. Li, V. Shrotriya, J. Huang, Y. Yao, T. Moriarty, K. Emery, and Y. Yang. High-efficiency solution processable polymer photovoltaic cells by self-organization of polymer blends. *Nature Materials*, 4:864–868, 2005.

[28] G. Li, Y. Yao, H. Yang, V. Shrotriya, G. Yang, and Y. Yang. "solvent annealing" effect in polymer solar cells based on poly(3-hexylthiophene) and methanofullerenes. *Advanced Functional Materials*, 17(10):1636–1644, 2007.

[29] C. Liu, E. Bonaccurso, and H.-J. Butt. Evaporation of sessile water/ethanol drops in a controlled environment. *Phys. Chem. Chem. Phys.*, 10:7150–7157, 2008.

[30] F. Padinger, R. S. Rittberger, and N. S. Sariciftci. Effects of postproduction treatment om plastic solar cells. *Advanced Functional Materials*, 13(1):85–88, January 2003.

[31] D. Vak, S.-S. Kim, J. Jo, S.-H. Oh, S.-I. Na, J. Kim, and D.-Y. Kim. Fabrication of organic bulk heterojunction solar cells by a spray deposition method for low-cost power generation. *Applied Physics Letters*, 91(8):081102, 2007.

[32] P. Vanlaeke, A. Swinnen, I. Haeldermans, G. Vanhoyland, T. Aernouts, D. Cheyns, C. Deibel, J. D'Haen, P. Heremans, J. Poortmans, and J. V. Manca. P3HT/PCBM bulk heterojunction solar cells: Relation between morphology and electro-optical characteristics. *Solar Energy Materials & Solar Cells*, 90(14):2150–2158, 2006.

[33] B. Widom. Line tension and the shape of a sessile drop. *Journal of Physical Chemistry*, 99(9):2803–2806, 1995.

[34] X. Xu, J. Luo, and D. Guo. Criterion for reversal of thermal marangoni flow in drying drops. *Langmuir*, 26(3):1918–1922, September 2009.